İSTANBUL TECHNICAL UNIVERSITY ★ GRADUATE SCHOOL OF SCIENCE ENGINEERING AND TECHNOLOGY

POSITION SENSORLESS FIELD ORIENTED CONTROL OF IPMSM UNDER PARAMETER UNCERTAINTIES

M.Sc. THESIS

İsa Eray AKYOL

Department of Control and Automation

Engineering Programme

JUNE 2016

İSTANBUL TECHNICAL UNIVERSITY ★ GRADUATE SCHOOL OF SCIENCE ENGINEERING AND TECHNOLOGY

POSITION SENSORLESS FIELD ORIENTED CONTROL OF IPMSM UNDER PARAMETER UNCERTAINTIES

M.Sc. THESIS

İsa Eray AKYOL
(504141117)

Department of Control and Automation

Engineering Programme

Thesis Advisor: Prof. Dr. Mehmet Turan SÖYLEMEZ

JUNE 2016

İSTANBUL TEKNİK ÜNİVERSİTESİ ★ FEN BİLİMLERİ ENSTİTÜSÜ

GÖMÜLÜ MIKNATISLI SENKRON MOTORUN PARAMETRİK BELİRSİZLİKLER ALTINDA KONUM SENSÖRSÜZ ALAN YÖNLENDİRMELİ KONTROLÜ

YÜKSEK LİSANS TEZİ

İsa Eray AKYOL
(504141117)

Kontrol ve Otomasyon Mühendisliği Anabilim Dalı

Kontrol ve Otomasyon Mühendisliği Programı

Tez Danışmanı: Prof. Dr. Mehmet Turan SÖYLEMEZ

HAZİRAN 2016

Isa Eray AKYOL, a M.Sc. student of İTU Graduate School of Science Engineering and Technology 504141117, successfully defended the thesis entitled "POSITION SENSORLESS FIELD ORIENTED CONTROL OF IPMSM UNDER PARAMETER UNCERTAINTIES", which he prepared after fulfilling the requirements specified in the associated legislations, before the jury whose signatures are below.

Thesis Advisor :	**Prof. Dr. M. Turan SÖYLEMEZ** İstanbul Technical University	.....
Jury Members :	**Prof. Dr. M. Turan SÖYLEMEZ** İstanbul Technical University	.....
	Prof. Dr. Metin GÖKAŞAN İstanbul Technical University	.....
	Yrd. Doç. Dr. İlker ÜSTOĞLU Yıldız Technical University	.....

Date of Submission : 2 May 2016
Date of Defense : 8 June 2016

To Nihan,

FOREWORD

First and foremost, I would like to thank to my advisor Prof. Dr. Mehmet Turan SÖYLEMEZ, for his valuable guidance and advice. His willingness to share his experience with me contributed tremendously to my project. Besides, I would like to thank Kann Bayka, Emrah Salman, Reyhan Türk, Namık Yılmaz, Safder Kayalı, Taner Yazıcı and all Arçelik R&D Center team for providing me an excellent environment to complete this work. Finally, an honorable mention goes to my family and Nihan Gündüz for their understandings and supports on me in everything. Without help of the particular that mentioned above, I would face many difficuilties while doing this.

June 2016

İsa Eray AKYOL
(Control Engineer)

TABLE OF CONTENTS

Page

FOREWORD ... **ix**
TABLE OF CONTENTS ... **xi**
ABBREVIATIONS ... **xiii**
SYMBOLS ... **xv**
LIST OF TABLES ... **xvii**
LIST OF FIGURES ... **xix**
SUMMARY ... **xxiii**
ÖZET ... **xxv**
1. INTRODUCTION ... **1**
1.1 Purpose of The Thesis ... 1
1.2 Literature Review ... 1
1.2.1 Sensorless speed control of IPMSM ... 2
1.2.1.1 State estimation ... 2
1.2.1.2 Wide speed range control ... 5
1.2.2 Parametric uncertainties related to the control system ... 5
1.3 Hypothesis ... 6
1.4 Organization of the Thesis ... 7
2. MATHEMATICAL MODEL OF IPMSM ... **9**
2.1 Alpha-Beta Reference Frame ... 11
2.2 D-Q Reference Frame ... 12
2.3 Extended BEMF Model ... 14
2.4 Control Strategy of The IPMSM ... 15
2.5 Field Weakening Operation ... 17
2.6 Parameter Uncertainties ... 18
3. SPEED ADAPTIVE PI OBSERVER DESIGN ... **19**
3.1 Observer Model ... 19
3.1.1 Convergence of estimation errors ... 20
3.2 Design By Using Classical Pole Assignment Method ... 21
3.3 Pole Colouring Concept ... 22
3.3.1 Several cost functions ... 26
3.3.1.1 Minimum perturbation based cost function ... 26
3.3.1.2 Settling time based cost function ... 26
3.4 Robust Pole Placement Via Pole Colouring ... 27
3.4.1 Using settling time and perturbation based cost functions together ... 30
3.5 Robust PI Observer Design Over Wide Speed Range ... 31
3.5.1 PI observer design for washing cycle ... 32
3.5.2 PI observer design for spinning cycle ... 33

3.6 Speed and Position Estimation 34
4. DESIGN OF ROBUST CURRENT CONTROLLERS 37
4.1 Mathematical Model of The Current loop 37
4.2 Open Loop Decoupling of The d-q Axes Currents 38
4.3 Design by Using Pole Colouring Concept 39
4.3.1 D-axis current controller design 40
4.3.2 Q-axis current controller design 40
5. DESIGN OF ROBUST SPEED CONTROLLER 43
5.1 PI-P Controller Design 45
6. POSITION SENSORLESS STARTUP ALGORITHM 47
6.1 Problem of Sensorless Starpup 47
6.2 A Novel Startup Algorithm 48
6.3 Open to Closed Loop Transition 49
7. FIELD WEAKENING OPERATION 53
7.1 Parameter Free Field Weakening Algorithm 53
7.2 Unbalanced Load Detection 55
8. SIMULATIONS AND EXPERIMENTAL RESULTS 59
8.1 Simulations 59
8.1.1 Washing cycle estimation errors 59
8.1.2 Spinning cycle estimation errors 61
8.2 Experimental Results 62
8.2.1 Washing cycle 62
8.2.2 Spinning cycle 64
8.2.3 Ramp condition at whole range 65
9. CONCLUSION 71
REFERENCES 73
APPENDICES 77
APPENDIX A.1 79
APPENDIX A.2 79
APPENDIX A.3 80
APPENDIX A.4 80
APPENDIX B.1 81
APPENDIX B.2 81
CURRICULUM VITAE 83

ABBREVIATIONS

IPMSM	**:** Interior Permanent Magnet Synchronous Motor
SPMSM	**:** Surface Permanent Magnet Synchronous Motor
PID	**:** Proportional-Integral-Derivative
MRAS	**:** Model Reference Adaptive System
SMO	**:** Sliding Mode Observer
EKF	**:** Extended Kalman Filter
DC	**:** Direct Current
AC	**:** Alternating Current
BEMF	**:** Back Electromotive Force
MMF	**:** Magnetomotive Force
SISO	**:** Single Input Single Output
MIMO	**:** Multiple Input Multiple Output
LQR	**:** Linear Quadratic Regulator

SYMBOLS

R	:	stator winding resistance
$i_{u,v,w}$	:	phase currents
$i_{d,q}$	:	d and q axes current
$i_{\alpha,\beta}$	:	α and β axes current
$i_{\gamma,\delta}$	:	γ and δ axes current
$L_{u,v,u}$	:	phase inductances
$L_{d,q}$	:	d and q axes inductances
$E_{u,v,w}$	:	phase back electromotive forces
$e_{d,q}$	:	d and q axes back electromotive forces
$e_{\gamma,\delta}$	:	γ and δ axes back electromotive forces
E_{ex}	:	extended back electromotive force
$v_{u,v,w}$	:	phase voltages
$v_{\alpha,\beta}$	:	α and β axes voltages
$v_{d,q}$	:	d and q axes voltages
$v_{\gamma,\delta}$	:	γ and δ axes voltages
ω_e	:	electrical angular velocity of the rotor
ω_m	:	mechanical angular velocity of the rotor
ω_{emax}	:	maximum electrical angular velocity of the rotor
$\hat{\omega}_e$	:	estimated electrical angular velocity of the rotor
J	:	moment of inertia
B	:	friction coefficient
k_t	:	torque constant
T	:	sampling period
θ_e	:	electrical angular position of the rotor
$\hat{\theta}_e$	:	estimated electrical angular position of the rotor
θ_{error}	:	angular position error between actual and estimated rotor position (electrical)
$\Psi^s_{u,v,w}$	:	phase stator linkages
Ψ_{PM}	:	magnet flux linkage

LIST OF TABLES

Page

Table 2.1 : Uncertain Parameters. 18
Table 4.1 : Parameter Space For R, L_d and L_q. 40
Table 5.1 : Parameter Space For The Speed Loop. 44

LIST OF FIGURES

Page

Figure 1.1 : Block Diagram of MRAS 3
Figure 1.2 : Block Diagram of Luenberger Observer 3
Figure 1.3 : Block Diagram of Sliding Mode Observer 4
Figure 1.4 : Block Diagram of Kalman Filter 4
Figure 2.1 : IPMSM Structure 9
Figure 2.2 : Single Phase Equivalent Circuit 10
Figure 2.3 : α-β Reference Frame 11
Figure 2.4 : $\alpha - \beta$ and $d - q$ Reference Frames 13
Figure 2.5 : Equivalent Circuit in $d - q$ Reference Frame 13
Figure 2.6 : Continuous Model of IPMSM in d-q Reference Frame 14
Figure 2.7 : Total Control Schema of The Control System 16
Figure 2.8 : Torque/Power vs. Speed Characteristic 17
Figure 3.1 : Pole Spread of the Observer, $\Omega_e = [-6300 \quad 0] \frac{rad}{s}$ 22
Figure 3.2 : Possible Pairing Options 25
Figure 3.3 : Nominal and Perturbed Poles 25
Figure 3.4 : Minimum Perturbation Based Cost Function 26
Figure 3.5 : Settling Time Based Cost function 27
Figure 3.6 : Closed Loop Pole Location when k=-0.5 and k=5 29
Figure 3.7 : Pole Spread when k=-0.5 29
Figure 3.8 : Pole Spread when k=5 30
Figure 3.9 : Pole Spread of the Closed Loop System for k=-8.5788 30
Figure 3.10 : Pole Spread of the Closed Loop System for k=-3.62 31
Figure 3.11 : Pole Spread of the observer, $\Omega_e = [-6300 \quad 0] \frac{rad}{s}$ 32
Figure 3.12 : Operation Region of the Washing Machine 33
Figure 3.13 : Pole Spread around $z_{1,2}$ and $z_{3,4}$ 33
Figure 3.14 : Pole Spread around $z_{1,2}$ and $z_{3,4}$ 34
Figure 3.15 : Pole Spread around $z_{1,2}$ and $z_{3,4}$ 34
Figure 3.16 : Pole Spread around $z_{1,2}$ and $z_{3,4}$ 35
Figure 3.17 : Actual And Imaginary Reference Frames 35
Figure 3.18 : Angle Tracking Observer 36
Figure 3.19 : Step Response of Angle Tracking Observer 36
Figure 4.1 : Set of SISO Representation of The Current Loop 38
Figure 4.2 : Current Control Loop Block Diagram 38
Figure 4.3 : Phase Current Without Decoupler 39
Figure 4.4 : Phase Current With Decoupler 39
Figure 4.5 : Pole Spread of The D Axis Current Closed Loop 41
Figure 4.6 : Closed Loop Step Response For D Axis Current Loop 41

Figure 4.7 : Pole Spread of The Q Axis Current Closed Loop 41
Figure 4.8 : Closed Loop Step Response For Q Axis Current Loop..... 42
Figure 5.1 : Pole Spread of The Closed Loop System With PI Controller 44
Figure 5.2 : PI-P Controller..... 45
Figure 5.3 : Pole Spread of The Closed Loop System With PI-P Controller..... 46
Figure 5.4 : Step Response of The Closed Loop System..... 46
Figure 5.5 : Comparison of Disturbance Rejection Performances..... 46
Figure 6.1 : Align State..... 48
Figure 6.2 : i_d-i_q Transition..... 49
Figure 6.3 : Flow Chart of The Startup Algorithm 50
Figure 6.4 : Novel Startup Realization 51
Figure 6.5 : Novel Startup Block Representation 51
Figure 7.1 : Control Schema of The Closed Loop 53
Figure 7.2 : Flow Chart of The Field Weakening Algorithm..... 54
Figure 7.3 : Control Schema of The Field Weakening Region 55
Figure 7.4 : The Free Body Diagram of The Unbalanced Load in Drum..... 55
Figure 7.5 : Equivalent Q-Axis Circuit 56
Figure 7.6 : Active Power Variation in The Presence of Unbalanced Load..... 56
Figure 7.7 : Unbalanced Load Estimation For Different Weights 57
Figure 8.1 : Estimated And Actual Reference Frames..... 59
Figure 8.2 : Washing Cycle State Estimation Errors..... 60
Figure 8.3 : Washing Cycle Rotor Position Errors..... 60
Figure 8.4 : Spinning Cycle State Estimation Errors 61
Figure 8.5 : Spinning Cycle Rotor Position Errors 61
Figure 8.6 : Drum Speed Under No Load Condition..... 62
Figure 8.7 : Drum Speed Under 400g Unbalanced Load Condition..... 63
Figure 8.8 : BEMF Voltages Under 400g Unbalanced Load Condition 63
Figure 8.9 : i_q Current Under 400g Unbalanced Load Condition..... 64
Figure 8.10: Estimated Position Error Under 400g Unbalanced Load Condition . 64
Figure 8.11: Drum Speed Under No Load Condition..... 65
Figure 8.12: Drum Speed Under 400g Unbalanced Load Condition..... 65
Figure 8.13: BEMF Voltages Under 400g Unbalanced Load Condition 66
Figure 8.14: i_q Current Under 400g Unbalanced Load Condition..... 66
Figure 8.15: Motor Speed Under Loaded Condition 67
Figure 8.16: Stator Currents Under Loaded Condition..... 67
Figure 8.17: Control Signals Under Loaded Condition 68
Figure 8.18: Estimated Extended BEMF Voltages Under Loaded Condition 68
Figure 8.19: Input Power Under Loaded Condition..... 68
Figure 8.20: Single Phase Current at The Maximum Speed..... 69
Figure 8.21: Single Phase Current at The Minimum Speed..... 69
Figure 8.22: Single Phase Current at Washing Speed Under 600g Unbalanced Load 69
Figure A.1 : Total SIMULINK Model of The Closed Loop System 79
Figure A.2 : PI Observer Model..... 79
Figure A.3 : IPMSM Model..... 80
Figure A.4 : Decoupler Model..... 80

Figure B.1 : MATHEMATICA Code for Minimum Perturbation Based Cost Function 81
Figure B.2 : MATHEMATICA Code for Settling Time Based Cost Function 81

POSITION SENSORLESS FIELD ORIENTED CONTROL OF IPMSM UNDER PARAMETER UNCERTAINTIES

SUMMARY

Permanent magnet synchronous motors are widely used in industry due to their high torque per volume ratio, low noise, efficiency and wide stable operation region. Especially in the home appliance applications, obtaining high torque by using small motors and low audible noise has crucial importance. Therefore, conventional DC motors have been replaced by the permanent magnet synchronous motors in the modern applications. Although, scalar control is a valid approach for many motor control applications, it is not preferred for high performance applications due to its low performance in the transient regions and lack of controllability of torque and flux separately. However, field oriented control presents important advantages over scalar control.

DC motors allow to control both air gap flux and torque separately, simplifying the control problem. However, it is not possible to control torque and air gap flux separately without using special control techniques in the PMSM. By using field oriented control approach, PMSM is turned into a DC motor mathematically, allowing to control flux and torque separately. In order to perform field oriented control, it is mandatory having rotor flux position information somehow. Conventional approach suggests to use position sensors such as hall effect sensors or resolvers. However, using additional sensors is not preferred due to the robustness concerns and cost constraints. In this study, position sensorless field oriented control approach have been carried out. Rotor flux position have been obtained by constracting an observable mathematical model of PMSM instead of using a position sensor. Mathematical model uses stator currents in order to estimate position related variables such as back electromotive force or flux.

Purpose of the thesis is to perform position sensorless field oriented control of PMSM which drives a washing machine drum, by considering the parametric uncertainties. Although, the closed loop system nominal parameters are assumed to be known, there are uncertainties due to operating conditions, changing temperature, unknown loads and production imperfectness. In order to obtain such a design, a PI observer has been designed to estimate the back electromotive force due to its simple and robust structure. By using an angle tracking observer, speed and position of the rotor have been estimated by evaluating the back electromotive forces. A PI-P controller has been designed in order to control the motor speed under changing moment of inertia, friction coefficient and torque constant conditions. This structure has also satisfactory disturbance rejection capability.

The current control loop consist of two part which are d axis and q axis control loops. Torque related q axes loop is coupled with the flux related d axes loop. In order to treat this problem under single input single output paradigm, a decoupling control has been

carried out. Current controllers have been designed by considering the uncertainties in the winding resistance and inductances.

Both observer and controllers have been designed by using pole coloring concept. This concept uses the degree of freedom of the controller (observer) structure in order to restrict the closed loop pole spread within defined regions. By assigning robustness related cost functions to each nominal closed loop poles, robust control problem has been turned in to an optimization problem. Resulting controllers (observers) are static and required complex mathematical calculations have been carried out offline. By using such an approach, computational effort of the microcontroller is minimized.

Position sensorless control shows low performance at the low speed regions due to presence of the effective unmodelled dynamics, noise and disturbances. So, the conventional approach is not to use observers until the rotor speed reaches a certain speed which the back electromotive forces are strong enough by comparison to the noise and disturbances. However, unknown load strongly effects the startup performance. A novel startup algorithm has been proposed in order to obtain satisfactory performance during the startup.

To sum up, rotor position sensorless control over wide speed range has been carried out under parametric uncertainties. Pole coloring concept has been used in control of a PMSM in an industrial setup for the first time. Novel startup algorithm has been proposed. Designs, results and simulations have been presented in the thesis.

GÖMÜLÜ MIKNATISLI SENKRON MOTORUN PARAMETRİK BELİRSİZLİKLER ALTINDA KONUM SENSÖRSÜZ ALAN YÖNLENDİRMELİ KONTROLÜ

ÖZET

Daimi mıknatıslı senkron motor gerek moment/hacim oranının yüksek olması ve verimi gerekse kararlı çalışma aralığının geniş olamsı nedeniyle günümüzde yaygın kullanım alanına sahiptir. Özellikle beyaz eşya uygulamalarında, gerekli momenti küçük hacimli ve verimli bir şekilde üretmek önemli bir önceliğe sahip olduğu için daimi mıknatıslı senkron motor çamaşır makinesi, buzdolabı, bulaşık makinesi gibi uygulamalarda sıklıkla kullanılır. Her ne kadar skaler kontrol yüksek performans gerektirmeyen uygulamalarda geçerli bir alternatif oluştursa da gerek geçici haldeki kontrol performansının düşük olması gerekse motora ilişkin akı ve moment büyüklüklerinin ayrı ayrı kontrol edilememesi nedenleriyle yüksek performans gerektiren uygulamalarda tercih edilmez. Bu nokta da alan yönlendirmeli kontrol skaler kontrole göre ciddi avantajlar sunmaktadır.

Doğru akım motorunda akı ve momentin ayrı ayrı kontrol edilebilmesi kontrol açısından büyük kolaylık sağlamaktadır. Ancak, alternatif akım motorlarında akı ve momentin özel yöntemler kullanılmadan ayrı ayrı kontrol edilmesi söz konusu değildir. Alan yönlendirmeli kontrol yöntemiyle alternatif akım motoru matematiksel olarak doğru akım motorunun kolay kontrol edilebilirlik özelliklerini kazanabilir. Clarke ve Park dönüşümleri yardımıyla eksenleri bir birine dik ve rotor akısı ile aynı frekansta dönen eksen takımında (d-q eksen takımı) ifade edilen motor modeli akı ve momente kontrol imkanı sağladığı gibi geçici hal performansının da kontrol edilmesini sağlar. Bu sayede hız kontrolü için kullanılan kontrolör moment kontrolörüne kaskat bağlanabilir. Ayrıca alan zayıflatma algoritması ve akı ilişkili akım kontrolörü yardımıyla motor akısı kontrol edilebilir ve motor dc bara gerilimi kısıtıyla belirlenen nominal hız değerinin üzerindeki hız değerlerine ulaşabilir. Motor modelini döner eksen takımında ifade etmek için rotor konumun bilinmesi gerekmektedir. Her ne kadar sensörler yardımıyla rotor konum bilgisi elde edilebilse de gerek maliyet gerekse sensörden kaynaklanabilecek sorunların önüne geçmek amacıyla konum sensörsüz kontrol uygulaması tercih edilmektedir.

Konum sensörsüz kontrol probleminde rotor konumu bir sensör yardımıyla değil, motor faz akımlarından alınan geri besleme yardımıyla matematiksel olarak kestirilir. Bunun için gözlenebilir bir matematiksel model oluşturulmuş ve rotor konumuyla ilgili olan büyüklükler (Ters elektromotor kuvvet veya akı) kestirilmiştir. Kestirilen büyüklükler yardımıyla rotor konumu ve hızı hesaplanmış ve kontrol için gerekli eksen takımı dönüşümleri yapılmıştır.

Her ne kadar motora ilişkin sistem parametreleri bilinse de çalışma koşullarının değişmesi, modelleme hataları, üretimdeki saçınıklıklar ve sıcaklık gibi nedenlerle model belirsizlikleri söz konusudur. Eğer belirsizlikleri dikkate alan bir tasarım yapılmazsa kontrol sisteminin performansında ciddi azalmalar meydana gelecektir.

Bu tezin amacı çamaşır makinelerinde kullanılmak üzere parametrik belirsizlikleri dikkate alarak dayanıklı kontrolör ve gözleyici tasarımlarının yapılmasıve tüm çalışma aralığında istenilen performans kriterlerinin sağlandığının garanti edilmesidir.

Daimi mıknatıslı senkron motor bu uygulamada çamaşır makinesinin tamburunun hız kontrolünü yapmak amacıyla kullanılmaktadır. Çamaşır makinesi gerek çalışma hız aralığının genişliği, gerek güç ihtiyacının büyük olması, gerekse çamaşır yükünün bilinmezliği nedeniyle tüm beyaz eşya uygulamalarındaki en kapsamlı motor kontrol problemidir. Çamaşır makinesinin tamburuna atılacak çamaşır yükü miktarı fiziksel olarak sınırlanmış olsa da çok geniş bir aralıkta değişebilmektedir. Çamaşır yüküne ve tambura alınan su miktarına bağlı olarak yük momenti ve tamburun eylemsizlik momenti geniş bir aralıkta değişmektedir. Bu büyüklükler makinenin çalışma hızına göre de farklılaşmaktadır. Düşük hızlarda çamaşır sürekli tambura çarparak belirli bir profilde yük momenti uygularken, yüksek hızlarda tamburun çepere yapışması nedeniyle tamburun eylemsizlik momenti değişmektedir. Ayrıca, bazı durumlarda çamaşırın tambur içinde çepere homojen bir şekilde dağılmamasından ötürü dengesiz yük oluşmakta, hem motor milinin gördüğü toplam eylemsizlik momenti hem de yük momenti çamaşırın konumuna bağlı olarak değişebilmektedir. Ayrıca, alan zayıflatma bölgelerinde hava aralığı akısı değiştiği için motorun moment sabiti de değişecektir. Dolayısı ile hız kontrol çevriminin bozucu bastırma performansının yüksek ve değişken eylemsizlik momenti, sürtünme katsayını ve moment sabitine karşı dayanıklı olması gerekmektedir.

Motorun elektriksel modeli göz önünde bulundurulursa motor sargı direnci ve endüktansı kapalı çevrim karakteristik polinomunun katsayılarını belirler. Motorun çalışma süresine ve çekilen akım miktarına bağlı olarak sargı direnci değişim göstermektedir. Ayrıca, endüktans değerleri akımın büyüklüğüne bağlı olarak değişmekte, yüksek akım çekildiğinde doymaya girebilmektedirler. Motorun akım çevrimi iki giriş ve iki çıkışlı sistem olarak modellenebilir. Farklı eksenler üzerindeki akımlar birbirlerine açısal hızla orantılı şekilde bağlıdırlar. Yüksek hızlara çıkıldığında bu etki kuvvetlendiği için kararlılığı garanti etmek amacıyla bu eksen takımları birbirlerinden ayrıştırılmıştır.

Gözleyici matematiksel modelinde açısal hız değişkeni değişken parametre olarak ele alınmıştır. Motorun çalışma hızı aralığı saat yönü ve saat yönünün tersinde yönde geniş bir aralığı kapsadığı için her koşulda kararlılığı garanti eden bir yöntem önerilmiştir.

Matematiksel modeldeki belirsizlikler parametrik belirsizlik yaklaşımıyla ele alınmıştır. Sistem parametrelerinin belirli aralıklarda değiştiği varsayılmış ve kapalı çevrime ilişkin kutup saçınımını en aza indirmek amacıyla dayanıklı tasarım yaklaşımı benimsenmiştir. Bu amaçla, gerek kapalı çevrim karakteristik polinomunun sınıfına bağlı olmaması gerekse tasarım sonucunda ortaya çıkan kontrolörün statik olması nedeniyle kutup renklendirme yöntemi kullanılmıştır. Bu yaklaşımla her bir kutup için dayanıklılıkla ilişkili ayrı maliyet fonksiyonları tanımlanmış ve tasarımda bu maliyet fonksiyonları minimize edilmiştir. Modellenmeyen dinamiklere ilişkin belirsizlikler bu tez kapsamında ele alınmamıştır.

Kutup renklendirme yöntemi, kullanılan kontrol yapısının serbestlik derecesini dayanıklılık kriterini sağlamak amacıyla kullanmaktadır. Bu amaçla dayanıklı kontrol problemi optimizasyon problemine dönüştürülmektedir. Yöntemin en büyük dezavantajı tasarım sürecinde yüksek matematiksel işlem gerektirmesidir. Ancak, tüm matematiksel işlemler gelişmiş tasarım ortamlarında yapılmakta, mikrodenetleyiciye

yazılan kontrol kodunda herhangi bir işlem yapılmamaktadır. Kontrolörlerin statik olması bu yöntemi parametrik belirsizlikleri olan sistemlerde kullanılabilecek uyarlamalı kontrol yöntemlerine göre en büyük avantajlarından biridir.

Bu amaçla dayanıklı bir gözleyici yapısı olan PI gözleyicisi tasarlanmış ve gerçeklenmiştir. PI gözleyicisi integratör terimi sayesinde hatanın geçmişteki değerlerini de geri besleme olarak kullandığı için modele etkiyecek farklı bozucu etkilere karşı dayanıklılık sağlamaktadır. Ayrıca, PI gözleyicisinin tasarımda sağladığı serbestlik kutup renklendirme yöntemi sayesinde dayanıklı kutup atama problemini çözmek için kullanılmıştır. Bu modelde bilinmeyen giriş olan ters elektromotor kuvveti kestirilmiştir. Gerçek rotor eksen takımı ile gözleyicinin gerçeklendiği eksen takımı arasındaki konum hatası bilgisi ters elektromotor kuvvet yardımıyla kestirilmiş ve açı takip gözleyici ile kompanze edilmiştir. Açı takip gözleyicisi yardımıyla rotor hızı ve konumu kestirilmiştir.

Hız kontrolörü olarak geleneksel yaklaşım olan PI kontrolör yerine PI-P yapısı tercih edilmiş, farklı yük ve hız koşullarında doğrulama yapılmıştır. PI-P kontrolör yapısı hem bozucu bastırma performansının PI kontrolöre göre daha yüksek olması hem de kutup renklendirme yönteminde kullanılmak üzere optimize edilebilecek fazladan bir parametre içermesi nedeniyle performans kriterlerini daha kolay sağlamıştır.

Akım kontrolörleri olarak dayanıklı PI yapıları tercih edilmiştir. Moment ve akı ile ilişkili eksenlerdeki akımlar arasında var olan kuplaj etkisini ortadan kaldırmak için uygun bir ayrıştırıcı yapısı önerilmiştir. Direnç ve endüktans değerlerinin değişimi göz önünde bulundurularak dayanıklı tasarım gerçeklenmiştir.

Konum sensörsüz kontrol uygulamalarında kestirilen büyüklüklerin düşük hızlarda çok fazla bozucu etkilere maruz kalması ve modellenmeyen dinamiklerden çok etkilenmesi nedeniyle problem teşkil eden değişken yüklerde başarılı bir kalkış gerçekleştirmek için özgün bir kalkış algoritması önerilmiştir. Özgün kalkış algoritması geleneksel çözümde olduğu gibi kalkış durumunda gözleyiciyi devre dışında bırakma yaklaşımının aksine, gözleyiciden belirli oranda yararlanarak kalkış profilini değiştirmektedir. Bu sayede çamaşır yüküne bağlı olarak kalkış profilinin değiştirilmesi ve belirli bir hıza kadar rotor konumu kestirilememesine rağmen motorun kritik hız seviyesine en az konum hatasıyla girmesi sağlanmıştır. Ayrıca makinanın tamburu yüksek hızlara çıkmadan evvel tambur içindeki dengesiz yükü ölçmek amacıyla dengesiz yük algılama algoritması önerilmiştir.

Yüksek hız koşullarında çalışma için alan zayıflatma algoritması gerçeklenmiştir. Bu sayede çamaşır makinesi her iki yönde maksimum hızda kararlı bir şekilde çalışabilmiştir. Tasarım, simülasyon ve deneysel sonuçlar tezde sunulmuştur. Tez kapsamında parametrik belirsizlikler altında konum sensörsüz DMSM kontrolü problemi için farklı bir yöntem önerilmiştir.

İlk defa endüstriyel bir uygulama çerçevesinde DMSM kontrolünde jutup renklendirme metodu kullanılmıştır. Ayrıca, basit yapılı ve dayanıklı PI gözleyici yapısı konum sensörsüz kontrol probleminde ters elektromotor kuvvetleri kestirmek için kullanılmıştır. Özgün bir kalkış algoritması önerilmiş ve farklı yük koşullarında yöntemin geçerliliği test edilmiştir.

1. INTRODUCTION

1.1 Purpose of The Thesis

The purpose of the thesis is to design a closed loop system in order to control the speed of the washing machine drum over wide speed range under parametric uncertainties without using a rotor position sensor. The controllers and observers are required to have simple structures which are applicable by using a low cost microcontroller. In order to solve rotor position sensorless startup problem, a novel startup algorithm is proposed. Validity of the design is proven by simulations and implementation.

1.2 Literature Review

In the last decade, great efforts have been made in the field of the position sensorless control of AC machines. The drive system is most commonly called as "sensorless drive" ambiguously in the literature despite the fact that the speed control system still include current sensors. In order to be consistent, these drive systems are called as "position sensorless drives" through this study.

Scaler control of AC machines show satisfying performance in the steady-state. Simple structure make it a valid control methods for many applications [1]. However, when it comes to high performance motor control application, field oriented control is a superior technique. The purpose of the field oriented control is to make real time control of torque, speed and phase currents not only in steady state but also during transients [2]. By decomposing the magnetic field and torque related components of the stator current vector, AC machine can be turned into a easily controllable DC machine in a sense [3]. The cost of achieving high performance control of AC machine is the necessity of rotor flux position information. This information can be obtained by a sensor which is vulnerable to the noise, vibrations and temperature variations. So the main purpose of the position sensorless drive is to eliminate the sensor in order to increase the robustness and reliability while reducing the hardware complexity and cost.

PMSMs are widely used in many industrial systems. The reason of absorbing too much attention by PMSM are their high torque/volume ratio, hign energy efficiency and reliable operation. Depending on the arrangements of the permanent magnets in the rotor, motor type can be classified in two categories; Surface mounted PMSM (SPMSM) and interior magnet PMSM (IPMSM). permanent magnets of the SPMSM are placed on in the rotor homogeneously so that the air gap does not depend on the rotor position. These machines uses only the excitation torque to produce mechanical power. IPMSM on the other hand uses both excitation and reluctance torque due to their saliency of the rotor structure. In this study, IPMSM motor drive is covered.

1.2.1 Sensorless speed control of IPMSM

The absence of the position sensor information leads the researchers to drive it from the mathematical model.There are two main stream in estimating the rotor position which are back electromotive force based models are stator flux based models. The rotating PM induces voltage in the stator windings depending on the speed and the position of the rotor position. Also, the magnetic flux is related to the speed and position as well. So, the mathematical model can be derived considering these values as states in order to obtain position information [4].

1.2.1.1 State estimation

The problem of the position estimation is moved to the state estimation area by relating the BEMF of flux values with the rotor position. Many researches have been done by focusing on different aspect of the control problem [5]. The methods that have been used can be crudely categorized as follows;

- Model Reference Adaptive Systems
- Luenberger Observer (Full or reduced order)
- Sliding Mode Observer
- Kalman Filter

The main idea of the MRAS is to use a desired mathematical model (Reference) besides an adaptive model which adapt the reference model [6]. The block diagram

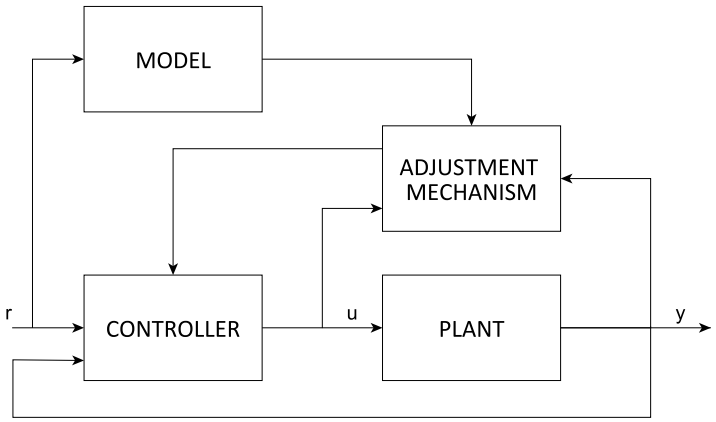

Figure 1.1 : Block Diagram of MRAS

of the MRAS is given in Figure 1.1. Full order state observer uses the measurable states (current) in order to estimate the measurable and unmeasurable states (BEMF, Flux etc.) by evaluating the error between motor mathematical model output and the measured currents [7]. Block representation is given in Figure 1.2. In reduced order observer, it is sufficient to design an observer for the partial states (unmeasurable states). The main problem of using Luenberger observer is its poor performance against disturbances and parametric uncertainties which are very critical in wide speed range control of AC machines. These requirements directed the researchers to use more robust topologies. The sliding mode observer is one of the most popular observers

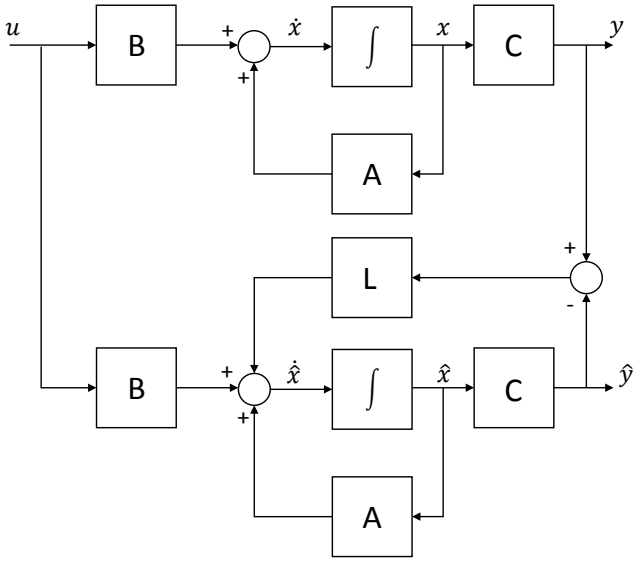

Figure 1.2 : Block Diagram of Luenberger Observer

among the position sensorless applications due to its easily implementable nature and robustness. Instead of using linear value as correction term (see Figure 1.3), sliding

mode observer uses a nonlinear switching function [6]. The chattering and the phase lag problems of the SMO are the main drawbacks [8]. Furthermore, calculation of the gains to ensure the convergence can be complex. The structure of the Kalman

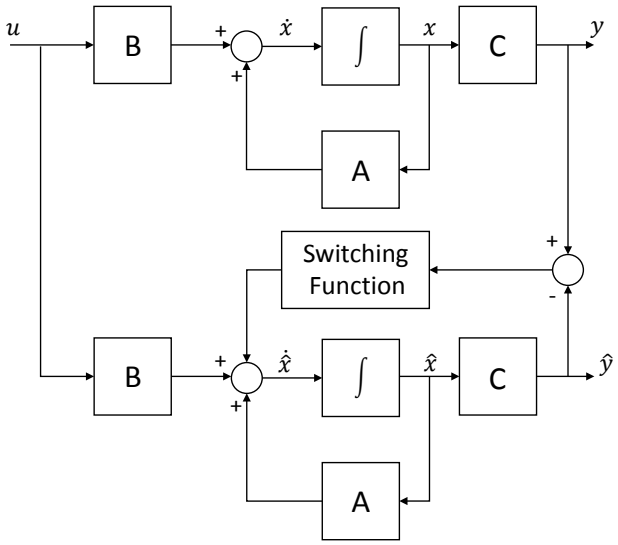

Figure 1.3 : Block Diagram of Sliding Mode Observer

filter is similar to the Luenberger observer. The main difference is the selection of the gain matrix which ensures the optimum state estimation of a quadratic quality criterion in linear case [6, 7]. Extended Kalman filter is widely used for estimating states of the nonlinear mathematical model of PMSM. The difficulty lies on the selection of the covariance matrices. Furthermore, sensitivity to the PM flux linkage and computationally extensive nature are main drawbacks of the EKF. Block diagram is given in Figure 1.4. Besides the methods mentioned above, there are different

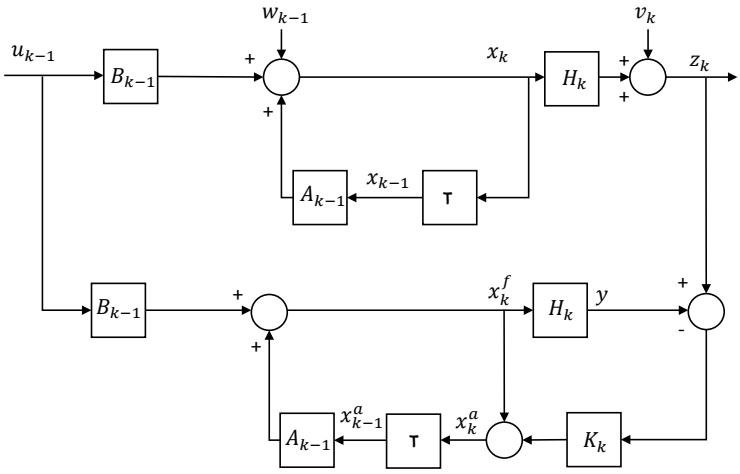

Figure 1.4 : Block Diagram of Kalman Filter

methods that are seldomly applied to the position sensorless problem such as artificial intelligence based methods and high frequency signal injection [7]. Computationally extensive nature of the artificial neural network is one of the drawbacks. Also there is no guideline to select the number of hidden layers in advance. HF injection method relates the saliency of the rotor with the rotor position. However, the noise reaches significant levels and it is required that the useful signal must be separated from the noise by using proper signal processing.

1.2.1.2 Wide speed range control

The speed control problem of an PMSM requires the control of torque and current components together. When it comes to wide speed range control, field weakening algorithm is a must due to the limitation of the stator voltage vector limitation. Field weakening requires the control of both torque and magnetic field related currents together. The mathematical model of PMSM shows that there are couplings between these two axes which are functions of speed. In order to achieve high performance drive these issues have to be handled properly.

Many methods have been suggested for the speed control from classical PID control to sliding mode control [9]. Although, some methods such as disturbance observer based techniques have been proposed in order to achieve robust solutions [10], the problem have been seldomly threatened as systems with parametric uncertainties. Some attempts have been done for induction machine using Kharitonov theorem [11]. Many robust topologies have been proposed for the current loop [12, 13]. Unfortunately, many of them require complex control structures and include computationally extensive design procedure.

1.2.2 Parametric uncertainties related to the control system

The field oriented control of PMSM includes many uncertainties especially in the case of wide speed range control. Influence of the parameter variations became a topic of many research [14–16]. Some of them focused on the BEMF based observer techniques [17, 18], which are the case of this study.

Parametric uncertainties related to the system can be listed as follows;

- Variations in winding resistance due to the temperature variations,

- Variations in the inductance values due to the saturations,
- Variations in the permanent magnet flux due to demagnetization and temperature,
- Variation of the moment of inertia and friction coefficient due to unknown load and changing speed,
- Variation of the torque constant due to field weakening operation
- Variation of the angular velocity if it is considered as a changing parameter in the observer model

In order to handle these uncertainties one may consider either adaptive structures or the robust approaches. In these study, controllers and the observer have been designed in a robust manner.

1.3 Hypothesis

The assumptions have been made during the design have been presented here. During the mathematical modeling following assumptions have been made;

- Stator windings produce sinusoidal MMF distribution. Space harmonics in the air-gap are neglected.
- Air-gap reluctance has a constant component as well as a sinusoidal varying component.
- Three phase sinusoidal voltage is balanced.
- Hysteresis and Eddy currents are omitted.
- Back electromotive force is limited within operational speed range and.
- Back electromotive force dynamics is sufficiently slow compared to the current dynamics.

Robust controllers and observer have been designed by considering the following assumptions;

- The uncertainties of the control system are structured and modeled as parametric uncertainties.
- The uncertain parameters are assumed to be changed between their maximum and minimum boundaries.
- Uncertainties related to unmodelled dynamics (inverter nonlinearities, measurement errors of current sensors etc.) are omitted.

1.4 Organization of the Thesis

The mathematical model of the IPMSM is given in Chapter 2. Mathematical model is represented in different reference frames. Control strategy, field weakening operation and parametric uncertainties are given in this chapter.

Chapter 3 is denoted to the PI observer design. Mathematical model and the design procedure is presented in this chapter. Pole coloring concept which is used for designing both observer and controllers, is also presented in this chapter. Angle tracking observer design have been carried out in this chapter.

Robust current controller designs have been presented in Chapter 4. Open loop decoupling and d-q axes current controllers have been carried out in this chapter.

Robust speed controller design have been explained in Chapter 5. Comparison between PI and PI-P structures have been presented.

Novel rotor position sensorless startup algorithm have been proposed in Chapter 6. Problem statement have been presented and the solution is explained in this chapter.

Field weakening algorithm which is used for high speed operations have been presented in Chapter 7. Unbalanced load detection algorithm is also presented here.

Experimental results and simulations have been presented in Chapter 8. Validation of the design is proven implementing the design in the real system and results related to the different operational conditions have been presented here.

Finally, conclusion is given in Chapter 9. Main results have been summarized and further works have been proposed.

2. MATHEMATICAL MODEL OF IPMSM

Interior magnet synchronous motor has a permanent magnet in the rotor creating a magnetic field. Three phase windings are placed in the stator such a way that corresponding currents have 120^o phase lag between each other. Structure of IPMSM is shown in Figure 2.1. Due to the Faraday's law, changing magnetic field induces

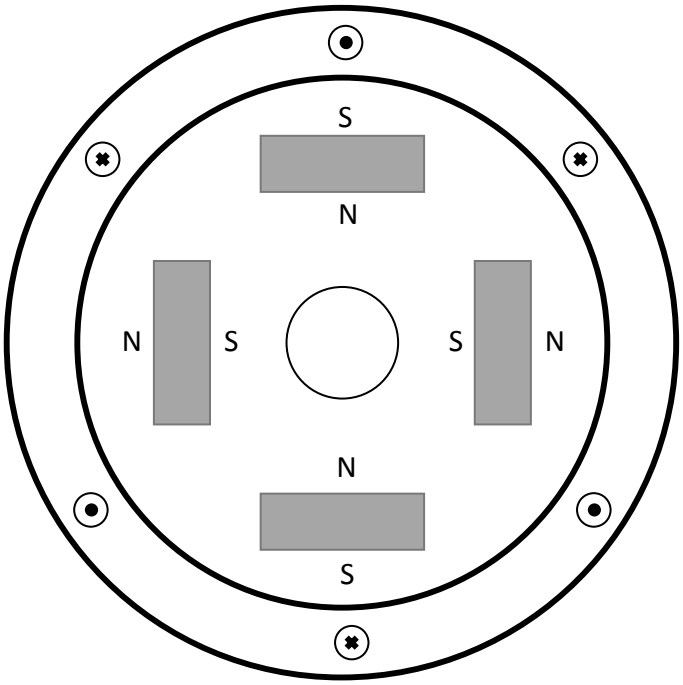

Figure 2.1 : IPMSM Structure

voltage. Correspondingly, rotating permanent magnet induces voltage which is called back electromotive force (BEMF) in the stator windings. Stator wingding has its own ohmic resistance and inductance due to the coils formed by the windings. By using these facts, equivalent circuit of a single phase can be modeled as follows; Through the mathematical model derivation following assumptions have been made;

- Stator windings produce sinusoidal MMF distribution. Space harmonics in the air-gap are neglected.
- Air-gap reluctance has a constant component as well as a sinusoidal varying component.

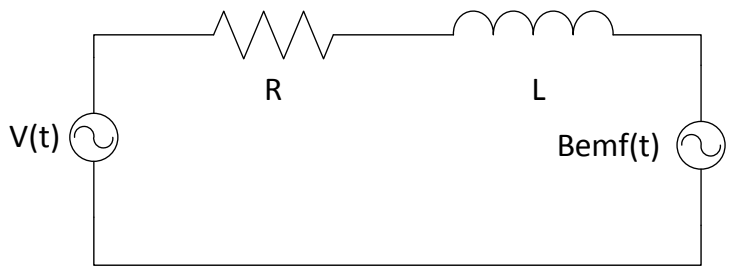

Figure 2.2 : Single Phase Equivalent Circuit

- Three phase sinusoidal voltage is balanced.
- Hysteresis and Eddy currents are omitted.

By applying Faraday's law to equivalent circuit in Figure 2.2, three phase equations have been obtained as follows;

$$v_u(t) = R_u i_u(t) + L_u \frac{di_u(t)}{dt} + E_u(t) \tag{2.1}$$

$$v_v(t) = R_v i_v(t) + L_v \frac{di_v(t)}{dt} + E_v(t) \tag{2.2}$$

$$v_w(t) = R_w i_w(t) + L_w \frac{di_w(t)}{dt} + E_w(t) \tag{2.3}$$

where $E(t)$ is the induced back electromotive force. For the sake of simplicity, time dependences are not going to be expressed in the equations explicitly unless otherwise is stated. Time derivative of the stator flux linkage corresponds BEMF due to the Faraday's law. The flux linkage of the each phase is given below;

$$\Psi_u^s = L_u i_u + \Psi_u^{PM} \tag{2.4}$$

$$\Psi_v^s = L_v i_v + \Psi_v^{PM} \tag{2.5}$$

$$\Psi_w^s = L_w i_w + \Psi_w^{PM} \tag{2.6}$$

By reevaluating the equations (2.1) and (2.4) together following form is obtained;

$$v_u = i_u + \frac{\Psi_u^s}{dt} \tag{2.7}$$

$$v_v = i_v + \frac{\Psi_v^s}{dt} \tag{2.8}$$

$$v_w = i_w + \frac{\Psi_w^s}{dt} \tag{2.9}$$

Equation (2.7) is the most general form of any alternating current machine. Any AC machine mathematical model can be derived from these equations .

The sum of instantaneous values of three phase signals would give 0 as shown in equation(2.11).

$$0 = v_u + v_v + v_w \tag{2.10}$$

$$0 = i_u + i_v + i_w \tag{2.11}$$

This result suggest that only the 2 component is needed in order to represent three phase quantities. Actually 2 phase symmetric windings (90^o phase lag between each other) can produce a rotating magnetic field as in the case of three phase machine.

2.1 Alpha-Beta Reference Frame

The Clarke transform is converts balanced three phase quantities into balanced two phase quantities. The Clarke transformation matrix is given below;

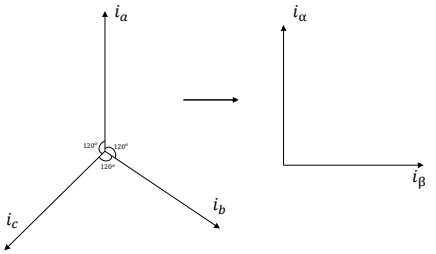

Figure 2.3 : α-β Reference Frame

$$\begin{bmatrix} f_\alpha \\ f_\beta \end{bmatrix} = \begin{bmatrix} 1 & -\frac{1}{2} & -\frac{1}{2} \\ 0 & \frac{\sqrt{3}}{2} & -\frac{\sqrt{3}}{2} \end{bmatrix} \begin{bmatrix} f_a \\ f_b \\ f_c \end{bmatrix} \tag{2.12}$$

By applying Clarke transformation to the equation (2.7), model in $\alpha - \beta$ reference frame can be obtained as follows;

$$\begin{bmatrix} v_\alpha \\ v_\beta \end{bmatrix} = \begin{bmatrix} R_a + p(L_0 + L_1 cos2\theta_e) & pL_1 sin2\theta_e \\ pL_1 sin2\theta_e & R_a + p(L_0 - L_1 cos2\theta_e) \end{bmatrix} \begin{bmatrix} i_\alpha \\ i_\beta \end{bmatrix} + \omega_e \Psi_{PM} \begin{bmatrix} -sin\theta_e \\ cos\theta_e \end{bmatrix} \tag{2.13}$$

i_α, i_β	α and β axes armature currents
v_α, v_β	α and β axes stator voltages
ω_e	electrical angular velocity of the rotor
θ_e	electrical angular position of the rotor
R_a	armature resistance
Ψ_{PM}	magnet flux linkage

$$L_0 = \frac{L_d + L_q}{2}, \quad L_1 = \frac{L_d - L_q}{2} \tag{2.14}$$

L_d and L_q are the d and q axes inductances and p is the differential operator. The rotor position information appears explicitly in the state matrix and disturbance matrix. During the construction of the observer it is required that only the BEMF or flux component include the rotor position information. Especially when the L_d and L_q inductances are different which is the case in IPMSM, mathematical expressions get complicated. Also, the mathematical model in $\alpha - \beta$ reference frame has no significant advantage from the controller point of view. Torque and flux related terms are not explicitly shown in this model. However, this reference frame still useful in constructing space vector modulation and DC bus ripple elimination algorithms. Also, $\alpha - \beta$ reference frame can be used for observer model with some modifications as in [19–21].

2.2 D-Q Reference Frame

Up to now, mathematical model is represented in stationary reference frames. Thus, voltage and current values are time varying due to changing magnetic field caused by the rotor movement. If the model is constructed from the rotor point of view, simpler and more useful mathematical model can be obtained. If the equations are represented in rotating reference frame, time varying AC components would turn into DC components. Park transform given in equation (2.15) is used to express the stationary reference frame values in rotating reference frame.

$$\begin{bmatrix} f_d \\ f_q \end{bmatrix} = \begin{bmatrix} cos(\theta_e) & sin(\theta_e) \\ -sin(\theta_e) & cos(\theta_e) \end{bmatrix} \begin{bmatrix} f_\alpha \\ f_\beta \end{bmatrix} \tag{2.15}$$

The IPMSM mathematical model is represented in d-q reference frame as shown in equation (2.16).

$$\begin{bmatrix} v_d \\ v_q \end{bmatrix} = \begin{bmatrix} R_a + p(L_d) & -\omega_e L_q \\ \omega_e L_d & R_a + p(L_d) \end{bmatrix} \begin{bmatrix} i_d \\ i_q \end{bmatrix} + \begin{bmatrix} 0 \\ \omega_e \Psi_{PM} \end{bmatrix} \tag{2.16}$$

where i_d and i_q are the d-q axes armature currents and v_d and v_q are the d-q axes stator voltages. Relationship of the $\alpha - \beta$ and $d - q$ reference frames is given in Figure 2.4. The main advantage of the $d - q$ reference frame representation is relating current components with the torque and flux linkage. Also, the currents and voltages in $d - q$ reference frame are not sinusoidal. The position dependencies of the parameters in the state matrix is not the case here. Torque equation is given below;

$$T_e = \frac{3}{2} Z_p [\Psi_{PM} + (L_d - L_q) i_d] i_q \tag{2.17}$$

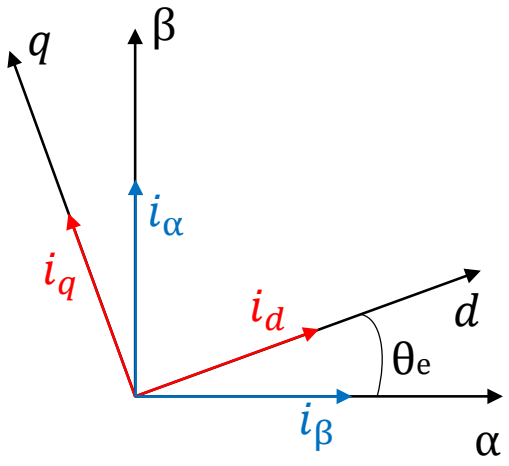

Figure 2.4 : $\alpha - \beta$ and $d - q$ Reference Frames

where Z_p is the number of pole pairs. In the d-q reference frame model q axis component of the current is related to the produced torque while d axis component is related to the flux linkage. Meaning of the currents is much more informative about the physical expressions than the model in $\alpha - \beta$ reference frame. The equivalent circuit in d-q reference frame is given in Figure 2.5. The state space representation of

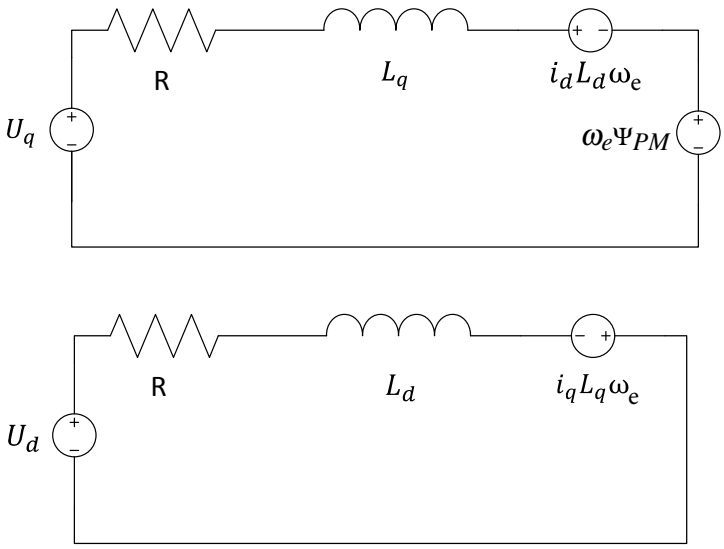

Figure 2.5 : Equivalent Circuit in $d - q$ Reference Frame

the system is given below;

$$\frac{d\mathbf{i_s}}{dt} = \mathbf{A}\mathbf{i_s} + \mathbf{B}\mathbf{u_s} + \mathbf{N}\mathbf{i_s}\omega_e + \mathbf{S}\psi_{PM}\omega_e \tag{2.18}$$

$$\mathbf{A} = \begin{bmatrix} -\frac{R}{L_d} & 0 \\ 0 & -\frac{R}{L_q} \end{bmatrix}; \mathbf{B} = \begin{bmatrix} \frac{1}{L_d} & 0 \\ 0 & \frac{1}{L_q}; \end{bmatrix}; \mathbf{N} = \begin{bmatrix} 0 & \frac{L_q}{L_d} \\ -\frac{L_d}{L_q} & 0 \end{bmatrix}; \mathbf{S} = \begin{bmatrix} 0 \\ -\frac{1}{L_q} \end{bmatrix} \tag{2.19}$$

where, **A** is system matrix, **B** is the input matrix, **N** is the nonlinear coupling matrix and **S** is the disturbance matrix. The block representation is givin in Figure 2.6. The

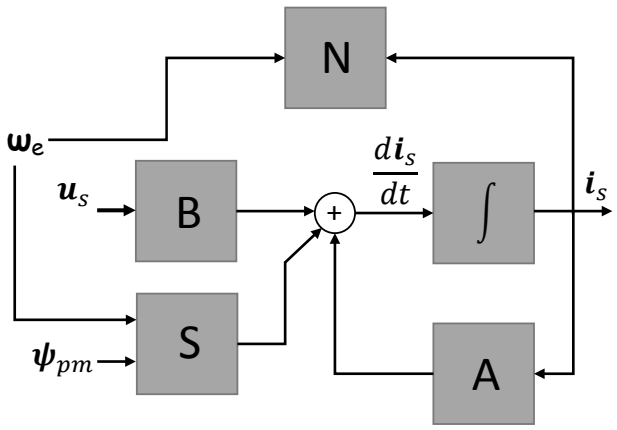

Figure 2.6 : Continuous Model of IPMSM in d-q Reference Frame

mathematical model is 2^{nd} order and the model shows bilinear characteristic due to term **N** which shows the multiplicative couplings between the input (ω) and the states (i_q and i_d).

2.3 Extended BEMF Model

The mathematical model in equation (2.16) is useful for control purpose. However, position estimation cannot be carried out by using this model due to the absence of the position information. If the rotating imaginary reference frame (γ-δ reference frame) which lags by θ_{error} from the d-q reference frame, is created position information can be obtained.

$$\begin{bmatrix} v_\gamma \\ v_\delta \end{bmatrix} = \begin{bmatrix} R_a + pL_d & -\omega_e L_q \\ \omega_e L_d & R_a + pL_q \end{bmatrix} \begin{bmatrix} i_\gamma \\ i_\delta \end{bmatrix} + \begin{bmatrix} \varepsilon_\gamma \\ \varepsilon_\delta \end{bmatrix} \tag{2.20}$$

where

$$\begin{bmatrix} \varepsilon_\gamma \\ \varepsilon_\delta \end{bmatrix} = \omega_e \psi_{pm} \begin{bmatrix} -sin\theta_{error} \\ cos\theta_{error} \end{bmatrix} + \mathbf{L_a} p \begin{bmatrix} i_\gamma \\ i_\delta \end{bmatrix} + \omega_e \mathbf{L_b} \begin{bmatrix} i_\gamma \\ i_\delta \end{bmatrix} + (\hat{\omega}_e - \omega_e)\mathbf{L_c} \begin{bmatrix} i_\gamma \\ i_\delta \end{bmatrix} \tag{2.21}$$

Although the position information appears in the imaginary BEMF terms, L_a, L_b and L_c matrices are also position dependent [22]. It is a computationally extensive duty to drag the position information from this complex model.

Equation (2.16) can be rewritten as follows [22];

$$\begin{bmatrix} v_d \\ v_q \end{bmatrix} = \begin{bmatrix} R_a + pL_d & -\omega_e L_q \\ \omega_e L_q & R_a + pL_d \end{bmatrix} \begin{bmatrix} i_d \\ i_q \end{bmatrix} + \begin{bmatrix} 0 \\ E_{ex} \end{bmatrix} \tag{2.22}$$

where

$$E_{ex} = \omega_e[(L_d - L_q)i_d + \psi_{pm}] - (L_d - L_q)(pi_q) \tag{2.23}$$

The term E_{ex} is called extended BEMF. By transforming this model into $\gamma - \delta$ reference frame observer model can be obtained as follow;

$$\begin{bmatrix} v_\gamma \\ v_\delta \end{bmatrix} = \begin{bmatrix} R_a + pL_d & -\omega_e L_q \\ \omega_e L_q & R_a + pL_d \end{bmatrix} \begin{bmatrix} i_\gamma \\ i_\delta \end{bmatrix} + \begin{bmatrix} e_\gamma \\ e_\delta \end{bmatrix} \tag{2.24}$$

where

$$\begin{bmatrix} e_\gamma \\ e_\delta \end{bmatrix} = E_{ex} \begin{bmatrix} -sin\theta_{error} \\ cos\theta_{error} \end{bmatrix} + (\hat{\omega}_e - \omega_e)L_d \begin{bmatrix} -i_\gamma \\ i_\delta \end{bmatrix} \tag{2.25}$$

The model in equation (2.24) is very simple compared to the model in equation (2.21). Also, extended BEMF term is the only term contains the position information. By taking the inverse tangent of e_γ and e_δ position information can be obtained.

2.4 Control Strategy of The IPMSM

According to the equation (2.17), if the i_d current is kept constant, it it obvious that electromechanical torque is proportional with the i_q current. So, it is possible to control the torque by changing q axis current. Also, torque constant can be adjusted by controlling the d axis current. This freedom is going to be used in field weakening operation. In order to control the speed, a speed controller have been utilized. Control signal of the speed controller has been fed to the current controller on the q axis. Control signal of the current controllers (both d and q axes) have formed the stator voltage. By applying inverse park transform, $\alpha - \beta$ components of the stator voltage have been obtained. These voltages is useful by deciding th stator current sector which is needed by the space vector modulation. Space vector modulation determines the switching sequence and drives the three phase inverter. Inverse Clarke transform has been used for obtaining three phase voltages.

In order to gain feedback information, three current sensor have been used. By applying Clarke and Park transformations, variables that are needed by controllers have been obtained. Extended BEMF based observer runs in the imaginary $\gamma - \delta$ reference frame and estimates the extended BEMF states. By using a angle tracking observer position estimation error, θ_{error}, have been compensated. Speed and position of the rotor shaft have been estimated by angle tracking observer. Block diagram of the control schema is given in Figure 2.7.

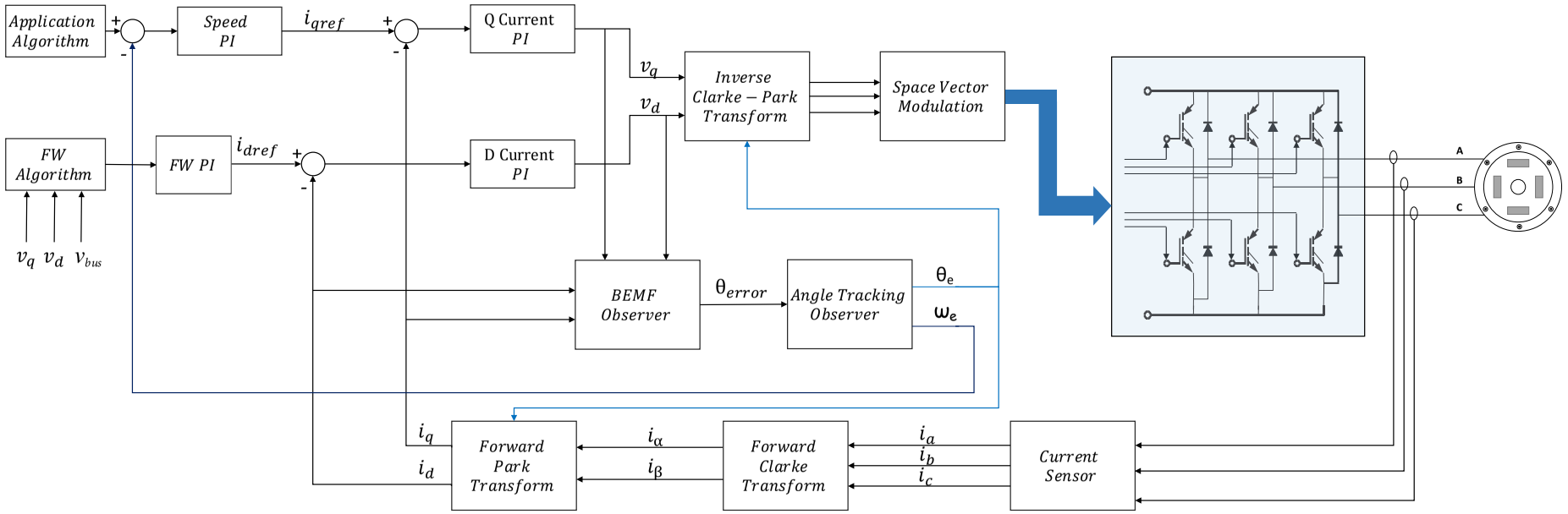

Figure 2.7 : Total Control Schema of The Control System

2.5 Field Weakening Operation

Once the motor reaches rated speed, the BEMF voltage reaches the maximum available terminal voltage. As the speed increases, torque drops rapidly. To overcome this problem and increase the operating speed above rated speed, demagnetizing current (d axis current) is increased in order to reduce the air gap flux. The operation is called field weakening. Torque/power vs. speed characteristic of the IPMSM is shown in Figure 2.8. At the steady state, state equations become;

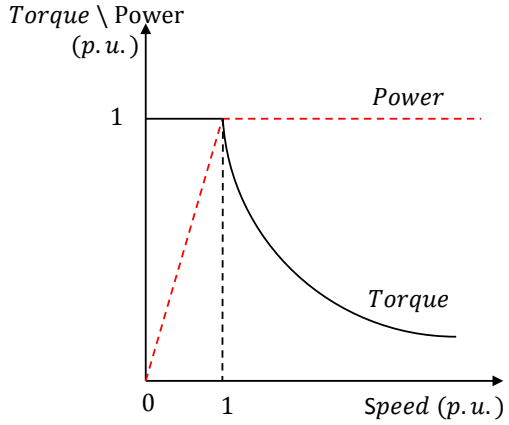

Figure 2.8 : Torque/Power vs. Speed Characteristic

$$v_d = Ri_d - \omega_e L_q i_q \tag{2.26}$$

$$v_q = Ri_q + \omega_e(L_d i_d + \psi_{pm}) \tag{2.27}$$

if the maximum speed is reached then $i_q = 0$ which yields;

$$v_d = Ri_d \tag{2.28}$$

$$v_q = \omega_{emax}(L_d i_d + \psi_{pm}) \tag{2.29}$$

$$v_{max}^2 = v_d^2 + v_q^2 = (Ri_d)^2 + \omega_{emax}^2(L_d i_d + \psi_{pm})^2 \tag{2.30}$$

Finally

$$\omega_{emax} = \frac{\sqrt{v_{max}^2 - (Ri_d)^2}}{L_d i_d + \psi_{pm}} \tag{2.31}$$

Obviously, i_d current can be adjusted in order to chance the maximum angular velocity. The i_d reference current have been obtained from another controller which is called field weakening controller. Detailed explanations of the field weakening algorithm is going to be presented in Chapter 7.

2.6 Parameter Uncertainties

The classical control theory assumes that the plant is perfectly modeled and controllers are designed without any error. However, this situation does not occur in practice. Due to the parameter changes, modeling errors (simplification, reductions etc.), measurement errors, disturbances, implementation errors and etc., closed loop system have many uncertainties. In this study, controllers and observer have been design by taking into account of uncertainties of the physical parameters. During the design procedure, parametric approach have been adopted. This paradigm allows to specify the parametric uncertainties exactly. The investigation of the effects of the different parameters is also possible. The resultant controllers are low ordered which makes the implementation easier. The drawback of this approach is that the procedures are computationally extensive and if there are any other kind of uncertainties in the system except for parametric uncertainties, results can be misleading. However, computationally extensive calculations have been made offline. So, there is no burden left to the microcontroller in which the control algorithm runs. Also, the main uncertainties of the position sensorless control system are parametric uncertainties. There may be other kind of uncertainties for examples concerning the inverter (actuator), however, it is effective at low speeds and can be compensated by using dead time compensation algorithm. So the assumptions have been made are;

- The uncertainties are structured
- The physical parameters take values between their maximum and minimum limits

The uncertain parameters are listed in Table 2.1.

Table 2.1 : Uncertain Parameters.

Parameter	Minimum Value	Maximum Value
k_t	0.6 $\frac{Nm}{A}$	0.65 $\frac{Nm}{A}$
L_d	10 mH	16.7 mH
L_q	20 mH	25 mH
R	3.15 Ω	4.5 Ω
ω_e	-6330 $\frac{rad}{s}$	6330 $\frac{rad}{s}$
J	0.0012 $kg \cdot m^2$	0.0024 $kg \cdot m^2$
B	0.00025$\frac{Nm \cdot s}{rad}$	0.00075$\frac{Nm \cdot s}{rad}$

3. SPEED ADAPTIVE PI OBSERVER DESIGN

3.1 Observer Model

In this part, the PI-Observer mathematical model is introduced [23]. For a class of systems described by

$$\hat{\dot{x}} = \mathbf{Ax(t)} + \mathbf{Bu}(t) + \mathbf{Nd}(\mathbf{x},t) + \mathbf{Eg}(\mathbf{x},t) \tag{3.1}$$

$$\mathbf{y}(t) = \mathbf{Cx}(t) \tag{3.2}$$

with the state vector $\mathbf{x}$(t) $\in \mathbb{R}^n$, the input vector $\mathbf{u}(t) \in \mathbb{R}^l$, the measurement vector $\mathbf{y}(t) \in \mathbb{R}^m$, the time variant and unknown inputs $\mathbf{d}(\mathbf{x},\mathbf{t}) \in \mathbb{R}^r$ and the unmodeled dynamics $\mathbf{Eg}(\mathbf{x},t)$ with $\mathbf{g}(\mathbf{x},t) \in \mathbb{R}^p$ and $\mathbf{E} \in \mathbb{R}^{nxp}$. The matrix $\mathbf{N}$ denoting the position of the unknown inputs effecting the system is assumed to be known. The purpose of the observer is to estimate the states and the unknown inputs which are going to be called as disturbances. Disturbances are assumed to be constant or slowly varying [24]. Extended system has been defined by

$$\begin{bmatrix} \dot{\mathbf{x}}(t) \\ \dot{\mathbf{d}}(t) \end{bmatrix} = \begin{bmatrix} \mathbf{A} & \mathbf{N} \\ 0 & 0 \end{bmatrix} \begin{bmatrix} \mathbf{x}(t) \\ \mathbf{d}(t) \end{bmatrix} + \begin{bmatrix} \mathbf{B} \\ \mathbf{0} \end{bmatrix} \mathbf{u}(t) + \begin{bmatrix} \mathbf{Eg}(t) \\ \mathbf{0} \end{bmatrix} \tag{3.3}$$

$$\mathbf{y}(t) = \begin{bmatrix} \mathbf{C} & \mathbf{0} \end{bmatrix} \begin{bmatrix} \mathbf{x}(t) \\ \mathbf{d}(t) \end{bmatrix} \tag{3.4}$$

The purpose of the PI observer is to estimate the states of the system described above robustly. The states $\mathbf{x}(t)$ and the disturbance $\mathbf{d}(t)$ can be estimated using the observer model below;

$$\begin{bmatrix} \dot{\hat{\mathbf{x}}} \\ \dot{\hat{\mathbf{d}}} \end{bmatrix} = \begin{bmatrix} \mathbf{A} & \mathbf{N} \\ \mathbf{0} & \mathbf{0} \end{bmatrix} \begin{bmatrix} \hat{\mathbf{x}} \\ \hat{\mathbf{d}} \end{bmatrix} + \begin{bmatrix} \mathbf{B} \\ \mathbf{0} \end{bmatrix} \mathbf{u}(t) + \begin{bmatrix} \mathbf{L_1} \\ \mathbf{L_2} \end{bmatrix} (\mathbf{y}(t) - \hat{\mathbf{y}}(t)) \tag{3.5}$$

$$\hat{\mathbf{y}}(t) = \begin{bmatrix} \mathbf{C} & \mathbf{0} \end{bmatrix} \begin{bmatrix} \hat{\mathbf{x}}(t) \\ \hat{\mathbf{d}}(t) \end{bmatrix} \tag{3.6}$$

By denoting the extended system matrix as $\mathbf{A_{ex}}$, input matrix as $\mathbf{B_{ex}}$, observer gains as $\mathbf{L_{ex}}$ and output matrix as $\mathbf{C_{ex}}$, observability can be determined by the observability

matrix Q.

$$\mathbf{Q} = \begin{bmatrix} \mathbf{C_{ex}} \\ \mathbf{C_{ex}}\ \mathbf{A_{ex}} \\ . \\ . \\ \mathbf{C_{ex}}\ \mathbf{A_{ex}^{n-1}} \end{bmatrix} \tag{3.7}$$

For the full observability, extended system A_{ex}, C_{ex} have to fulfill $Rank(Q) = n + r$.

3.1.1 Convergence of estimation errors

Considering the equations above, estimation errors have been defined as $\mathbf{e}(t) = \hat{\mathbf{x}}(t) - \mathbf{x}(t)$ and $\mathbf{f}(t) = \hat{\mathbf{d}}(t) - \mathbf{d}(t)$. Finally, error dynamics can be expressed as follows,

$$\begin{bmatrix} \dot{\mathbf{x}} \\ \dot{\mathbf{f}} \end{bmatrix} = \begin{bmatrix} \mathbf{A} - \mathbf{L_1 C} & \mathbf{N} \\ -\mathbf{L_2 C} & \mathbf{0} \end{bmatrix} \begin{bmatrix} \mathbf{e}(t) \\ \mathbf{f}(t) \end{bmatrix} - \begin{bmatrix} \mathbf{Eg}(\mathbf{x},t) \\ \dot{\mathbf{d}}(t) \end{bmatrix} \tag{3.8}$$

It is obvious that eigenvalues of the system matrix of error dynamics determine the convergence dynamics. Observer gains have to be chosen such a way that $\mathbf{e}(t) \to 0$ and $\mathbf{f} \to 0$ as $t \to \infty$ while minimizing the effect of the $\dot{\mathbf{d}}(t)$. Two requirement rise here;

- $Re(\lambda_i) < 0$, where λ_i are the all eigenvalues of A_{ex}
- $\|L_2\|_F >> \|L_1\|_F$

where $\|\cdot\|$ is the Frobenius norm, $\|A\|_F = \sqrt{trace(A^*A)}$. In the frequency domain, convergence the estimation error can be expressed as follows,

$$\mathbf{e}(s) = \mathbf{G^{-1}f(s)} - \mathbf{G^{-1}Eg(s)} \tag{3.9}$$

$$\mathbf{f}(s) = -[s\mathbf{I} + \mathbf{L_2 C G^{-1} N}]^{-1} s\mathbf{d}(s) + [s\mathbf{I} + \mathbf{L_2 C G^{-1} N}]^{-1} \mathbf{L_2 C G^{-1} Eg}(s) \tag{3.10}$$

where $\mathbf{G} = [s\mathbf{I} - \mathbf{A} - \mathbf{L_1 C} + \hat{\mathbf{N}}[s\mathbf{I}]^{-1}]$. The transfer function from $s\mathbf{d}(s)$ to $\mathbf{f}(s)$ must satisfy $\|[\mathbf{I}s + \mathbf{L_2 C G^{-1} N}]^{-1}\|_\infty \leq \gamma$, where $\gamma \to Minimum$ in order to minimize the effect of $\mathbf{d}$ on $\mathbf{f}$.

Observer model can be constructed by using permanent magnet synchronous motor model. Back EMF input has been considered as disturbance in this model.

Since the closed loop system is a digitally controlled system, mathematical model has to be constructed in the discrete domain. By denoting the sampling time as T, discrete model can be obtained as follows;

$$\begin{bmatrix} \dot{i_d} \\ \dot{i_q} \\ \dot{e_d} \\ \dot{e_q} \end{bmatrix} = \begin{bmatrix} 1-\frac{RT}{L_d} & \frac{L_qT\Omega_e}{L_d} & \frac{T}{L_d} & 0 \\ -\frac{L_qT\Omega_e}{L_d} & 1-\frac{RT}{L_d} & 0 & \frac{T}{L_d} \\ 0 & 0 & 1 & 0 \\ 0 & 0 & 0 & 1 \end{bmatrix} \begin{bmatrix} i_d \\ i_q \\ e_d \\ e_q \end{bmatrix} + \begin{bmatrix} \frac{T}{L_d} & 0 \\ 0 & \frac{T}{L_d} \\ 0 & 0 \\ 0 & 0 \end{bmatrix} \begin{bmatrix} v_d \\ v_q \end{bmatrix} \tag{3.11}$$

where $e_d = 0$.

State space mathematical model of the motor has been constructed in the d-q reference frame. However, observer model cannot be obtained in the same reference frame because of the unknown rotor position. So the observer model has been constructed in the rotating $\gamma - \delta$ reference frame.

$$\begin{bmatrix} \dot{i_\gamma} \\ \dot{i_\delta} \\ \dot{e_\gamma} \\ \dot{e_\delta} \end{bmatrix} = \begin{bmatrix} 1-\frac{RT}{L_d} & \frac{L_qT\Omega_e}{L_d} & \frac{T}{L_d} & 0 \\ -\frac{L_qT\Omega_e}{L_d} & 1-\frac{RT}{L_d} & 0 & \frac{T}{L_d} \\ 0 & 0 & 1 & 0 \\ 0 & 0 & 0 & 1 \end{bmatrix} \begin{bmatrix} i_\gamma \\ i_\delta \\ e_\gamma \\ e_\delta \end{bmatrix} + \begin{bmatrix} \frac{T}{L_d} & 0 \\ 0 & \frac{T}{L_d} \\ 0 & 0 \\ 0 & 0 \end{bmatrix} \begin{bmatrix} v_\gamma \\ v_\delta \end{bmatrix} + \begin{bmatrix} L_{11} & L_{12} \\ L_{13} & L_{14} \\ L_{21} & L_{22} \\ L_{23} & L_{24} \end{bmatrix} \begin{bmatrix} i_d - i_\gamma \\ i_q - i_\delta \end{bmatrix} \tag{3.12}$$

3.2 Design By Using Classical Pole Assignment Method

It is obvious that the back emf signals have relatively slow dynamics by comparison to the current dynamics. So the eigenvalues of the current error dynamics have to be closer to the origin than the eigenvalues of the back emf signals in the Z-Domain. Sampling period is $T = 50\mu s$ and the error dynamics of the current are required to be settled in 10 sampling period. Furthermore, the error dynamics of the back emf signals are required to be settled in $20ms$. Finally, suggested desired poles have been determined as follows;

$$Desired poles = [0.651 \quad 0.651 \quad 0.99 \quad 0.99] \tag{3.13}$$

The main problem here the presence of the angular velocity in the state matrix. Angular velocity is not constant and closed loop pole locations depend on the angular velocity. Eigenvalues of A matrix are given as follows.

$$\lambda = \frac{L_d - RT}{L_d} \pm i\frac{L_qT\Omega_e}{L_d} \tag{3.14}$$

As the ω chances between $[-6300 \quad 6300]\frac{rad}{s}$, imaginary part of the eigenvalues varies dramatically. One may consider to use a certain angular velocity value in order to make

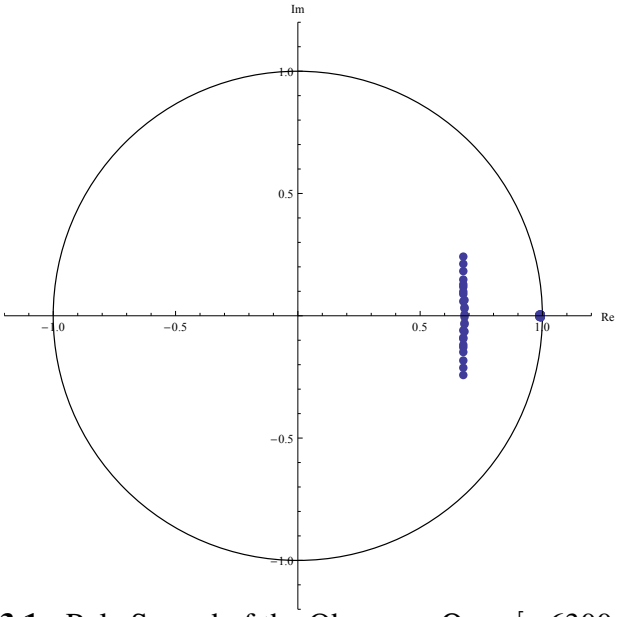

Figure 3.1 : Pole Spread of the Observer, $\Omega_e = [-6300 \quad 0]\ \frac{rad}{s}$

a pole assignment. However, when the operational speed of the motor is changed, closed loop pole locations vary and error dynamic of the observer can get unwillingly slower causing the violate the separation property of the closed loop system. The example design has been carried out by taking $\Omega_e = -4000\ \frac{rad}{s}$. As it can be seen in Figure 3.1, poles of the observer have been spread very large area causing the error dynamics of the estimated error get slower.

The observer gains have to be chosen such a way that the pole spread of the observer poles are restricted in a certain stability region called as D-region. Event the parameter have been perturbed, observer must fulfill certain convergence criteria. Solution is to consider the angular velocity as a parameter uncertainty with the bounds $[-6300 \quad 6300]\frac{rad}{s}$. The concept of pole colouring is going to be introduced in the next section.

3.3 Pole Colouring Concept

It is known that poles of closed loop system roughly define the closed loop system dynamic behavior besides stability. Although element zeros have effects on system dynamic behavior, they do not effect the stability. So, the design approach is finding controller in order to meet closed loop dynamic behavior requirements by considering the effects of closed loop zeros. Pole assignment problem can be defined as follows;

Design a gain matrix **K** such that

$$|sI-(A-BK)| = (s-p_1)(s-p_2)...(s-p_n) \tag{3.15}$$

where p_1,p_2...p_n are the desired closed loop poles. There are many pole assignment techniques in the literature [25, 26] and a crude classification can be made for state and output feedback cases as follows [27];

1) **Classical methods:** Transform system into one or several SISO or canonical forms and solve the equations involving determinants or characteristic polynomials [28], [25].

2) **Direct Methods:** Transform system into canonical forms using stable unitary matrices [29].

3) **Matrix Equation Methods:** Solve Sylvester-like matrix equations [30]

$$AX - X\Lambda = BG \tag{3.16}$$

with the feedback matrix $K = GX^{-1}$

4) **Eigenvector methods:** Select the closed loop eigenvectors x_j, the columns of the matrix X, from some admissible subspaces.

In linear feedback compensation, nominal mathematical model is used for designing controllers. However, there are many uncertainties related to the physical model in practice due to linearization error, changing in environment, modeling errors, changing operating conditions etc. Static controllers can perform satisfactory when the nominal plant is the case. However, when the uncertainties are included, it is possible that closed loop system poles can go unstable regions. Model uncertainty can be categorized into two types: parametric uncertainty, which represents the parameter variations in model and unstructured uncertainty, which represents the unmodeled effects. In this study, parametric uncertainties are concerned. Former description of an uncertain system is follows;

$$\dot{x} = A(q)x + B(q)u \tag{3.17}$$

$$y = C(q)x + D(q)u \tag{3.18}$$

where A, B, C and D are functions of the uncertainty vector **q**

$$q = [q_1 \quad q_2 ... q_n] \tag{3.19}$$

whose elements are interval parameters

$$q_i^- \leq q_i \leq q_i^+ \quad for(i = 1,2,...,n) \tag{3.20}$$

Robust control problem addresses to designing controller such a way that closed loop system behavior can satisfy predefined robustness requirements by considering the uncertainties. There are useful tools that can be used in analysis and design such that value set concept, however, it involves evaluation of the system for a range of frequency value which is not practical [28]. The generalized Kharitonov approach is also considered however it includes conservatisms for many classes of the systems [31]. Many attempts are made in order to move the problem to the optimization area.In [32] and [33], LQR technique is used to robust pole placement. Although, the method guarantees the robustness, it allows pole placement only in a specific region. In [34] and [35], different robustness measures are minimized via optimization. However, selecting the robustness measure is an issue and different robustness measures can not be assigned for different closed loop poles. Here, pole colouring concept [36] gives a powerful idea by using the freedom in the pole assignment problem in order to minimize cost functions which are defined for each nominal and perturbed pole pairs. Technique also gives an insight into problem by using only pole spread of the closed loop system.

Depending on the number of the poles,n, there are $n!$ possible paring options. Here there are 6 possible paring options (Figure 3.2) and it is reasonable to make the paring such that the distance between nominal and perturbed poles are minimum. Then the problem can be expressed as follows:

$$J_q = \min_{q=1,...n!} (\max_{i=1,..n} F_i) \tag{3.21}$$

where, n is the order of the closed loop system and F_i is the robustness assesment function. Since the number of permutation is increased as the order of the closed loop system is increased, a suitable algorithm has to be used in order to obtain fast pairing. Linear bottleneck assignment problem is addressed here [37]. A simple cost function

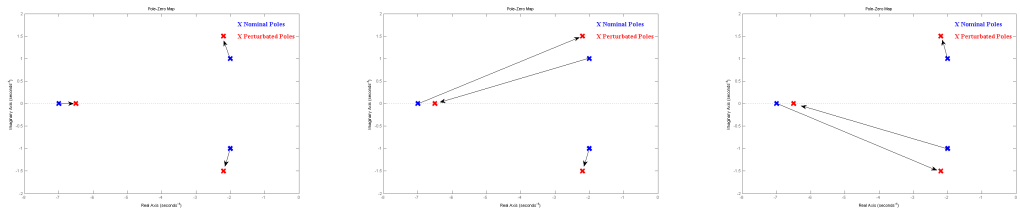

(a) Case 1 (b) Case 2 (c) Case 3

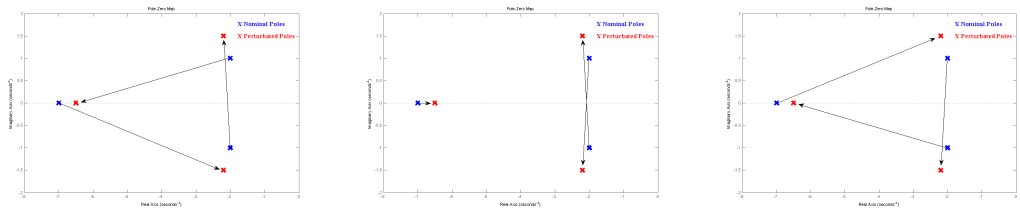

(d) Case 4 (e) Case 5 (f) Case 6

Figure 3.2 : Possible Pairing Options

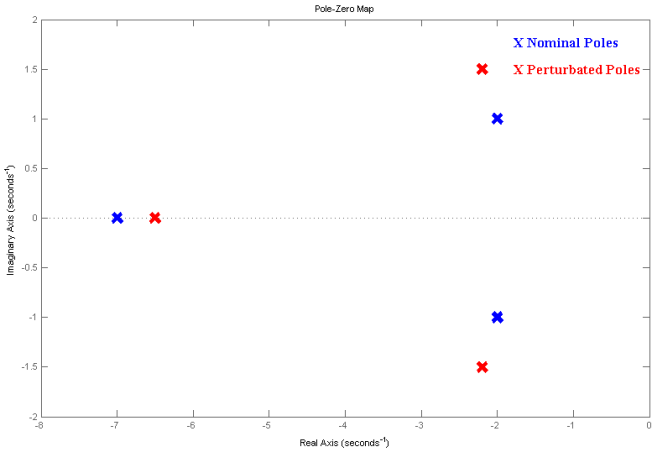

Figure 3.3 : Nominal and Perturbed Poles

may be defined as the Euclidean distance between nominal and perturbed poles.

$$F_i = \sqrt{\sum_{i=1}^{n} (p_{pi} - p_{ni})^2} \tag{3.22}$$

Note that, if there are no perturbation, $F_i = 0$. The power of the technique is allowing the designer to assign a different cost functions to each pole pair. By doing so, dominant pole assignment can be relaxed by selecting less strict cost function for the undominant poles. Since problem usually involves many local minimum, a global optimization technique has to be used in order to obtain optimum result. Possible cost functions are presented in the next section. Also, a design example is presented. Perturbation based cost function has been used during the observer and controller designs.

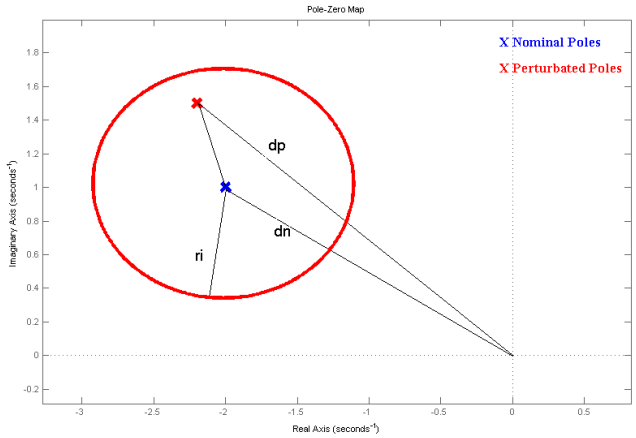

Figure 3.4 : Minimum Perturbation Based Cost Function

3.3.1 Several cost functions

Usually, performance criteria for each pole is different. For example, designer may not want to allow much perturbation for the dominant pole and it can be sufficient to assign simple settling time requirement for the poles which are far away from the dominant region. Also, in order to obtain specific time domain characteristics like rise time and damping ratio, several cost functions can be used together for a specific pair. Here, minimum perturbation based and settling time based cost functions are presented. Further information can be fount in [25, 36].

3.3.1.1 Minimum perturbation based cost function

By defining a disk in root space, perturbed poles can be limited to stay in this disk which center is the corresponding nominal pole. By changing the radius of the disk different cost functions can be assigned for the different pole pairs. Mathematical representation is follows [36]:

$$J_{1i} = \frac{|d_{ni} - d_{pi}|}{r_i} \tag{3.23}$$

where r_i is the radius of the disc, d_ni and d_pi are the distances from nominal and perturbed poles to the origin respectively.

3.3.1.2 Settling time based cost function

While making dominant pole placement, it is required that the poles which are not in that region, are to be far away from the dominant region. A settling time based cost function can be assigned for the poles which are not in dominant region. By doing

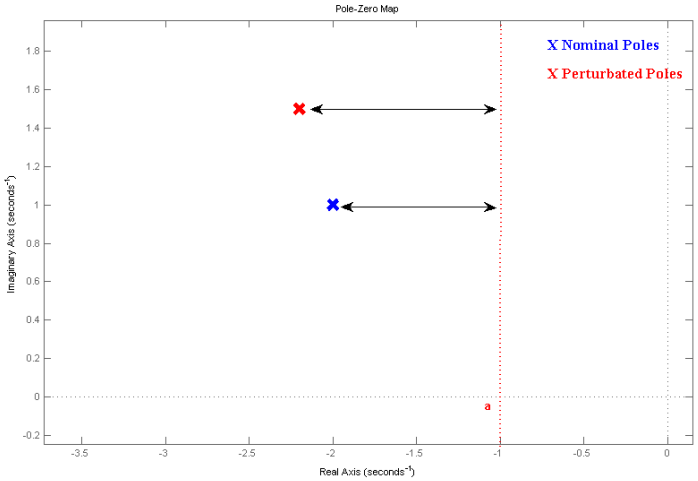

Figure 3.5 : Settling Time Based Cost function

this, it can be guaranteed that the undominant poles are going to be stayed outside the dominant region under parametric uncertainties. Settling time based cost function can be defined as follows [36]:

$$J_{2i} = \frac{Re(d_{ni}) - Re(d_{pi})}{Re(d_{ni}) - \sigma_i} \tag{3.24}$$

where σ_i corresponds the location of the related right boundary.If the all the poles are to the left of their right boundaries, the cost function is going to be less than one. Similarly, for the poles are required to be the right of the corresponding left boundary, cost function can be define as follows [36]:

$$J_{2i} = \frac{Re(d_{pi}) - Re(d_{ni})}{\sigma_i - Re(d_{ni})} \tag{3.25}$$

3.4 Robust Pole Placement Via Pole Colouring

Let's consider the system below

$$A(q) = \begin{bmatrix} 1 & -1 & 0 \\ 0 & -1+q_1 & 2+q_2 \\ 2 & 1 & -2 \end{bmatrix} B(q) = \begin{bmatrix} 0 & 1 \\ -1+q_3 & 0 \\ 1 & 1 \end{bmatrix} \tag{3.26}$$

where parameter are known to be vary as follows,

$$q_1 = [-0.25 \quad 0.25] \tag{3.27}$$

$$q_2 = [-0.35 \quad 0.35] \tag{3.28}$$

$$q_3 = [-0.20 \quad 0.25] \tag{3.29}$$

where nominal values are $q_1 = q_2 = q_3 = 0$. Since there are two input of the system and system order is 3, state feedback gain matrix is $2x3$ matrix. Since there are 6 parameters to adjust, it is impractical to use this structure during optimization. So dyadic feedback approach which belongs to classical methods can be used in order to design a state feedback controller. By doing so, 2 input system is turn into pseudo-single input system whose input signal is weighted sum of two inputs. In this approach, state feedback matrix **K** is an outher product of two vectors,

$$\mathbf{K} = f_o \mathbf{k} \tag{3.30}$$

$$b = B f_o \tag{3.31}$$

where f_o is called fan-out vector and b is pseudo single input matrix [25]. By taking fan-out vector as follows,

$$f_o = \begin{bmatrix} 1 \\ k \end{bmatrix} \tag{3.32}$$

input matrix can be expressed as follows,

$$b = \begin{bmatrix} k \\ -1 + q_3 \\ 1 + k \end{bmatrix} \tag{3.33}$$

Desired closed loop pole locations are

$$s = -2 + i \quad s = -2 - i \quad s = -7 \tag{3.34}$$

By simply using desired characteristic polynomial, state feedback k is found as follows,

$$\mathbf{k} = (k1 \quad k2 \quad k3) \tag{3.35}$$

where

$$k1 = \frac{90 - 8(-2+k)k}{2 + k(11 + 4k(7+2k))} \tag{3.36}$$

$$k2 = \frac{13 + 254k + 76k^2}{2 + k(11 + 4k(7+2k))} \tag{3.37}$$

$$k3 = \frac{31 + 8k(29 + 10k)}{2 + k(11 + 4k(7+2k))} \tag{3.38}$$

by obtaining state feedback matrix by $\mathbf{K}=f_o\mathbf{k}$

$$K = \begin{pmatrix} \frac{90-8(k-2)k}{k(4k(2k+7)+11)+2} & \frac{76k^2+254k+13}{k(4k(2k+7)+11)+2} & \frac{8k(10k+29)+31}{k(4k(2k+7)+11)+2} \\ \frac{k(90-8(k-2)k)}{k(4k(2k+7)+11)+2} & \frac{k\left(76k^2+254k+13\right)}{k(4k(2k+7)+11)+2} & \frac{k(8k(10k+29)+31)}{k(4k(2k+7)+11)+2} \end{pmatrix} \tag{3.39}$$

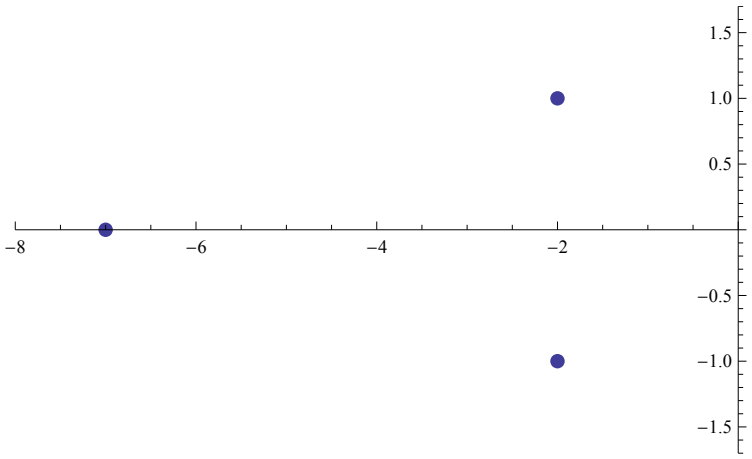

Figure 3.6 : Closed Loop Pole Location when k=-0.5 and k=5

Whatever the value of the free parameter k is, closed loop poles are going to be located at the desired locations as shown in Figure 3.6. However, when the uncertainties are included, pole spread varies dramatically as shown in Figure 3.7 and Figure 3.8.

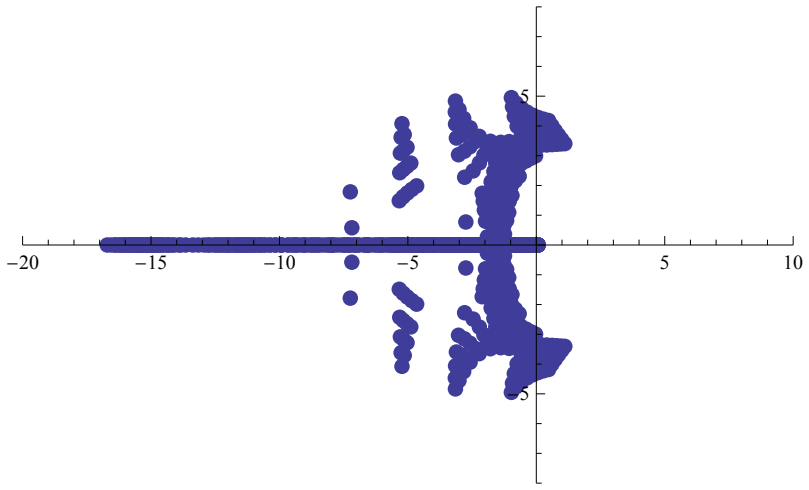

Figure 3.7 : Pole Spread when k=-0.5

Here, value k is a free parameter that can be used for fulfilling robustness requirement. Now let us consider the minimum perturbation based cost functions where

$$r_1 = 1 \tag{3.40}$$

$$r_2 = 1 \tag{3.41}$$

$$r_3 = 2 \tag{3.42}$$

For this purpose a simple MATHEMATICA code has been written (Figure B.1). As a result optimum value of k has been found as -8.5788. Resulting pole spread of the closed loop system has been given in Figure 3.9. As it can be seen in Figure 3.9,

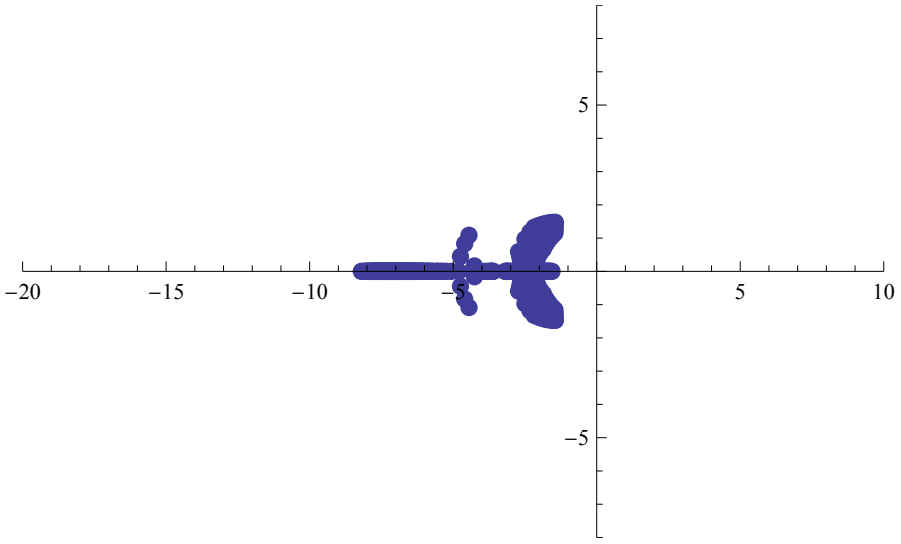

Figure 3.8 : Pole Spread when k=5

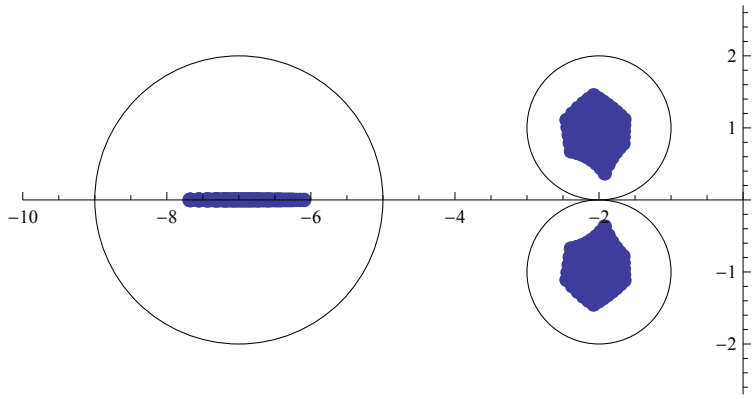

Figure 3.9 : Pole Spread of the Closed Loop System for k=-8.5788

perturbed poles are in the defined D-regions.

3.4.1 Using settling time and perturbation based cost functions together

For the real root, settling time based cost function can be defined. It is required that real roots are to be left of the $\sigma = -6.5$ boundary. Perturbation based cost function is relaxed by setting $r_{1,2} = 1.5$. For this purpose MATHEMATICA code has been written (Figure B.2).

Result of the optimization gives the k value as $k = -3.62$. Related pole spread is given in Figure 3.10. As it can be seen in Figure 3.10, real poles are on the left of the $\sigma = -6.5$. However, complex poles are not in the D-region. Related cost function value $J_2 = 3.94 > 1$, means that perturbed poles are not in the D-region. In this case

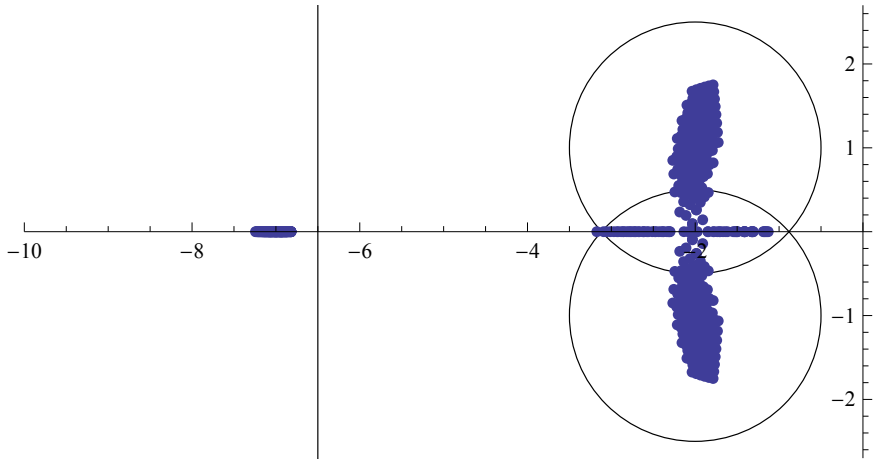

Figure 3.10 : Pole Spread of the Closed Loop System for k=-3.62

cost function should be relaxed and optimization should be redone. For $\sigma = -6.3$ and $k = -3.676$, pole spread stays in defined D-regions.

3.5 Robust PI Observer Design Over Wide Speed Range

Pole colouring concept can be easily applied on the robust observer design problem. Here, the angular velocity is going to be considered as a parameter uncertainty with the bounds of $[-6300 \quad 6300]\frac{rad}{s}$. Since motor rotation has two direction, different optimization can be made for both rotation. First, the ω_e is assumed to be changed between $[-6300 \quad 0]\frac{rad}{s}$. By applying minimum perturbation based cost function, observer gain have been calculated as follows;

$$L = \begin{bmatrix} 0.47 & -0.21 \\ -0.18 & 0.43 \\ -5.54 & 0.18 \\ 0.27 & -5.22 \end{bmatrix} \tag{3.43}$$

As it can be seen in Figure 3.11, poles of the observer are not in the desired D-region. This means that observer model has not enough degree of freedom to assign all poles to the desired region. Either D-region can be relaxed or the parameter variation assumption can be changed. Fortunately, operation range of the motor can be separated into two region (See Figure 3.12).

In washing machine application, motor runs at relatively low speed during washing cycles which takes much more time than the spinning cycles. So, different optimizations are going to be used for washing and spinning cycles.

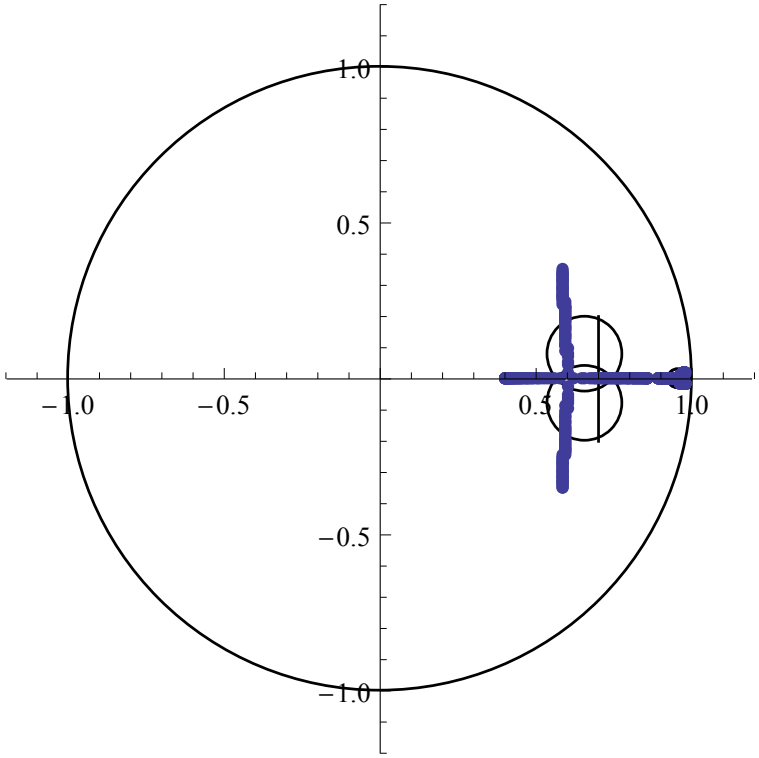

Figure 3.11 : Pole Spread of the observer, $\Omega_e = [-6300 \quad 0]\frac{rad}{s}$

3.5.1 PI observer design for washing cycle

Angular velocity of the motor is assumed to be changed between $\omega_e = [0 \quad 2000]\ \frac{rad}{s}$. Desired nominal poles are $z_{1,2} = 0.651 \pm 0.05i$ and $z_{3,4} = 0.95 \pm 0.002j$. D-Regions related to the optimization have been defined such that perturbation radius for the $z_{1,2}$ is $r_1 = 0.12$ and for the $z_{3,4}$ is $r = 0.005$. The observer gains have been calculated by using pole colouring method are given below;

$$\begin{bmatrix} 0.3759 & 0.1 \\ -0.099 & 0.371 \\ -4.94 & -0.544 \\ 0.1 & -5.419 \end{bmatrix} \tag{3.44}$$

After optimization, Poles are restricted to the given D-regions. Pole spread of the observer dynamics are given in Figure 3.13. For the negative rotation direction, where angular velocity changes between $\omega_e = [0 \quad -2000]\ \frac{rad}{s}$, same procedure has been applied.Resulting pole spread is given in Figure 3.14 and observer gains have been calculated as follows;

$$\begin{bmatrix} 0.3544 & -0.0491 \\ 0.067 & 0.3746 \\ -4.889 & -0.5146 \\ -0.2485 & -5.8664 \end{bmatrix} \tag{3.45}$$

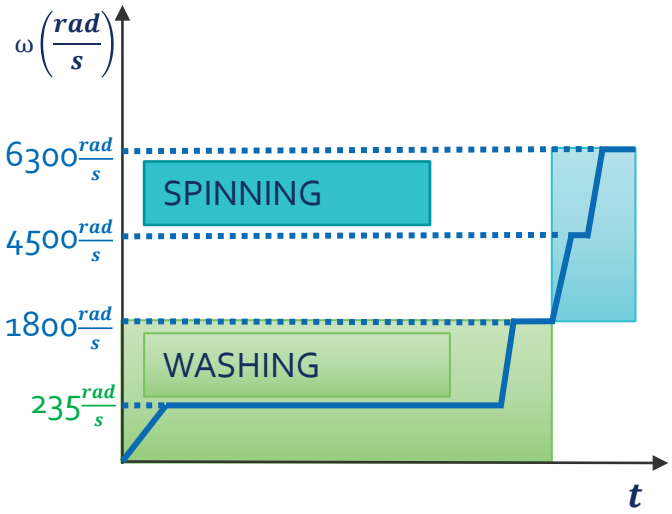

Figure 3.12 : Operation Region of the Washing Machine

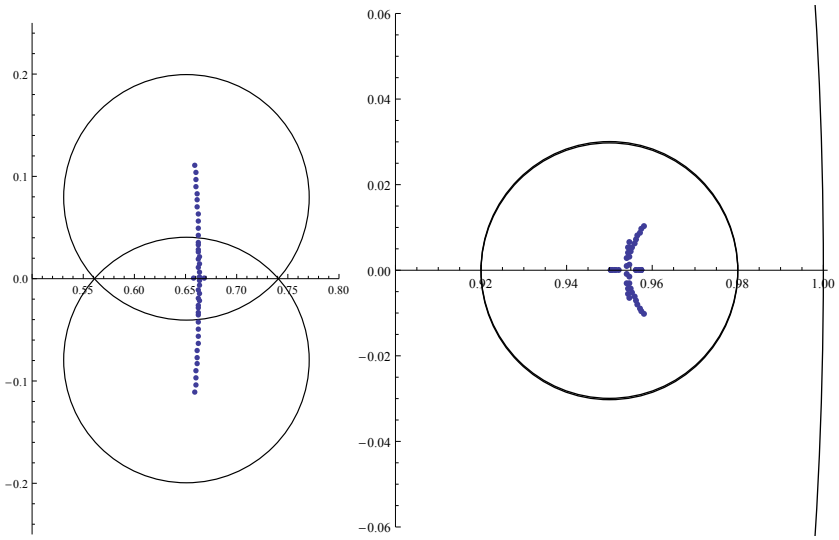

(a) $Z_{1,2}$ (b) $Z_{3,4}$

Figure 3.13 : Pole Spread around $z_{1,2}$ and $z_{3,4}$

3.5.2 PI observer design for spinning cycle

Angular velocity of the motor is assumed to be changed between $\omega_e = [2000 \quad 6300]$ $\frac{rad}{s}$ in spinning cycle. Desired nominal poles are $z_{1,2} = 0.651 \pm 0.1i$ and $z_{3,4} = 0.99 \pm 0.002j$. D-Regions related to the optimization have been defined such that perturbation radius for the $z_{1,2}$ is $r_1 = 0.12$ and for the $z_{3,4}$ is $r = 0.005$. The observer gains have been calculated by using pole colouring method are given below;

$$\begin{bmatrix} 0.3616 & 0.2821 \\ -0.213 & 0.403 \\ -4.90 & 0.20 \\ -0.098 & -5.31 \end{bmatrix} \tag{3.46}$$

Related pole spread is given in Figure 3.15. For the negative rotation direction, angular

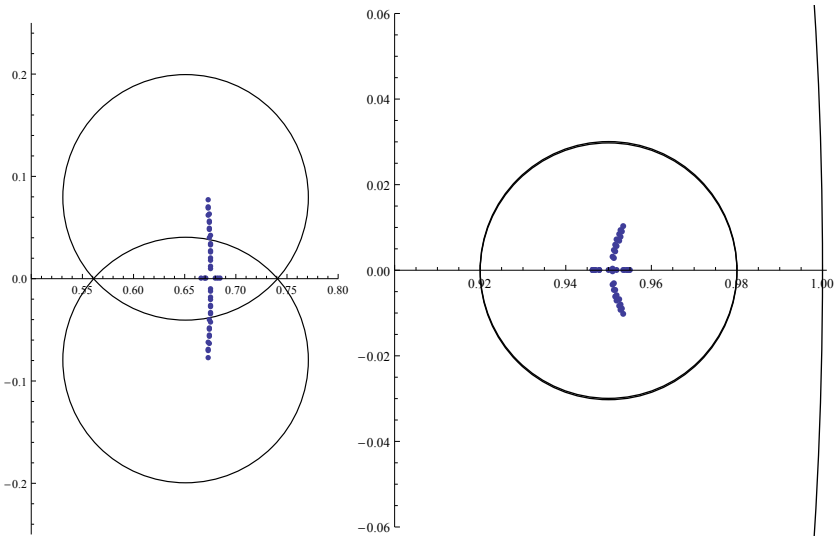

(a) $Z_{1,2}$ (b) $Z_{3,4}$

Figure 3.14 : Pole Spread around $z_{1,2}$ and $z_{3,4}$

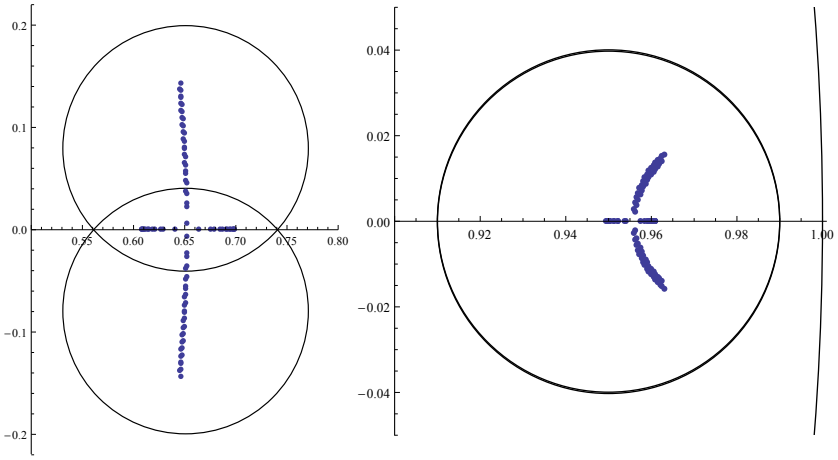

(a) $Z_{1,2}$ (b) $Z_{3,4}$

Figure 3.15 : Pole Spread around $z_{1,2}$ and $z_{3,4}$

velocity is assumed to be changed between $\omega = [-2000 \quad -6300]\ \frac{rad}{s}$. Observer gains for negative rotation direction spinning cycle is given below;

$$\begin{bmatrix} 0.3994 & -0.2732 \\ 0.2158 & 0.3868 \\ -5.4971 & -0.5449 \\ 0.0437 & -5.8361 \end{bmatrix} \tag{3.47}$$

Related pole spread is given in Figure 3.16.

3.6 Speed and Position Estimation

Back electromotive force estimation has been carried out by the PI observer. The next step is to estimate speed and angular position of the rotor. Since the rotor position

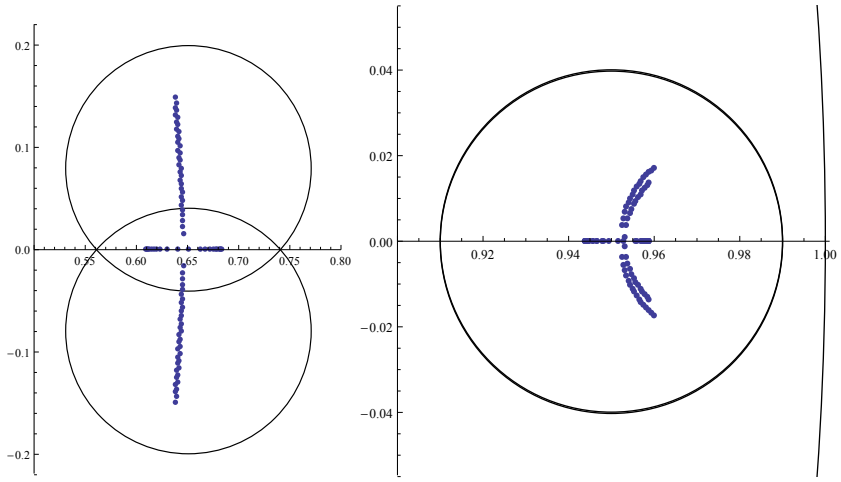

(a) $Z_{1,2}$ (b) $Z_{3,4}$

Figure 3.16 : Pole Spread around $z_{1,2}$ and $z_{3,4}$

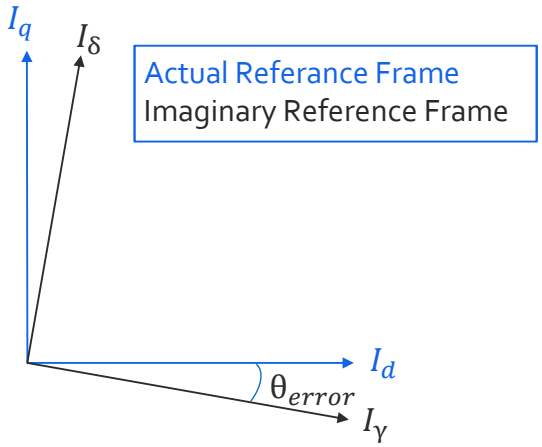

Figure 3.17 : Actual And Imaginary Reference Frames

information is related to the BEMF (see Figure 3.17), rotor position error between imaginary and the actual reference frame can be calculated as follows;

$$\begin{bmatrix} E_\gamma \\ E_\delta \end{bmatrix} = E \begin{bmatrix} -sin(\theta_{error}) \\ cos(\theta_{error}) \end{bmatrix} \tag{3.48}$$

$$\theta_{error} = tan^{-1}(\frac{-E_\gamma}{E_\delta}) \tag{3.49}$$

The position error between actual and imaginary reference frame can be compensated by using proper controller-like structure. When the position error θ_{error} is driven to zero, actual speed and rotor position information can be filtered. Selected structure is called Angle Tracking Observer given in Figure 3.18. By using forward Euler approximation, discrete domain transfer function has been obtained as follows;

$$T = \frac{K_1K_2Tz + K_1T(T-K_2)}{z^2 + z(K_1K_2T-2) + T^2K_1 + 1 - TK_1K_2} \tag{3.50}$$

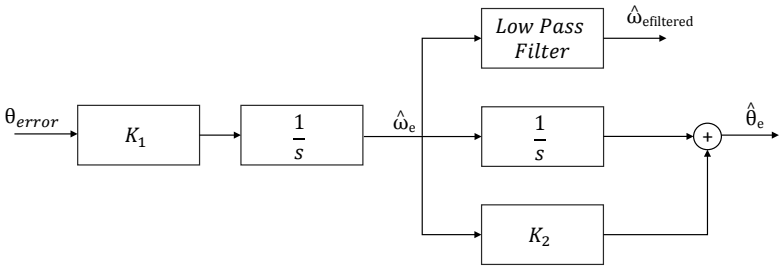

Figure 3.18 : Angle Tracking Observer

Where T is the sampling period, K_1 and K_2 are observer gains. Desired settling time is 0.2 ms and overshoot is zero. Gains have been calculated as;

$$K_1 = 300000 \quad K_2 = 0.4 \tag{3.51}$$

Step response of the angle tracking observer is given in Figure 3.19. Speed estimation has been used in order to update the PI observer system matrix in order to make nominal and observer system matrix error minimum.

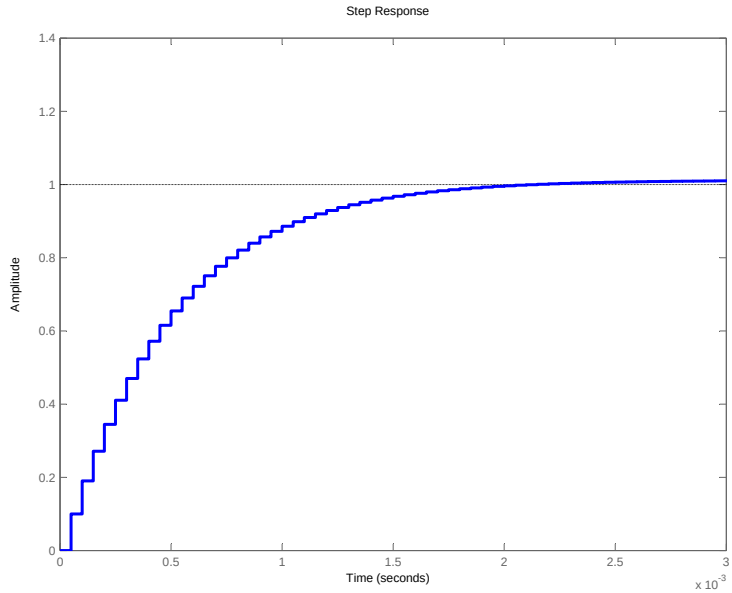

Figure 3.19 : Step Response of Angle Tracking Observer

4. DESIGN OF ROBUST CURRENT CONTROLLERS

4.1 Mathematical Model of The Current loop

The mathematical model of the current loop is given below;

$$V_d = RI_d + L_d \frac{dI_d}{dt} - \omega_e L_q I_q \tag{4.1}$$

$$V_q = RI_q + L_q \frac{dI_q}{dt} + \omega_e L_d I_d + \omega_e \Psi_{pm} \tag{4.2}$$

The model includes multiplication of angular velocity and the currents. However, angular velocity changes slowly by comparison to current. So the angular velocity is going to be treated as time varying parameter instead of a state. The main problem of the mathematical model above is coupling effects among the d and q axes currents. Furthermore, these coupling effects get stronger as the angular velocity increase. For this reason, it is very hard to obtain satisfying performance at high speed applications without suppressing these coupling effects.

Before considering fully interacting multivariable design, it is useful to check if the problem can be treated as set of SISO system which have interactions between each other. Advantages of using decentralized approach over MIMO desing are that it has straightforward procedure and it is easy to understand by considering classical control arguments [38]. As it can be seen in Figure 4.1, the inputs (V_d and V_q) affect both I_d and I_q. One may consider to design two controller for each loop by considering the coupling effect as disturbances. By making aggressive controller in order to suppress the disturbance effects may show satisfactory performance in the cases where small coupling effects are present. However, the mathematical model in equation (4.1) and equation (4.2) shows that coupling effects increase dramatically as the angular velocity increase. Also, current controllers have settling time limits because of the separation property due to the observer in the closed loop. So, the coupling effects have to be compensated by using a proper structure.

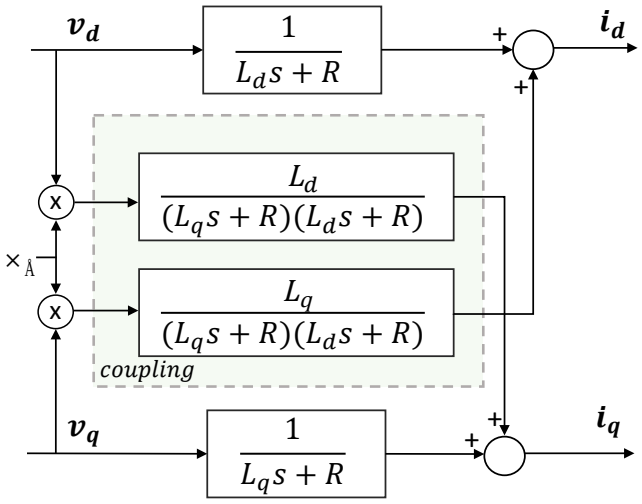

Figure 4.1 : Set of SISO Representation of The Current Loop

4.2 Open Loop Decoupling of The d-q Axes Currents

Selection of which decoupling method is going to be used can be complicated and each method address different problem [39]. Simplified decoupling method is going to be used in this section. Open loop transfer function of the system is given below;

$$G(s) = \begin{bmatrix} \frac{1}{L_d s+R} & \frac{\omega_e L_q}{(L_q s+R)(L_d s+R)} \\ \frac{\omega_e L_d}{(L_q s+R)(L_d s+R)} & \frac{1}{L_q s+R} \end{bmatrix} \tag{4.3}$$

The desired open loop transfer function has following form;

$$T = \begin{bmatrix} T_1(s) & 0 \\ 0 & T_2(s) \end{bmatrix} \tag{4.4}$$

Where $T(s) = D(s)G(s)$. Resulting decoupler has been found as follows;

$$D(s) = \begin{bmatrix} 1 & \frac{\omega_e L_q}{L_q s+R} \\ \frac{\omega_e L_d}{L_d s+R} & 1 \end{bmatrix} \tag{4.5}$$

Updated current loop control block diagram is given in Figure 4.2. Since the angular

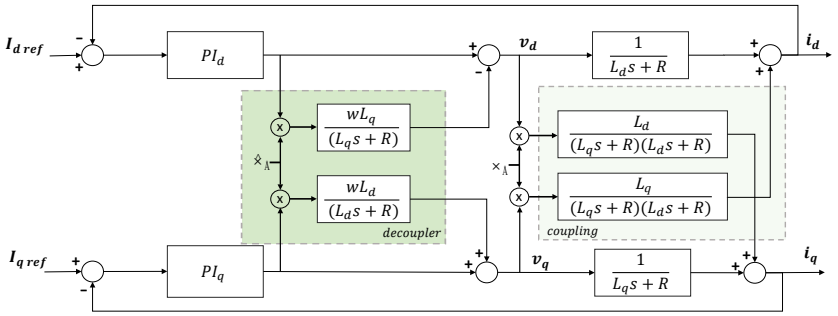

Figure 4.2 : Current Control Loop Block Diagram

velocity is estimated by the angle tracking observer, it is possible to update the

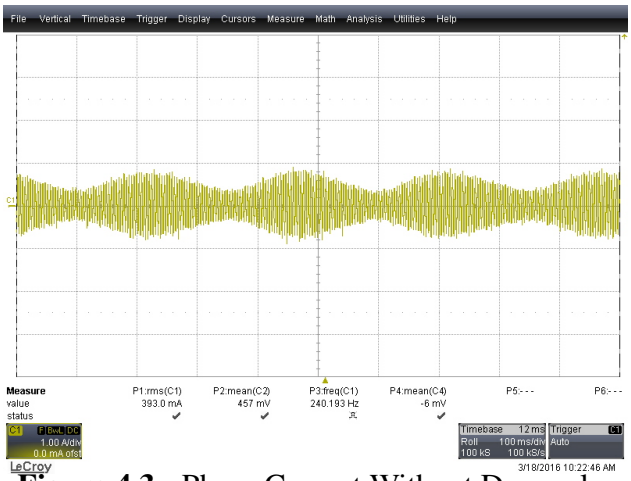

Figure 4.3 : Phase Current Without Decoupler

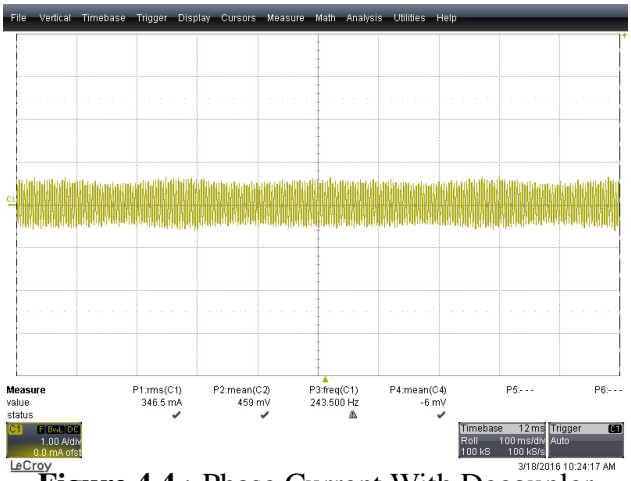

Figure 4.4 : Phase Current With Decoupler

decoupling transfer function as the speed changes. Because the speed is the major coupling effect, the main idea of the decoupling of I_d and I_q current loop is to cancel the speed dependent terms. Although, there exist parameter mismatches between motor model and the decoupling transfer functions, these effects can be considered as disturbances affecting the system input now. The PI controllers can be design in order to suppress these disturbance effects. The pole coloring concept is going to be used in order to design robust current PI controllers under parameter uncertainties. Single phase currents with and without decoupler have been given in Figure 4.3 and Figure 4.4.

4.3 Design by Using Pole Colouring Concept

The resistor of the stator windings is affected by the temperature rise due to high current or operational duration. Inductance of the d and q axes may go saturate if the corresponding current values increases. by considering all these variations, robust

Table 4.1 : Parameter Space For R, L_d and L_q.

Parameter	R(ohm)	L_d(mH)	L_q(mH)
Min	3.15	0.01 A	0.02
Max	4.5	0.0167	0.025

current controllers can be designed by using pole colouring concept. Parameter space related to the current loop mathematical model is given in Table 4.1.

4.3.1 D-axis current controller design

For the d-axis current loop, discrete domain open loop system is given below;

$$G(z) = \frac{1}{R}(1 - \frac{z-1}{z - e^{\frac{-RT}{L_d}}}) \tag{4.6}$$

Where T is the sampling period. The main strategy is to assign the zero of the PI controller far enough to stay out of the dominant region while the closed loop poles are located in the dominant region satisfying certain settling time and overshoot requirements. Desired closed loop poles is given below;

$$z_{1,2} = 0.985 \pm 0.01 \tag{4.7}$$

Where the poles correspond a settling time which is $10ms$ and percentage overshoot is 6 . Controller coefficients have been found as follows;

$$K_p = 3.43 \tag{4.8}$$

$$K_i = 0.089 \tag{4.9}$$

Pole spread after the optimization is given in Figure 4.5. Related step response is given in Figure 4.6.

4.3.2 Q-axis current controller design

Same procedure has been repeated for the q-axis current controller loop. Nominal poles are $z_1 = 0.975$ and $z_2 = 0.9922$. Controller coefficients have been found as follows;

$$K_p = 12.94 \tag{4.10}$$

$$K_i = 0.1 \tag{4.11}$$

Pole spread of the closed loop system is given in Figure 4.7. Related step response is given in Figure 4.8.

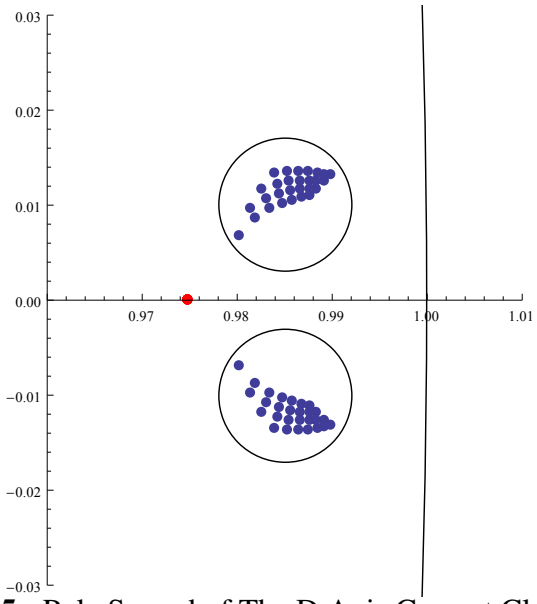

Figure 4.5 : Pole Spread of The D Axis Current Closed Loop

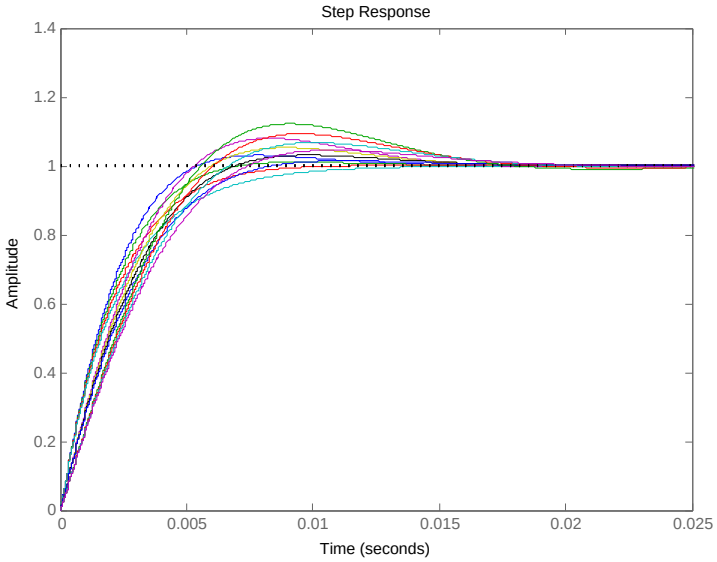

Figure 4.6 : Closed Loop Step Response For D Axis Current Loop

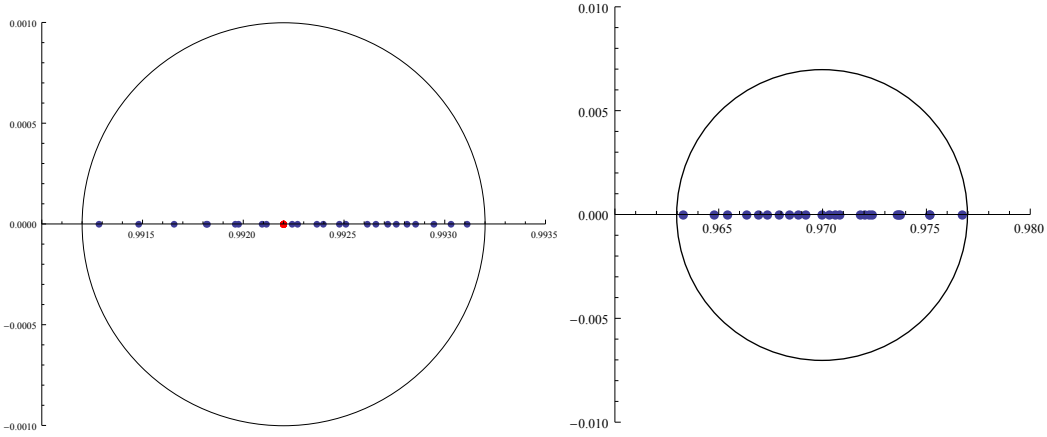

(a) Z_1 (b) Z_2

Figure 4.7 : Pole Spread of The Q Axis Current Closed Loop

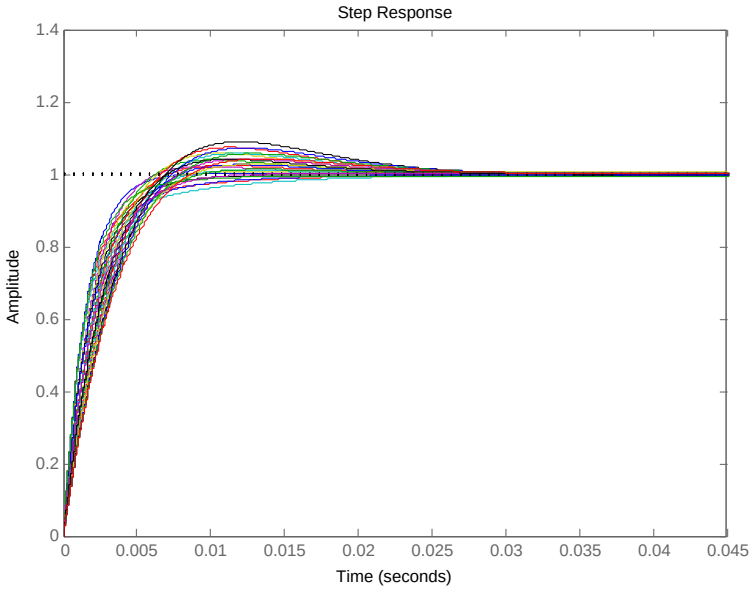

Figure 4.8 : Closed Loop Step Response For Q Axis Current Loop

5. DESIGN OF ROBUST SPEED CONTROLLER

The mathematical model of the speed loop is given below;

$$T_E - T_L = J\frac{d\omega_m}{dt} + B\omega_m \tag{5.1}$$

Where T_E is the produced torque by the machine, T_L is the load torque, J is the moment of inertia and B is the friction coefficient. In the washing machine application, motor shaft is connected to the drum via a belt-pulley mechanism which has turn ratio of 10.8. This ratio keeps the operating speed of the motor in the stable region and also decreases the torque applied on the motor. Moment of inertia and the friction coefficients of the drum are going to be reflected with the ration of $\frac{1}{10.8^2}$ due to belt-pulley mechanism. This result also shrinks the parameter spread on the motor side due to

$$J_{total} = \frac{J_{drum}}{10.8^2} + J_{motor} \tag{5.2}$$

$$B_{total} = \frac{B_{drum}}{10.8^2} + B_{motor} \tag{5.3}$$

Since the loads to be put in the drum is unknown, moment of inertia of the mechanical system may change dramatically. Moment of inertia also changes during the operation due to the changing speed. At low speeds, clothes roll over in the drum and hit the drum surface causing torque disturbance and changing moment of inertia. At the high speed, clothes sticks to the drum surface leading to the changing moment of inertia. Furthermore, clothes do not always stick to the drum surface homogeneously. Some parts of the clothes may be gathered to the specific area on the surface causing the unbalanced load torque. To sum up, speed controller has to be robust to the parameter variation and has good disturbance rejection capability. The torque equation of the motor is given

$$T = \frac{3}{2}Z_p(\Psi_{pm} + (L_d - Lq)I_d)I_q \tag{5.4}$$

Where Z_p is the number of pole pair of the motor which is 4. By taking the torque constant as $k_t = \Psi_{pm} + (L_d - Lq)I_d$, motor torque can be expressed as

$$T = k_t I_q \tag{5.5}$$

Table 5.1 : Parameter Space For The Speed Loop.

Parameter	Moment of Inertia	Friction Coefficient	Torque Constant
Min	0.0012 $(kg \cdot m^2)$	0.00025 $(\frac{Nm \cdot s}{rad})$	0.6 $\frac{Nm}{A}$
Max	0.0024 $(kg \cdot m^2)$	0.00075 $(\frac{Nm \cdot s}{rad})$	0.65 $\frac{Nm}{A}$

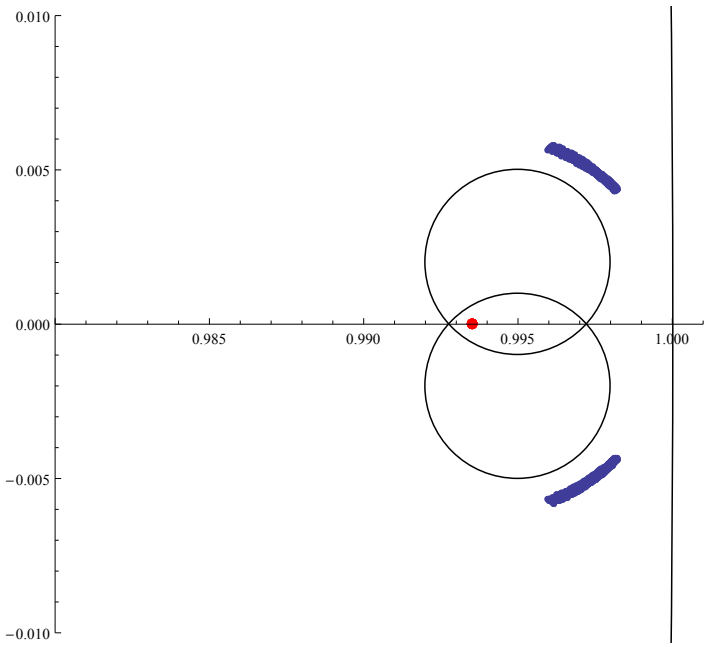

Figure 5.1 : Pole Spread of The Closed Loop System With PI Controller

with assumption that I_d current is constant. Up to field weakening region, I_d current is kept constant at $0A$. When the motor speed is increased further, negative current reference is applied to the d axis current loop. By changing I_d current, torque constant is changed. So, the torque constant is also going to be considered as parameter uncertainty. Parameter space related to the motor side is given in Table 5.1. By taking account these uncertainties a PI controller has been design for nominal poles at

$$z_{1,2} = 0.995 \pm 0.002i \tag{5.6}$$

and also the zero location is restricted to the $z_{zero} < 0.9935$. Resulting PI controller coefficients are given below;

$$K_p = 0.0136 \tag{5.7}$$

$$K_i = 0.000089 \tag{5.8}$$

Pole spread of the closed loop system is given in Figure 5.1. The pole spread exceeds the defined D-regions. This is because the PI controller has not enough degree of

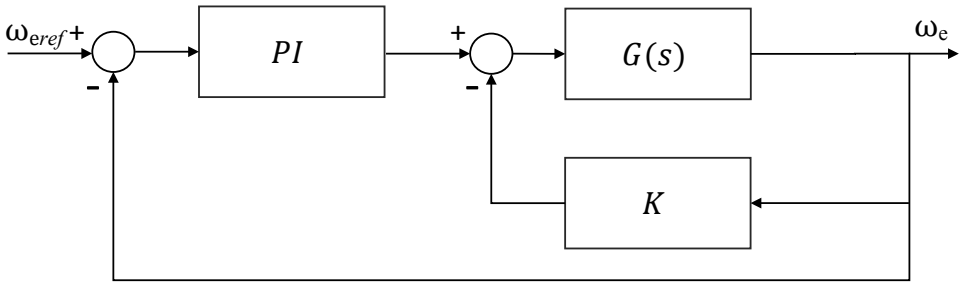

Figure 5.2 : PI-P Controller

freedom to restrict all poles to the defined D-region. For this reason PI-P controller structure is going to be implemented.

5.1 PI-P Controller Design

PI-P controller structure given in Figure 5.2 has more degree of freedom than the PI controller. Also, disturbance rejection capability is much higher than PI controller due to the inner loop. Same design procedure is going to be repeated for the PI-P controller. In this case further design constrain comes from the inner loop. If the feedback gain is too high, inner loop dynamics is going to be excessively fast causing the large control signal. It also amplifies the noise in the speed feedback. If the feedback gain is kept too low, than the advantages of the PI-P structure would not be observed. So, during the optimization, feedback gain, K, is restricted between 0 and 0.01. Also zero of the closed loop system is restricted to be left of the $z = 0.9935$. After optimization, design parameter have been calculated as follows;

$$K = 0.01 \tag{5.9}$$

$$K_p = 0.0158 \tag{5.10}$$

$$K_i = 0.0001 \tag{5.11}$$

Pole spread of the closed loop is given in Figure 5.3. Step response of the closed loop system is given in Figure 5.4. Comparison of the two controller performance for the ramp and step disturbances is given in Figure 5.5. PI-P controller shows better disturbance rejection performance for ramp and step type disturbances.

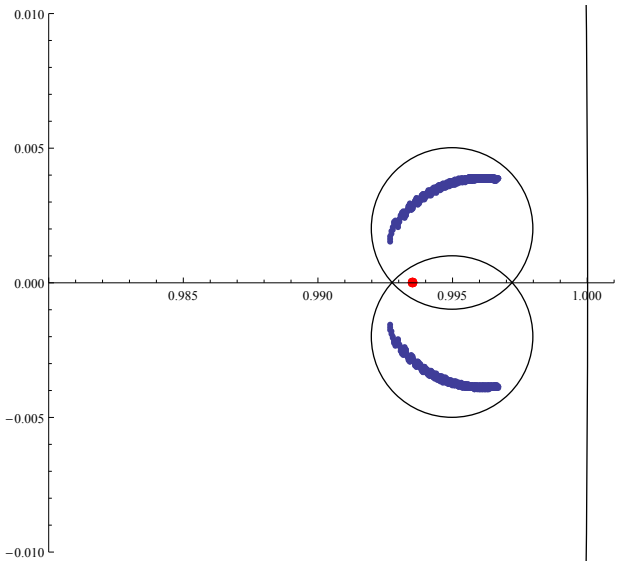

Figure 5.3 : Pole Spread of The Closed Loop System With PI-P Controller

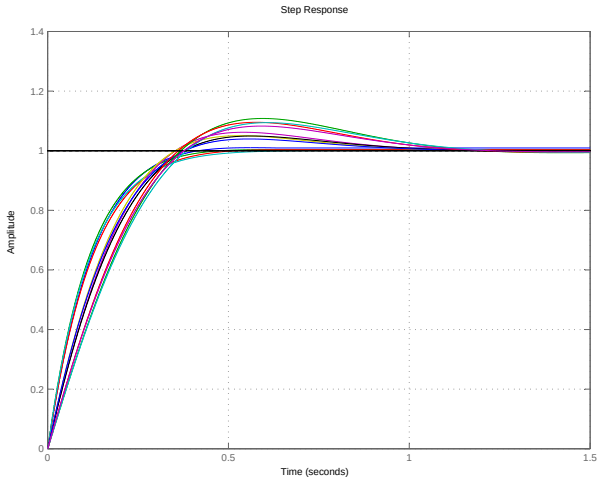

Figure 5.4 : Step Response of The Closed Loop System

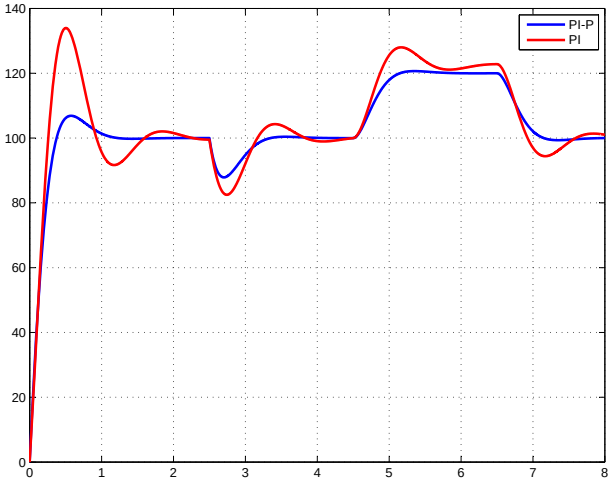

Figure 5.5 : Comparison of Disturbance Rejection Performances

6. POSITION SENSORLESS STARTUP ALGORITHM

6.1 Problem of Sensorless Starpup

The BEMF based position sensorless control methods are very effective in the middle and high speed range. However, when it comes to low speed operation, closed loop system performance may decrease dramatically. One reason of that is the unmodeled dynamics.

$$\mathbf{v_s} = \mathbf{R i_s} + \mathbf{L}\frac{\mathbf{di_s}}{\mathbf{st}} + \mathbf{e} + \mathbf{v_d} \tag{6.1}$$

where $\mathbf{v_s}$ is stator voltage, $\mathbf{i_s}$ is stator current, $\mathbf{L}$ is the inductance matrix and $\mathbf{v_d}$ is the disturbance voltage. As it can be seen in equation (6.1), disturbance voltage $\mathbf{v_d}$ takes place in more detailed model. The reason of this disturbances are usually inverter nonlinearities and noise. At the high speed operations, stator voltage is sufficiently high by comparison to the disturbance voltage. So, elimination of the disturbance voltage in the model does not cause any dramatic effects. However, at the low speed operation, the effects of the disturbance voltage cannot be omitted and it degrades the controllers performance. The unknown initial rotor position is also a problem. If the distance between applied current vector and the rotor flux vector is too large, then unnecessarily huge currents can be required to produce torque.

On the other hand, current demand is high in order to overcome the mechanical inertia. High currents cause noisy environment because of the switching components in the inverter. So, it is hard to filter the BEMF signal in the noisy environment. BEMF signal is also low at the low speed since it is proportional to the angular velocity.

This problems lead the engineers to search efficient startup algorithms. High frequency injection based methods is a valid alternative as discussed in Chapter 1. However, it increases the noise in the layout and has some limitations due to the switching elements. A practical approach is to align the rotor position with the current vector by applying a flux related i_d current. Since the permanent magnets is going to be aligned with the produced magnetic field vector, at least the distance between current and rotor flux vector can be decreased. However, rotating the current vector with only i_d current

leads the vibration in the rotor movement due to the holding torque. Once the rotor is aligned (or assumed to be aligned), torque related current component, i_q, is applied in order to produce startup torque. By applying i_q current, motor speed is increased until the BEMF signal is matured to be correctly estimated. So, this procedure is called open loop startup due to absence of speed and position information.

The main problem in such an approach is how to rotate the current vector. Since the

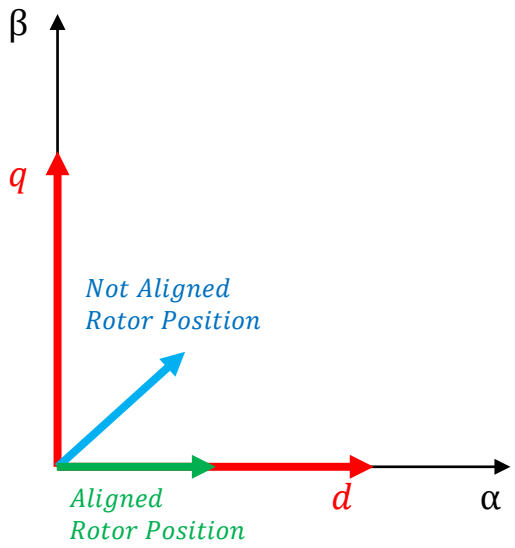

Figure 6.1 : Align State

rotor velocity and position is unknown, Clarke and Park transform cannot be utilized and space vector modulation cannot be performed in order to derive the motor. Usually and open loop speed and position calculation is performed in the algorithm with the assumption that constant speed ramp. By using the relation below, speed and position information can be obtained in the open loop.

$$\int a_e dt = \omega_e \tag{6.2}$$

$$\int \omega_e dt = \theta_e \tag{6.3}$$

However, speed ramp may change dramatically due to the load. If the load and inertia are not constant, such an approach may fail for a specific condition.

6.2 A Novel Startup Algorithm

A novel startup algorithm is proposed here. The main idea of the algorithm is that although the position and speed informations are corrupted with noise and

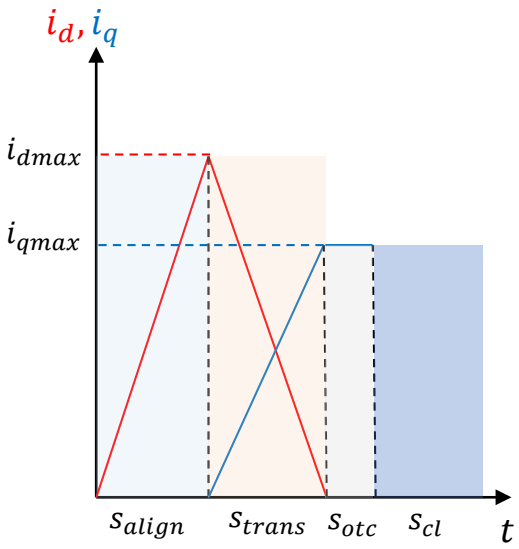

Figure 6.2 : i_d-i_q Transition

disturbances, the acceleration ramp of the filtered speed estimation gives an idea about the load torque and inertia during transient. So the open loop speed ramp information can be updated depending on the filtered speed estimation in order to derive speed and position information (See Figure 6.5). If the inertia and the load torque is high, motor accelerates slowly under the constant current amplitude. By decreasing the open loop speed ramp value, position error between rotor and current vector is decreased to a acceptable levels. Similarly, open loop speed ramp value is increased if the load and inertia is low which the speed estimation indicates. Flow chart of the algorithm is given in Figure 6.3.

6.3 Open to Closed Loop Transition

The BEMF based observer can operate properly once the angular velocity reaches a certain level. At this point, observer output have to be used in order to obtain closed loop control. Although, the position error between current vector and the rotor flux vector is decreased by using the startup algorithm mentioned in Section 6.2, there may be still difference between position information obtained from observer and open loop derivation. If the error is not compensated somehow, oscillations and ripples are take place during the open loop to closed loop transition.

In order to minimize these unwanted behaviors, a smooth transition algorithm has been

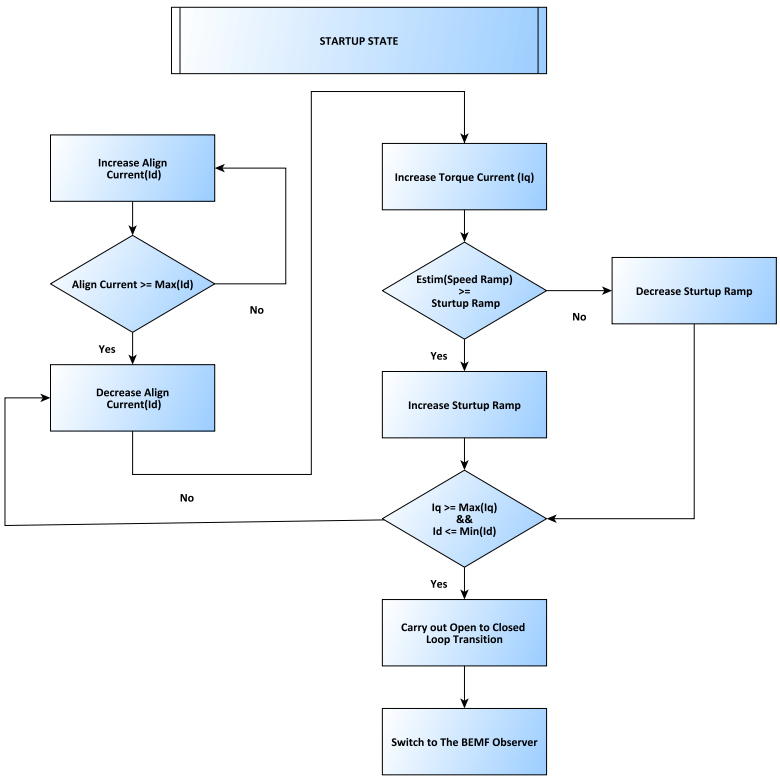

Figure 6.3 : Flow Chart of The Startup Algorithm

used. Algorithm utilizes a convex conjugate function which is defined below;

$$f_{out} = \alpha f_{cl} + (1-\alpha) f_{ol} \tag{6.4}$$

$$\int_0^1 \Delta dt = \alpha \tag{6.5}$$

where Δ is the merge step, f_{out} is the updated value, f_{ol} is the value in the open loop algorithm and f_{cl} is the value in the observer. α changes between 0 and 1 with the predefined merge steps. Once the α reaches its maximum value, value in the open loop algorithm has no effect and the observer outputs are running. Selection of the merge steps depends on transition speed. Merge step has to be selected such a way that, there have to be left enough time for controllers to recover the transient disturbances.

The stator current values are high by comparison to the closed loop. This is because the position error is much less in when the observer is online and required torque is high during the startup. When the control algorithm switches to the closed loop, stator current drops depending on the load. Since the startup stator current is high, overshoots may occur in the transition if the load is low. This degrades the startup quality and causes sudden changes in the rotor position which may be hard to estimated by the observer and recovered by the controllers. In order to obtain smooth transition,

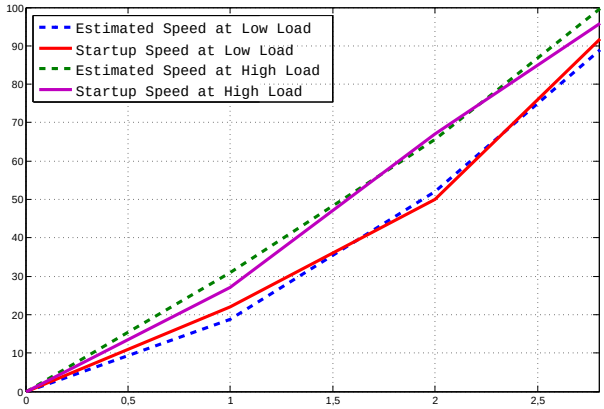

Figure 6.4 : Novel Startup Realization

startup stator current amplitude is decreased by the information which is obtained from the previous startup. Since the washing machine makes run and stop operation all the time, motor is started up for the worst case scenario once, then the startup stator current amplitude is adjusted depending on the load information which is obtained from the previous startup. The estimated and the calculated value of the rotor speed is shown in Figure 6.4.

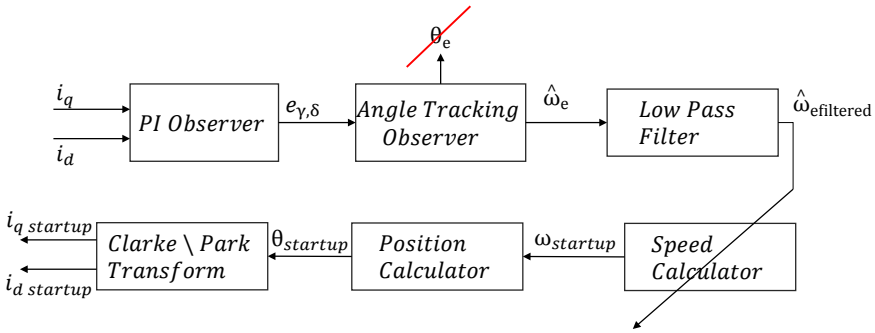

Figure 6.5 : Novel Startup Block Representation

7. FIELD WEAKENING OPERATION

The control system hardware is supplied by the grid. An AC-DC converter rectifies the sinusoidal input voltage in order to feed the three phase inverter. A large capacitor in the DC bus reduces the voltage ripples and it is assumed that DC bus voltage is fixed or fluctuates in a small range. When the motor speed is increased to the rated value, induced BEMF voltage is also increased and the motor cannot accelerates further due to the voltage limitation [40, 41].

$$\omega_{emax} = \frac{\sqrt{v_{max}^2 - (Ri_d)^2}}{L_d i_d + \psi_{pm}} \tag{7.1}$$

On the other hand, the current which is applied to the motor is limited due to the inverter ratings and stator winding temperature. Voltage and current limits is shown in Figure 7.1. Several approaches are proposed as in [40, 42], However, many of them

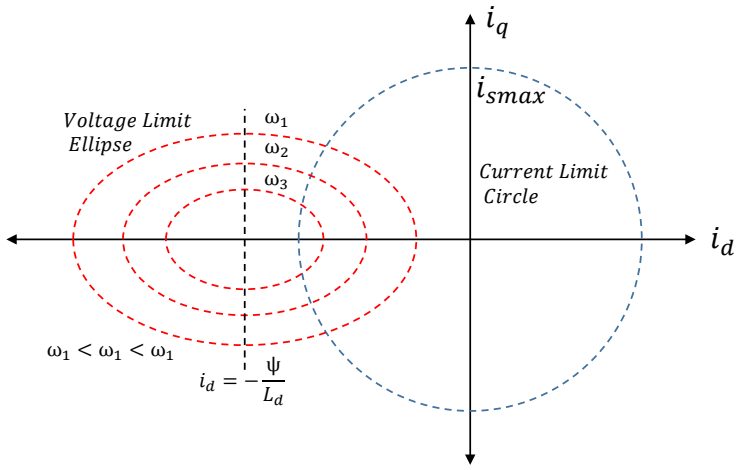

Figure 7.1 : Control Schema of The Closed Loop

are parameter dependent. Including too much parameter in the algorithm leads to degradation in the control performance when the parameters have chanced.

7.1 Parameter Free Field Weakening Algorithm

The parameter free field weakening algorithm is based on a single fact. Stator voltage vector cannot exceed the available DC bus voltage.

$$v_{bus}^2 > v_d^2 + v_q^2 \tag{7.2}$$

or alternatively;

$$|v_{bus}| > |v_s| \tag{7.3}$$

where v_s is the stator voltage vector which is $v_s^2 = v_d^2 + v_q^2$. This is actually the starting condition of the field weakening algorithm. Since the realizable vector space is limited due to the practical considerations [43], voltage limitation error is rewritten below;

$$v_{bus}^2 \cdot K_{marg} = v_d^2 + v_q^2 \tag{7.4}$$

Once the motor reaches its allowable rated speed, v_{bus} is equal to v_s. At this point a PI controller can be used in order to increase (negative direction) demagnetization current (i_d) for keeping the relation of $|v_{bus}| > |v_s|$ is held. As the i_d current increase, motor accelerates further due to the reduction in the air gap flux. By applying such an algorithm motor maximum speed is increased four times to its rated speed which is determined by the hardware. The maximum speed is limited to the mechanical considerations and winding temperature anyway. Also applying too much demagnetizing current may lead to the permanent demagnetization. So the demagnetization current (i_d) is limited. Flow chart of the control algorithm is given in Figure 7.2;

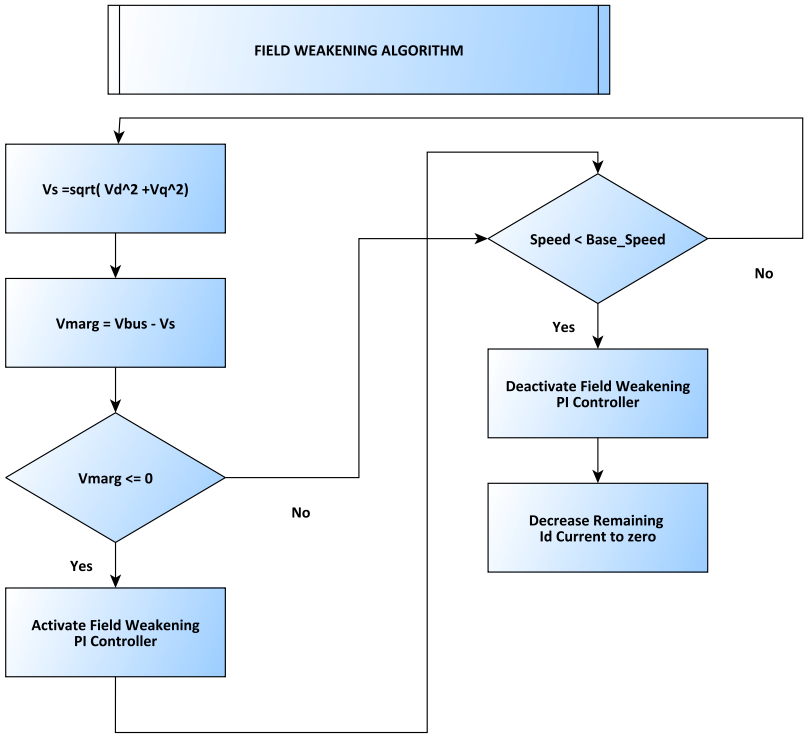

Figure 7.2 : Flow Chart of The Field Weakening Algorithm

Block representation is given in Figure 7.3.

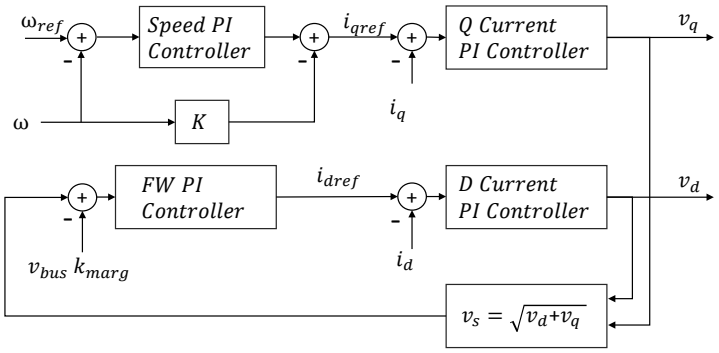

Figure 7.3 : Control Schema of The Field Weakening Region

7.2 Unbalanced Load Detection

In order to operate safely at high speed regions, load distribution in the drum has to be balanced which means that the clothes have been distributed homogeneously in the drum. Usually, this is not the case. This causes unbalanced load distribution and may cause excessive power consumption besides vibration. In order to prevent this situations, equivalent unbalanced load weight have to be calculated. If the unbalanced load wight is higher than the predefined limit, than drum speed have to be limited below the maximum operating speed. Certain speed profile may be applied to the drum.
In order to estimate equivalent unbalanced load, active power demand of the rotor is considered.

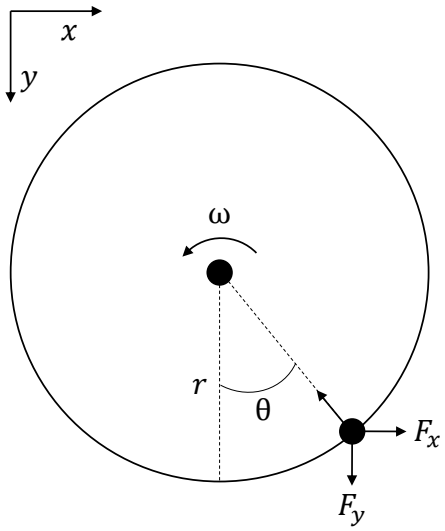

Figure 7.4 : The Free Body Diagram of The Unbalanced Load in Drum

$$F_y = m\omega_m^2 r\cos(\theta) + mg \tag{7.5}$$

$$F_x = m\omega_m^2 r\sin(\theta) \tag{7.6}$$

Since the clothes are stuck to the drum at 100 rpm speed, unbalanced load detection can be carried out at constant 100 rpm drum speed. By considering the vertical force applied by the load, it can be assumed that the active power required by the drum chances sinusoidally. Due to the friction, active power demand of the rotating drum is denoted as P_{100rpm} which is constant. By considering the drum radius, measurement speed and the gravitational acceleration, power equation can be approximated.

$$P_{unbalanced} \approx P_{100rpm} + m\frac{\omega_m^3 r^2}{2} \tag{7.7}$$

By considering the power requirement, unbalanced load weight can be determined since the radius of the drum and P_{100rpm} are known.

$$m \approx \frac{2(P_{unbalanced} - P_{100rpm})}{\omega_m^3 r^2} \tag{7.8}$$

Active power can be calculated by using q axis equivalent circuit at steady state in Figure 7.5. Since the active power transferred to the rotor can be calculated by knowing

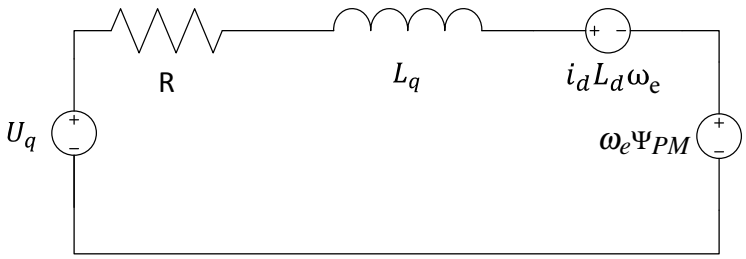

Figure 7.5 : Equivalent Q-Axis Circuit

i_q current and back electromotive force, it can be used to calculate the unbalanced load weight. 633 g unbalanced load has been used in order to the validate the concept. Active power transferred to the rotor is given in Figure 7.6. By considering the

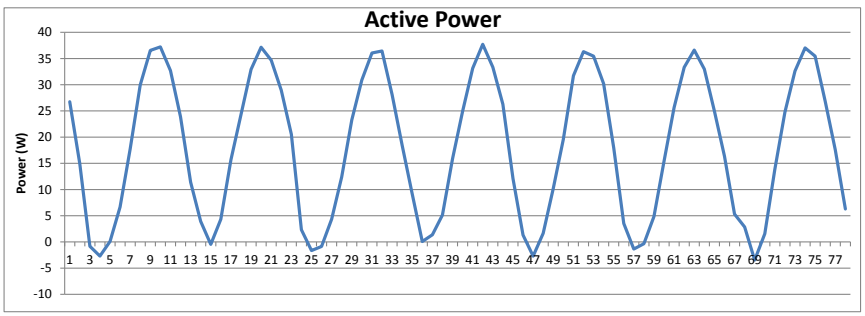

Figure 7.6 : Active Power Variation in The Presence of Unbalanced Load

unbalanced load equation, load weight has been calculated as 672g. Since drum has

its own unbalanced load due to imperfect mechanical structure, it can be said that this approach can be used in order to detect equivalent unbalanced load in the drum. The unbalanced load estimation for different weight have been given in Figure 7.7.

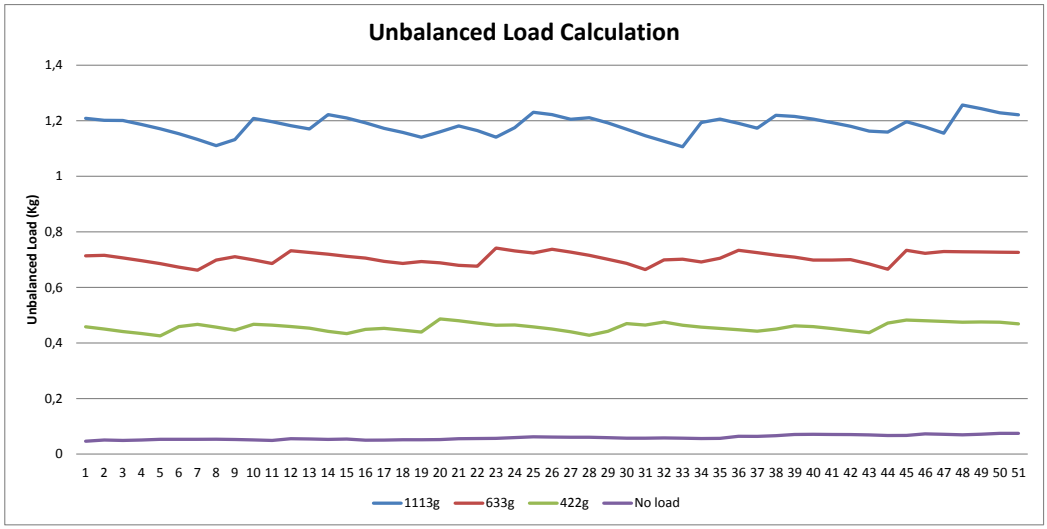

Figure 7.7 : Unbalanced Load Estimation For Different Weights

8. SIMULATIONS AND EXPERIMENTAL RESULTS

8.1 Simulations

In order to validate the design, MATLAB/SIMULINK model of the closed loop system has been constructed. The aim is to observe the position error between actual and estimated rotor position. As it is discussed in chapter 3, state estimation (i_d, i_q) errors go to zero in the steady state. However, depending on the uncertainties, extended back emf estimation error is kept below a certain limit, γ, so the estimated rotor position in Figure 8.1. Since the structure of the observer and the controllers are PI type, estimation errors have been simulated also during ramp state. Uncertain parameters have been chanced between their limits during simulation and the worst case results are presented in this section. SIMULINK block are given in the APPENDIX.

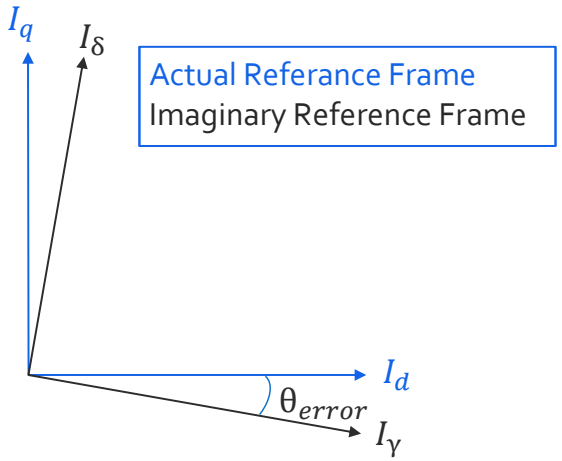

Figure 8.1 : Estimated And Actual Reference Frames

8.1.1 Washing cycle estimation errors

During washing cycle, motor mechanical speed is below 1000 rpm. Since the observer has $\omega_e \frac{L_q}{L_d}$ terms, the back electromotive force estimation error caused by L_d and L_q is expected to be lower than the high speed case. State estimation errors under parameter uncertainties and noisy environment is given in Figure 8.2. Similarly, rotor position estimation is given in Figure 8.3. As it can bee seen in the Figure 8.2 and Figure 8.3, stator current estimation is satisfying. Estimated states track the actual states

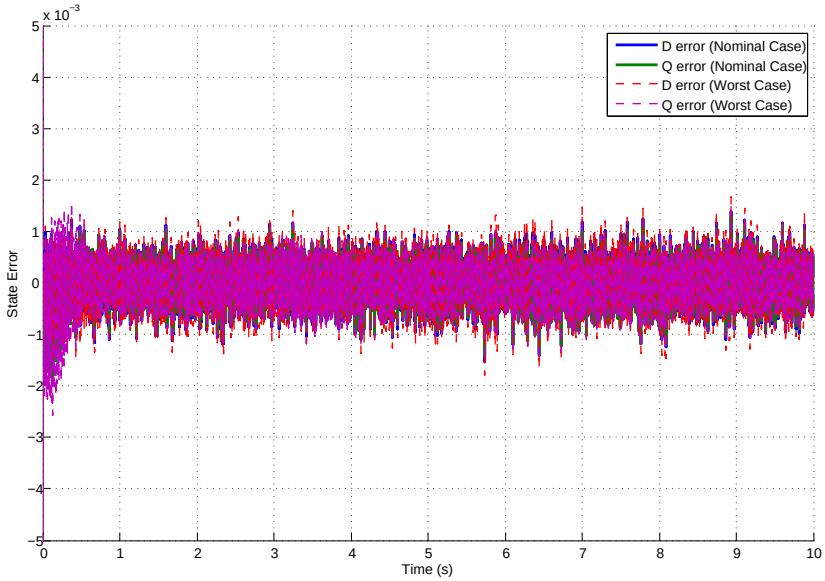

Figure 8.2 : Washing Cycle State Estimation Errors

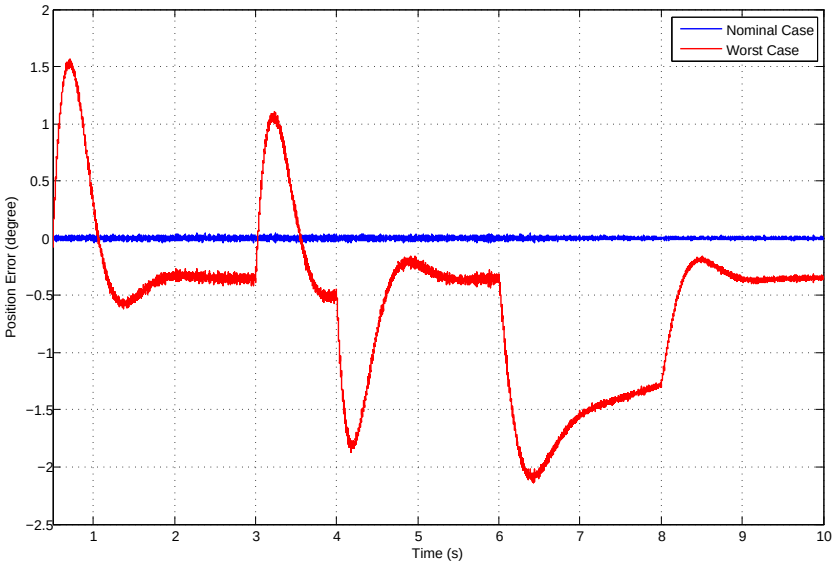

Figure 8.3 : Washing Cycle Rotor Position Errors

without steady state error in both nominal and worst case. However, rotor position error has steady state error when the parameters are chanced. During nominal (ideal) case steady state error is zero. Position error is also increased when the load is chanced and motor is accelerated (or decelerated). However, rotor position error is limited due to predefined speed ramps and parameter variation limits. Position error at worst case is below 3^o. Up to $20^o - 30^o$ position error, control performance does not chance dramatically. Depending on the position error, required stator current is increased leading to inefficient drive performance. So the design is valid. Motor control closed loop system can tolerate this position error.

8.1.2 Spinning cycle estimation errors

Motor mechanical speed reaches up to 15120 rpm. So, the estimation errors caused by the $\omega \frac{L_q}{L_d}$ term is more effective by comparison to the washing cycle case. Therefore, spinning cycle is more challenging case. Although state estimation steady state error converges to zero, position estimation error is relatively high compared to the washing cycle. Spinning cycle state estimation error is given in Figure 8.4. At worst case, there

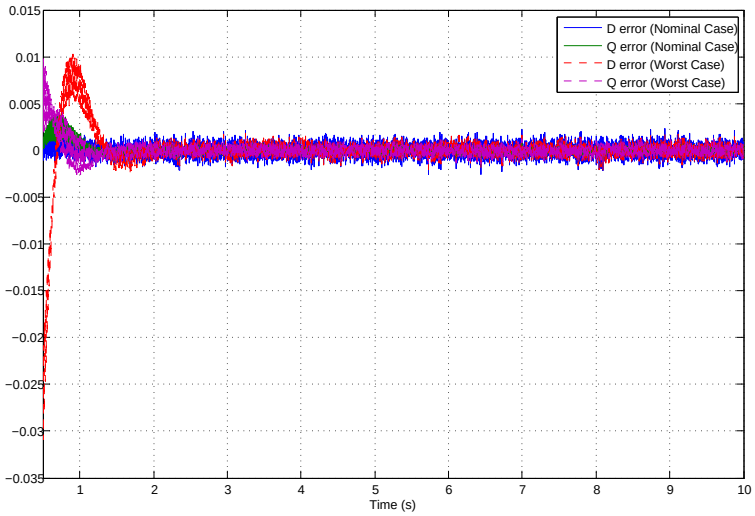

Figure 8.4 : Spinning Cycle State Estimation Errors

are overshoots in the transient period. However, estimation error goes to zero at the steady state. Position estimation error is given in Figure 8.5. As it can be seen in

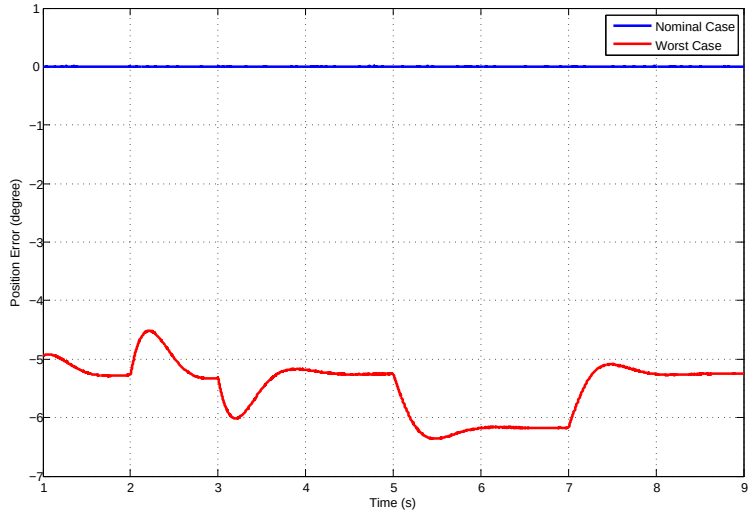

Figure 8.5 : Spinning Cycle Rotor Position Errors

Figure 8.5, estimated position error is higher than the washing cycle case. However, position error is kept below 7^o. This result is also satisfying. This position error shows

itself as the unnecessarily high stator current due to the projection as given in Figure 8.1. However, current increment is tolerably low due to low position error.

8.2 Experimental Results

By using E2Studio IDE, real time variables have been captured to the text file. In this section, control system variables have been presented under different load and speed conditions.

8.2.1 Washing cycle

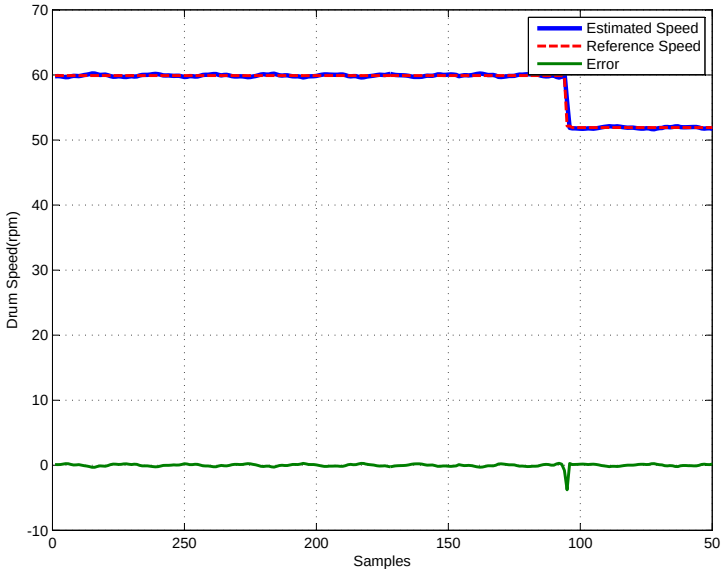

Figure 8.6 : Drum Speed Under No Load Condition

As it can be seen in Figure 8.6, drum speed tracks the reference speed without making steady state error. In order to make more realistic experiments, washing machine is load with 400g unbalanced load. The unbalanced load creates sinusoidal load torque and the frequency of the sinus depends on the rotor speed. Speed estimation under 400g unbalanced load is given in Figure 8.7. Estimated extended back electromotive forces under 400g unbalanced load have been given in Figure 8.8. Since the load torque chances sinusoidally, back electromotive forces are also oscillate. D axis back electromotive force fluctuates around zero. This means the observer estimates the rotor position very closely. Depending on the uncertainties, error between real and estimated rotor position may chance as indicated before. However, current estimation error is expected to be zero. Torque component of the current ,i_q, is given in Figure 8.9. Unbalanced load in the drum creates sinusoidal load torque, causing the torque

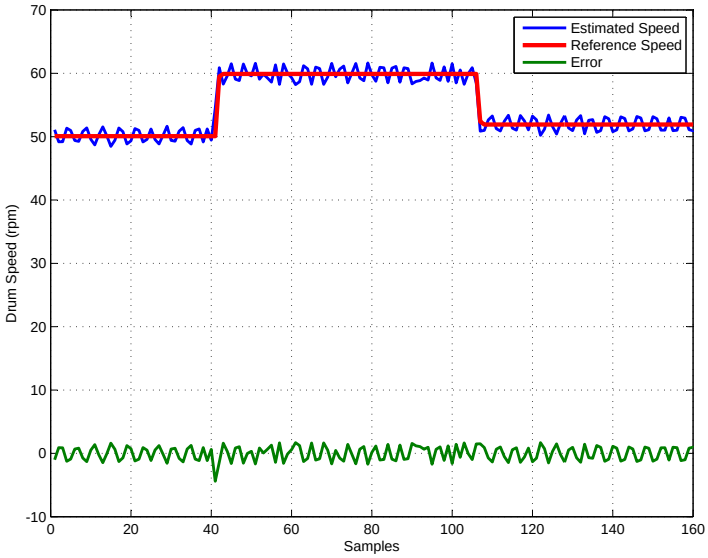

Figure 8.7 : Drum Speed Under 400g Unbalanced Load Condition

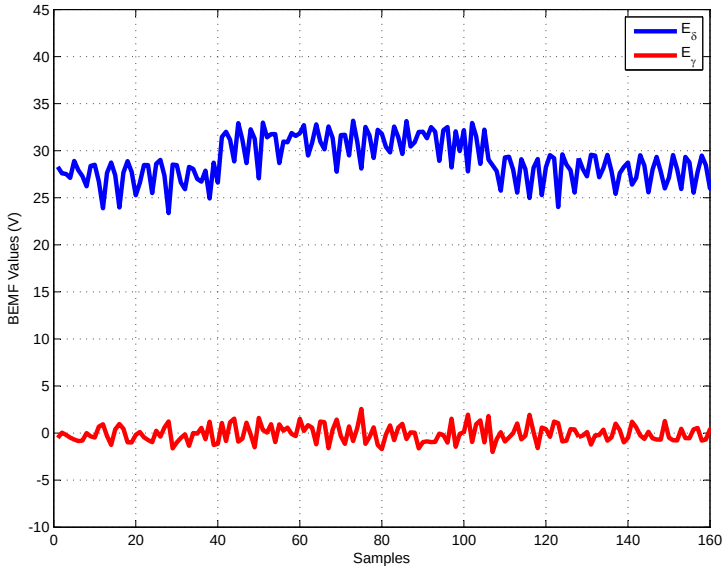

Figure 8.8 : BEMF Voltages Under 400g Unbalanced Load Condition

component of the stator current oscillates. However, mean value, which compensates the torque caused by the friction, is almost constant. Estimated position error which is $atan(\frac{-E_\gamma}{E_\delta})$, is given in Figure 8.10. Estimated position error between actual and imaginary reference frames is calculated by using back electromotive forces. Since the unbalanced load causes the back electromotive force oscillations, estimated position error is also oscillates. The other reason of the oscillation is the observer dynamics. Observer tries to compensate the error between actual and the observer model output. So, during the transient period, estimation error may not be zero depending on the error dynamics.

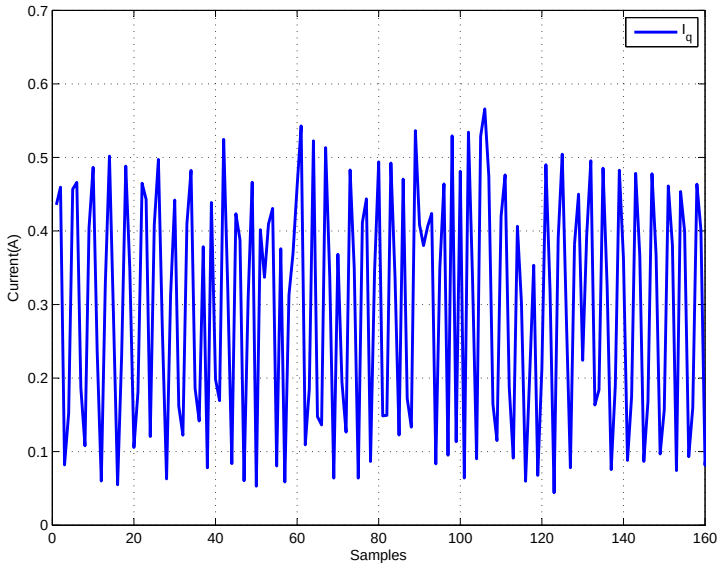

Figure 8.9 : i_q Current Under 400g Unbalanced Load Condition

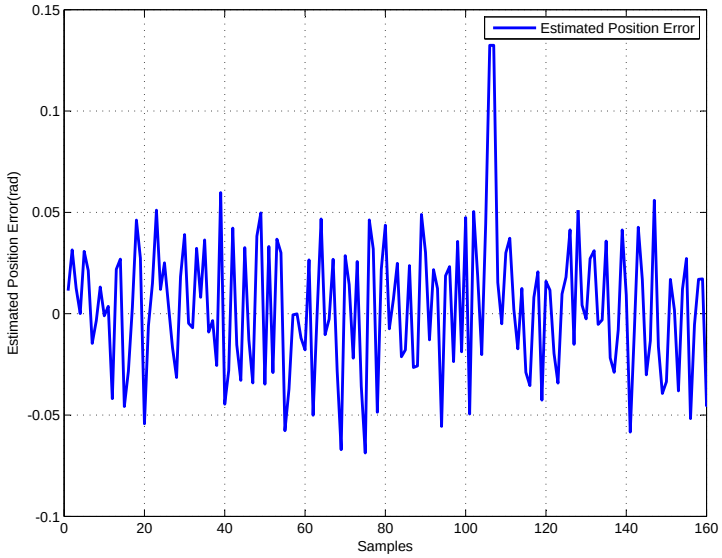

Figure 8.10 : Estimated Position Error Under 400g Unbalanced Load Condition

8.2.2 Spinning cycle

As the motor speed increased, sinusoidal load torque frequency is also increased. Furthermore, stator winding resistance is increased as the stator current is increased. So the spinning cycle is a suitable region in order to test the performance of the closed loop system. Speed Estimation under no load condition and 400g unbalanced load condition is given in Figure 8.11 and Figure 8.12. Drum speed tracks the reference signal for different load conditions. Estimated back electromotive forces is given in Figure 8.13. Depending on the rotor speed, extended electromotive forces change. Since the d axis is aligned with the permanent magnet, there is no back electromotive force in the d axis. However, depending on the estimation quality and the operational

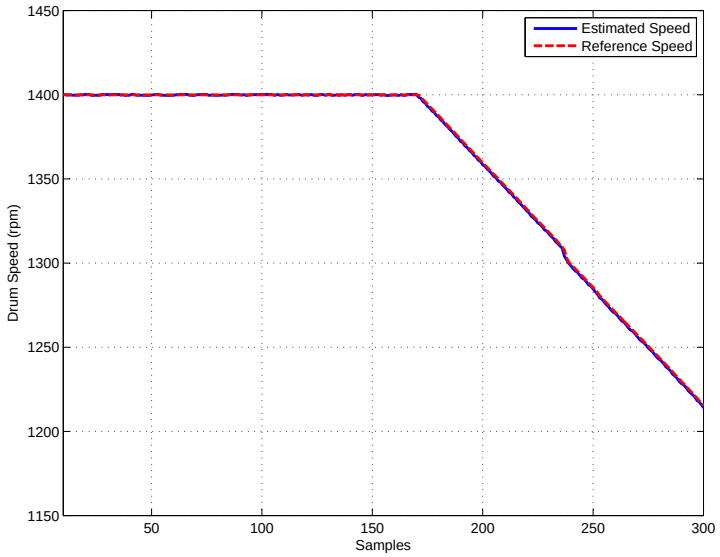

Figure 8.11 : Drum Speed Under No Load Condition

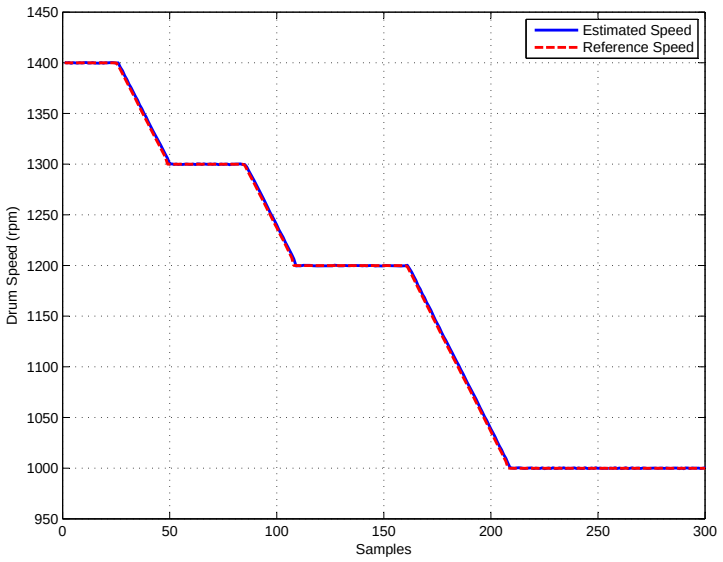

Figure 8.12 : Drum Speed Under 400g Unbalanced Load Condition

conditions, d axis back electromotive force takes values different from zero. But as it is observer, d axis back electromotive force is always near to zero. Torque related i_q current is given in Figure 8.14.

8.2.3 Ramp condition at whole range

Since rotor position error is increased during acceleration (or deceleration), it is also important to observe the closed loop variables during the ramp case. Washing machine is loaded with clothes and related closed loop variables have been observed. Motor speed profile which covers full range is given in Figure 8.15. Motor speed tracks the reference without making any steady state error. Figure 8.16 and Figure 8.17 show

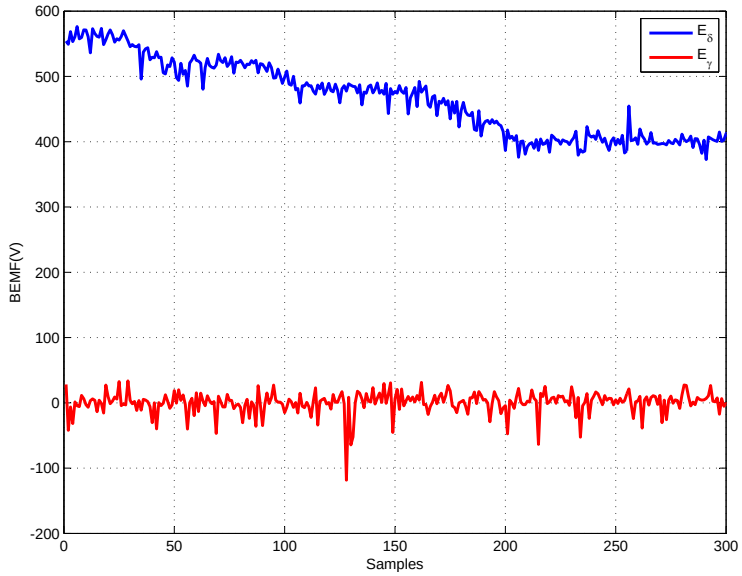

Figure 8.13 : BEMF Voltages Under 400g Unbalanced Load Condition

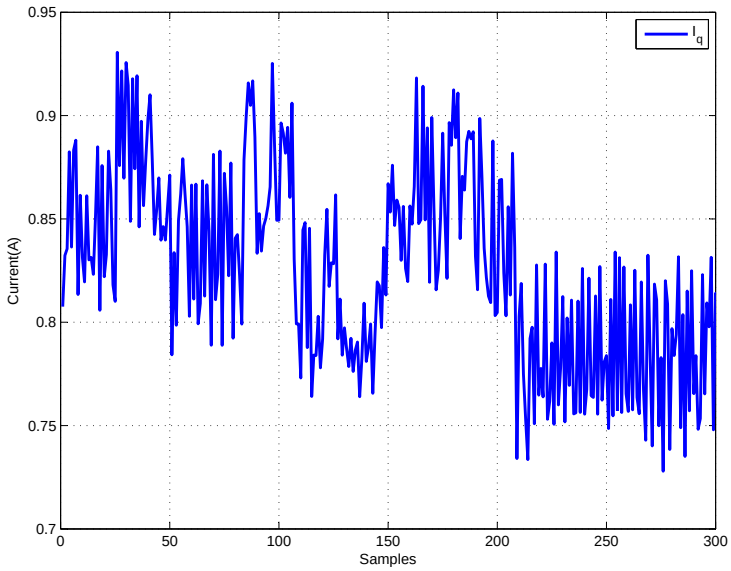

Figure 8.14 : i_q Current Under 400g Unbalanced Load Condition

the stator currents and the control signals. Especially at high speed operation, stator current variation is increased due to the coupling effects and high frequency sinusoidal load torque. However, controllers compensate the effect of these disturbances. Control signal oscillations are satisfactorily low. Control signals also do not exceed the stator voltage limits during the whole operational range. Estimated extended back electromotive forces, E_γ and E_δ, are shown in Figure 8.18. E_γ stays at zero as expected and E_δ reaches high voltages depending on the motor speeds. Since the extended back electromotive forces are fictive variables, exceeding 300 V DC bus voltage is not a problem. By using an oscilloscope, stator phase current can be measured. Stator current can be considered as the vectorial sum of the i_q and i_d. So, by observing

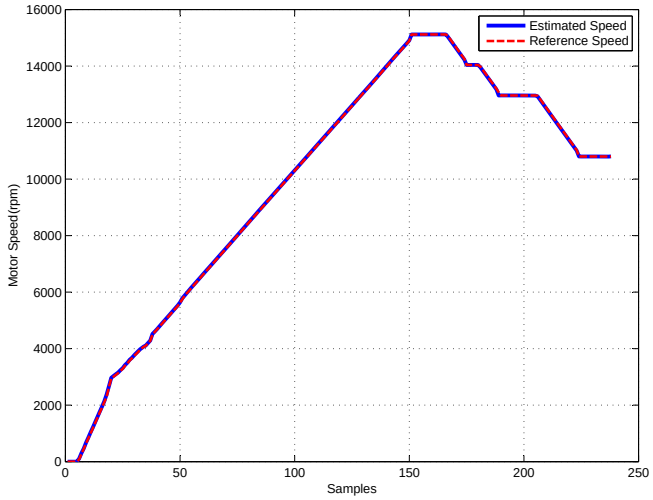

Figure 8.15 : Motor Speed Under Loaded Condition

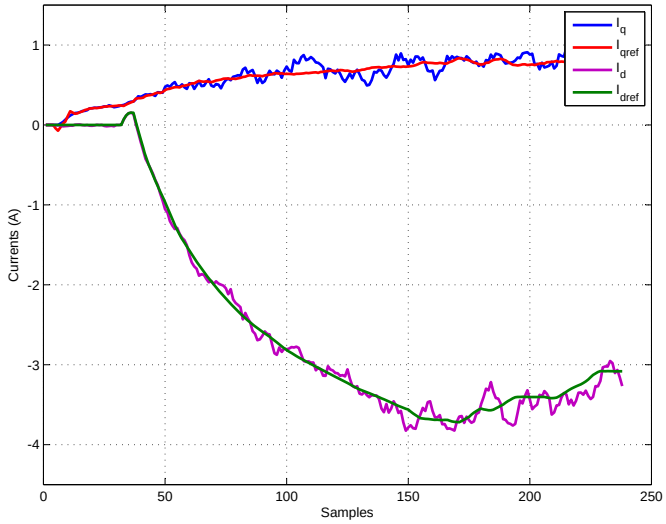

Figure 8.16 : Stator Currents Under Loaded Condition

the phase current, many information can be obtained. First of all, phase current is sinusoidal. Amplitude of the phase current is proportional to $\sqrt{i_d^2 + i_q^2}$ and the frequency is directly proportional to the rotor speed. Since the number of pole pairs is 4, electrical rotor speed can be found by multiplying the electrical frequency by 15. Position estimation quality can be also observed up to certain point. Harmonics of the phase current increases with the rotor position error. So, pure sinusoidal phase current means that the rotor position estimation is satisfactory. Phase currents at maximum speed, at minimum speed and washing speed under unbalanced load condition are given in Figure 8.20, Figure 8.21 and Figure 8.22.

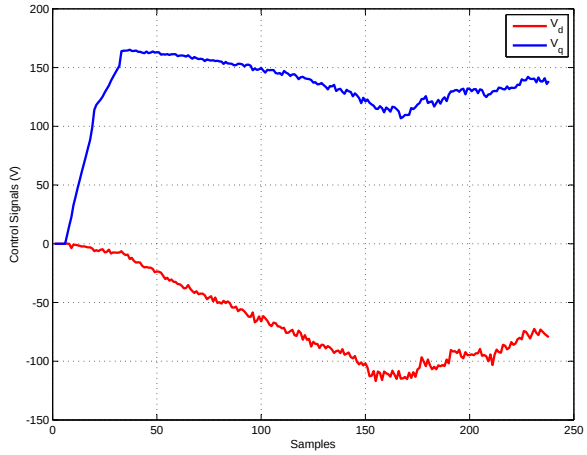

Figure 8.17 : Control Signals Under Loaded Condition

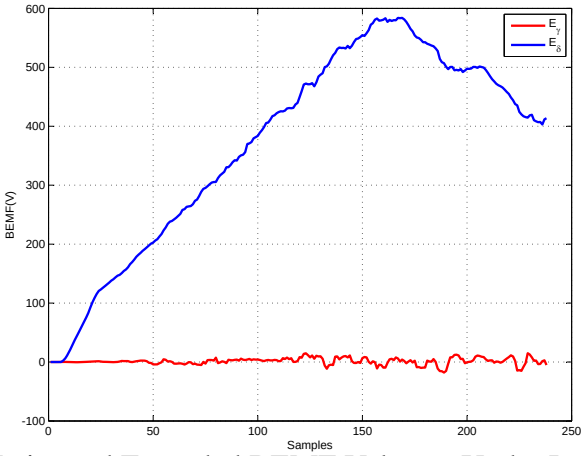

Figure 8.18 : Estimated Extended BEMF Voltages Under Loaded Condition

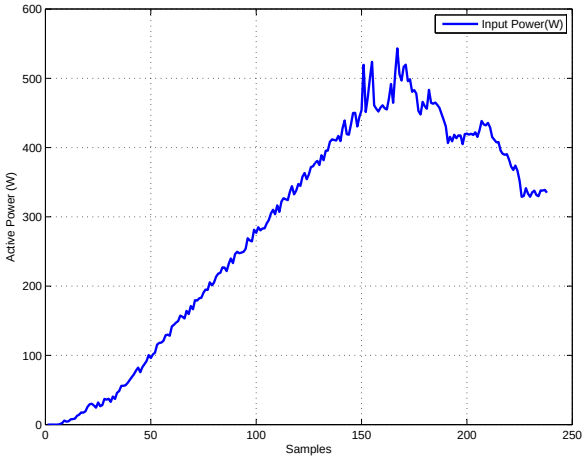

Figure 8.19 : Input Power Under Loaded Condition

Figure 8.20 : Single Phase Current at The Maximum Speed

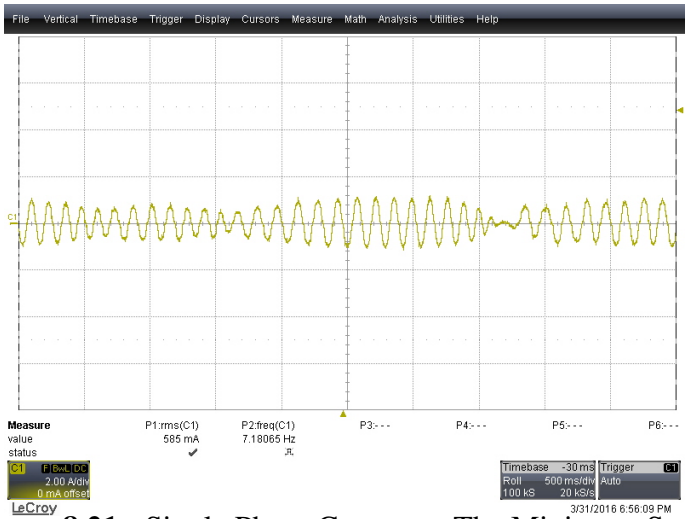

Figure 8.21 : Single Phase Current at The Minimum Speed

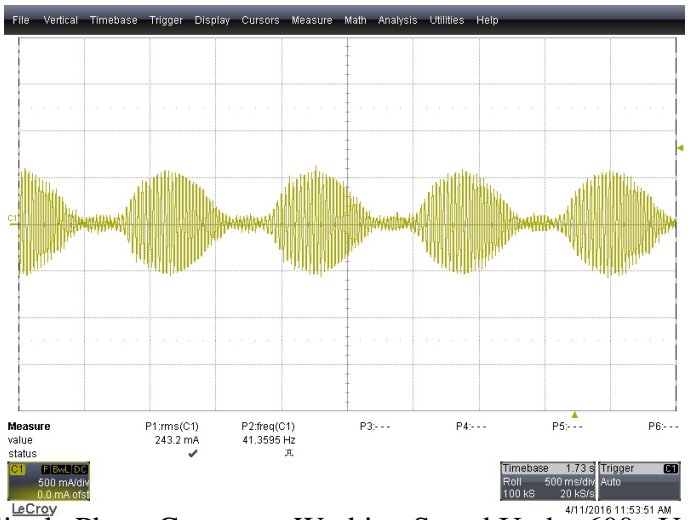

Figure 8.22 : Single Phase Current at Washing Speed Under 600g Unbalanced Load

9. CONCLUSION

In this study, interior magnet synchronous motor has been controlled under parametric uncertainties without using any rotor position sensor. The designed closed loop system has been applied to a washing machine application. Pole coloring concept has been applied to a real industrial problem for the first time in order to obtain satisfactory design under parametric uncertainties. By using this approach, controller coefficients remain unchanged during the whole operational range. This led to simple control algorithm without using adaptive structures.

PI observer has been selected as state and disturbance observer due to its simple structure, easily applicable nature to the low cost microcontroller, and its satisfactory robustness properties. Results in Chapter 8 show that controller and observer designs fulfill the requirements of washing machine application. Field weakening algorithm has been applied in order to extend the motor speed which is limited by the DC bus voltage. Also, decoupling control structure has been designed in order to minimize the cross coupling effects between d and q axes currents.

In order to overcome the robust startup problem, a novel startup algorithm has been proposed and applied. By using the algorithm, it was observed that motor has always been able to perform successful startup for different load conditions.

Unbalanced load detection algorithm has also been proposed. However, the current version of the algorithm can only detect the unbalanced load. When the drum is loaded with balanced and unbalanced load, algorithm shows poor performance and is needed to be improved.

At the end of the study following issues are proposed to be improved as further works.

- Steady state error of the state estimation converges to the zero for the estimated currents. However, disturbances (back electromotive forces) estimation error does not converges to zero but to a small number. In order to improve the observer robustness, degree of freedom of the observer may be increased.

- In order to overcome the decoupling problem, open loop transfer functions have been decoupled by using 2 transfer function. However, uncertainty analysis have not been covered. More improved decoupling techniques may be applied to the closed loop system (Observers may be used in order to estimate the decoupling signals).

- Low speed operation has not been covered in this study. However, washing machine drum can still rotates at $8rpm$ under loaded condition without loosing the stability. Further improvement may be proposed in order to improve low speed performance such as including detailed model of the inverter, using active disturbance rejection techniques and using different mathematical model and structure for the observer.

- Uncertainties have been treated as parametric uncertainties and unstructured uncertainties are now covered. Further study may cover the frequency domain in order to increase robustness.

- Parameter identification has not been covered in this study. Estimating the certain parameters like load moment of inertia and the stator resistance may improve the closed loop system performance besides improving the application algorithm (winding temperature estimation, amount of water to be used etc.).

REFERENCES

[1] **Mishra, A.**, **Makwana, J.**, **Agarwal, P. and Srivastava, P.** (2012). Modeling and implementation of vector control for PM synchronous motor drive, *International Conference on Advances in Engineering, Science and Management (ICAESM)*, Nagapattinam.

[2] **Harib, K.H.**, **Khousa, E.A. and Ismail, A.** (2011). Field oriented motion control of a 3-phase permanent magnet synchronous motor, *2nd International Conference on Electric Power and Energy*, Sharjah.

[3] **A. Rafiq, M.G. Sarwer, M.D. and Ghosh, C.** (2005). Fast speed response field-orientation control induction motor drive with adaptive neural integrator, *IEEE International Conference on Industrial Technology*.

[4] **Bayka, K.** Comparison of Three IPMSM Sensorless Position Estimation Methods Through Simulations And Experiments, Master's thesis, ITU.

[5] **Benjak, O. and Gerling, D.** (2010). Review of Position Estimation Methods for IPMSM Drives Without a position Sensor Part I: Nonadaptive Methods, *XIX International Conference of Electrical Machines*, Rome, Italy.

[6] **Benjak, O. and Gerling, D.** (2010). Review of Position Estimation Methods for IPMSM Drives Without a position Sensor Part 2: Adaptive Methods, *XIX International Conference of Electrical Machines*, Rome, Italy.

[7] **Agrawal, J. and Bodkhe, S.** (2013). Sensorless Permanent Magnet Synchronous Motor Drive: A Review, *National Conference on Innovative Paradigms in Engineering & Technology*, Nagpur, India.

[8] **Kazraji, S.M.**, **Soflayi, R.B. and Sharifian, M.B.B.** (2014). Sliding-Mode Observer for Speed and Position Sensorless Control of Linear-PMSM, *Scientific Journal of RTU/ Electircal, Control and Communication Engineering*, *5*, 20 – 26.

[9] **Deo, H.V. and Shekokar, R.** (2014). A Review of Speed Control Techniques Using PMSM, *International Journal of Innovative Research in Technology*, *1*(11).

[10] **Kim, K.**, **Baik, I.**, **Moon, G. and Youn, M.** (1999). A Current Control or a Permanent Magnet Synchronous Motor With a simple disturbance estimation scheme, *IEEE Trans. Control System Technol.*, *7*(5), 630–633.

[11] **Moaveni, B. and Khorshidi, M.** (2015). Robust speed controller design for induction motors based on IFOC and Kharitonov theorem, *Turkish Journal of Electrical Engineering and Computer Sciences*, *23*, 1173–1186.

[12] **Turker, T.**, **Buyukkeles, U. and Bakan, A.F.** (2016). A Robust Predictive Current Controller for PMSM Drives, *IEEE Transactions on Industrial Electronics*, (99).

[13] **Hassaine, S.**, **Moreau, S.**, **Gherbi, S.**, **Sedraoui, M. and Mazari, B.** (2012). Real time implementation of a robust controller for PMSM drive system using H_{inf} norm, *38th Annual Conference on IEEE Industrial Electronics Society*, Montreal.

[14] **Zhou, C.**, **Quach, D.C.**, **Xiong, N.**, **Huang, S.**, **Zhang, Q.**, **Yin, Q. and Vasilakos, A.V.** (2015). An Improved Direct Adaptive Fuzzy Controller of an Uncertain PMSM for Web-Based E-Service Systems, *IEEE Transactions on Fuzzy Systems*, *23*, 58–71.

[15] **Zhao, D.**, **Tian, W.**, **Zhang, T. and Hu, H.** (2010). Adaptive Control Design for Permanent Magnet Synchronous Motor with Uncertain Parameters: An LMI Approach, *IEEE International Conference on Information and Automation (ICIA)*, Harbin.

[16] **de Sousa, M.A.T.F.**, **Caux, S.**, **Fadel, M. and Lima, A.M.N.** (2007). Adaptive Control Design for Permanent Magnet Synchronous Motor with Uncertain Parameters: An LMI Approach, *European Conference on Power Electronics and Applications*, Alborg.

[17] **Wang, Z.**, **Lu, K.**, **Ye, Y.**, **Jin, Y. and Hong, W.** (2011). Analysis of influence on back-EMF based sensorless control of PMSM due to parameter variations and measurement errors, *International Conference on Electrical Machines and Systems (ICEMS)*, Beijing.

[18] **Lee, K.W. and Ha, J.I.** (2012). Evaluation of Back-EMF Estimators for Sensorless Control of Permanent Magnet Synchronous Motors, *Journal of Power Electronics*, *12*.

[19] **Boldea, I. and Agarlita, S.** (2011). The Active Flux Concept For Motion-Sensorless Unified AC Drives:a Review, *International Aegean Conference on Electrical Machines and Power Electronics and Electromotion Joint Conference (ACEMP)*, Istanbul.

[20] **Guoqiang, Z.**, **Gaolin, W.**, **Ronggang, N. and Dianguo, X.** (2014). Active flux based full-order discrete-time sliding mode observer for position sensorless IPMSM drives, *17th International Conference on Electrical Machines and Systems (ICEMS)*, Hangzhou.

[21] **Foo, G. and Rahman, M.F.** (2010). Sensorless Direct Torque and Flux-Controlled IPM Synchronous Motor Drive at Very Low Speed Without Signal Injection, *IEEE Transactions on Industrial Electronics*, *57*(1), 395 – 403.

[22] **Morimoto, S.**, **Kawamoto, K.**, **Sanada, M. and Takeda, Y.** (2001). Sensorless control strategy for salient-pole PMSM based on extended EMF in rotating reference frame, *Proc. IEEE Ind. App. Soc. Annual Meeting*, *4*, 2637 – 2644.

[23] **Liu, Y.** (2011). Robust Nonlinear Control Design with Proportional-Integral-Observer Technique, *Ph.D. thesis*, University of Duisburg-Essen, Essen, Germany.

[24] **Bakhshande, F. and Söffker, D.** (2015). Proportional-Integral-observer A brief survey with special attention to the actual methods using ACC Benchmark, *8th Vienna International Conference on Mathematical Modelling*, *48*(1), 532 – 537.

[25] **Soylemez, M.** (1999). *Pole Assignment For Uncertain Systems*, Research Studies Press.

[26] **Davidson, E. and Wang, S.** (1975). On Pole Assignment in Linear Multivariable Systems Using Output Feedback, *IEEE Trans. Automat. Contr.*, *20*(8), 516 – 518.

[27] **Chu, E.** (2011). Optimization And Pole Assignment In Control System Design, *Int. J. Appl. Math. Compu. Sci*, *11*(5), 1035 – 1053.

[28] **Ackermann, J.** (2002). *Robust Control: The Parameter Space Approach*, Springer.

[29] **G.G. Miminis, C.** (1982). An Algorithm For Pole Assignment of time Invariant Multi-Input Linear Systems, *21st IEEE Conference on Decision and Control*, Orlando, Florida, USA.

[30] **Bhattacharyya, S. and Sousa, E.D.** (1982). Pole Assignment Via Sylvester Equations, *Syst. Contr. Lett.*, *1*(5), 261 – 263.

[31] **S.P. Bhattacharyya, H.C. and Keel, L.** (1995). *Robust Control: The parametric Approach*, Prentice Hall.

[32] **Nath, V. and Mitra, R.** (2014). Robust Pole Placement Using linear Quadratic Regulator Weight Selection Algorithm, *International Journal of Scientific Research Engineering and Technology*, *3*(3), 329–333.

[33] **Moheimani, S. and Petersen, I.** (1996). Quadratic quarenteed Cost Control with Robust Pole Placement in a Disk, *IEE Proc-Control Theory Appl.*, *143*(1), 37 – 43.

[34] **R.Byers and S.G.Ñash** (1996). Approaches to Robust Pole Assignment, *Int. J. Contr.*, *49*(1), 97 – 117.

[35] **Yang, Y. and Tits, A.**, (1995), Globally Convergent Algorithm For Robust Pole Assignment By State Feedback, Tech. Rep., Dept. Electr. Eng. and Inst. Syst. Res., University of Maryland at College Park.

[36] **Soylemez, M. and Munro, N.** (1997). Robust Pole Assignment in Uncertain Systems, *Proc. IEE-Cont. Theo. and Appl.*, *144*(3), 217 – 224.

[37] **R. Burkard, M.Dell'Amico, S.M.**, (2009). Assigment Problems, Society for Industrial and Applied Mathematics, Philadelphia.

[38] **G.G. Goodwin, S. Graebe, M.S.** (2000). *Control System Design*, Prentice Hall, Incorporated.

[39] **Hariz, M.B. and Bouani, F.** (2015). Design of controllers for decoupled TITO systems using different decoupling techniques, *2015 20th International Conference on Methods and Models in Automation and Robotics (MMAR)*, Miedzyzdroje.

[40] **Chi, S.** (2007). Position Sensorless Control of Permanent Magnet Synchronous Machines Over Wide Speed Range, *Ph.D. thesis*, Ohio State Univercity, Ohio, USA.

[41] **PED4-1038C, G.** (2009). Torque Control in Field Weakening Mode, *Ph.D. thesis*, Institute of Energy Technology, Aalborg University, AAlborg, Denmark.

[42] **Huawei Zhou, Xuhui Wen, F.Z.J.Z.J.M.** (2012). An Improved Flux-weakening Strategy for Field-oriented-controlled PMSM Drives, *7th International Power Electronics and Motion Control Conference*, Harbin.

[43] **N.P. Quang, J.D.** (2015). *Vector Control of Three-Phase AC Machines*, Springer.

APPENDICES

APPENDIX A.1 : Total SIMULINK Model of The Closed Loop System
APPENDIX A.2 : PI Observer SIMULINK Model
APPENDIX A.3 : IPMSM SIMULINK Model
APPENDIX A.4 : Decoupler SIMULINK Model
APPENDIX B.1 :MATHEMATICA Code for Perturbation Based Cost Function
APPENDIX B.2 : MATHEMATICA Code for Settling Time Based Cost Function

APPENDIX A.1

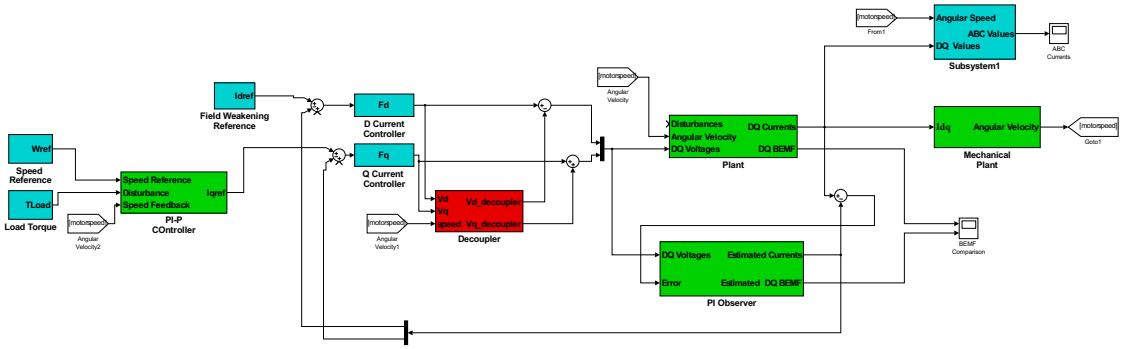

Figure A.1 : Total SIMULINK Model of The Closed Loop System

APPENDIX A.2

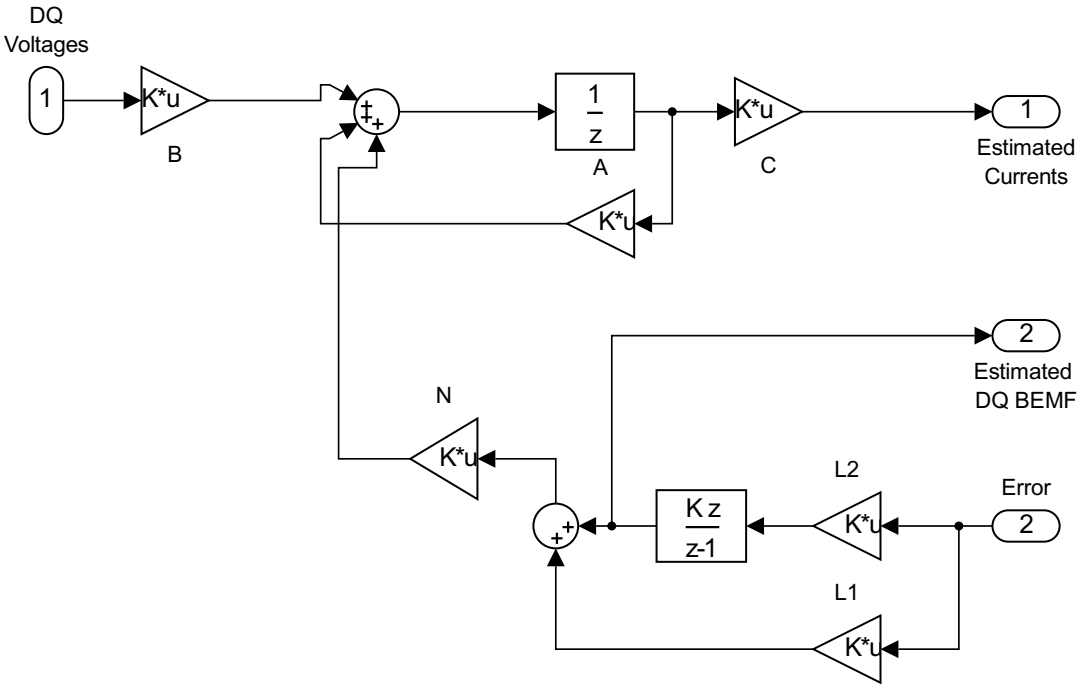

Figure A.2 : PI Observer Model

APPENDIX A.3

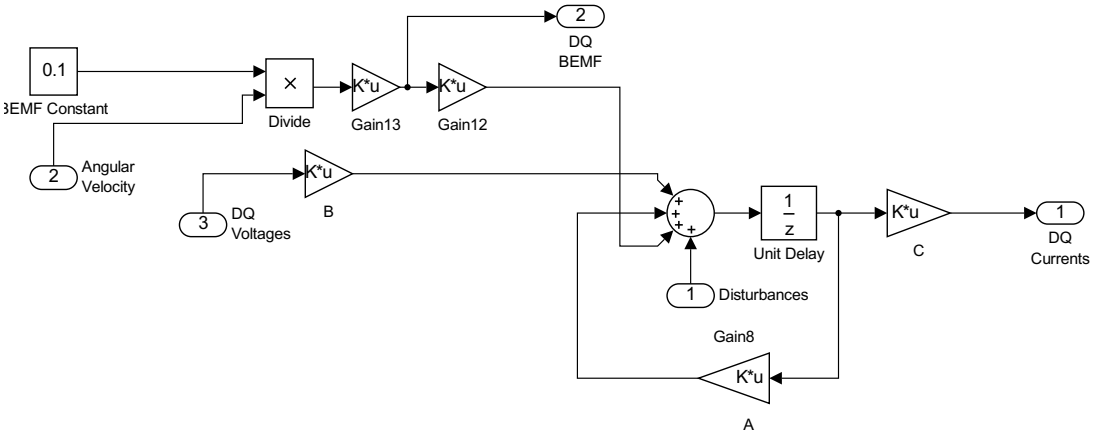

Figure A.3 : IPMSM Model

APPENDIX A.4

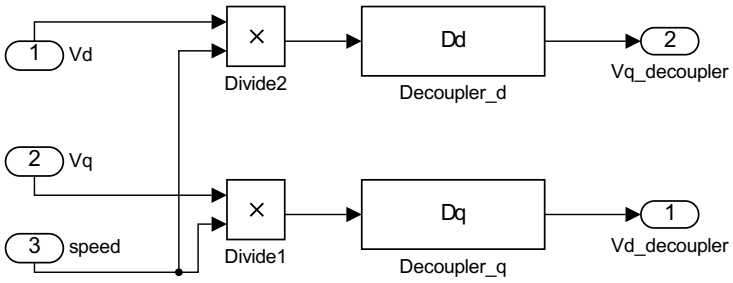

Figure A.4 : Decoupler Model

APPENDIX B.1

```
cost1 = N[Table[(Abs[Permutations[{-7, -2 + i, -2 - i}][[counter]][[1]]
          - Eigenvalues[A - B.Fs][[1]]] / r1), {counter, 1, 6}]];
cost2 = N[Table[(Abs[Permutations[{-7, -2 + i, -2 - i}][[counter]][[2]]
         - Eigenvalues[A - B.Fs][[2]]] / r2), {counter, 1, 6}]];
cost3 = N[Table[(Abs[Permutations[{-7, -2 + i, -2 - i}][[counter]][[3]]
         - Eigenvalues[A - B.Fs][[3]]] / r3), {counter, 1, 6}]];

Jpair = Min[cost1 + cost2 + cost3];

Jpc = Max[Table[Jpair, {q1, -0.25, 0.25, 0.25}, {q2, -0.35, 0.35, 0.35},
    {q3, -0.2, 0.25, 0.2}]]

Minimize[Jpc, k, Reals]
```

Figure B.1 : MATHEMATICA Code for Minimum Perturbation Based Cost Function

APPENDIX B.2

```
cost1 = N[Table[(Abs[Permutations[{-7, -2 + i, -2 - i}][[counter]][[1]]
          - Eigenvalues[A - B.Fs][[1]]] / r1), {counter, 1, 6}]];
cost2 = N[Table[(Abs[Permutations[{-7, -2 + i, -2 - i}][[counter]][[2]]
          - Eigenvalues[A - B.Fs][[2]]] / r2), {counter, 1, 6}]];
cost3 = N[Table[(Re[Permutations[{-7, -2 + i, -2 - i}][[counter]][[3]]]
         - Re[Eigenvalues[A - B.Fs][[3]]]) / (Re[Permutations[{-7, -2 + i, -2 - i}]
            [[counter]][[3]]] + 6.5), {counter, 1, 6}]];

Jpair = Min[cost1 + cost2 + cost3];

Jpc = Max[Table[Jpair, {q1, -0.25, 0.25, 0.25}, {q2, -0.35, 0.35, 0.35},
    {q3, -0.2, 0.25, 0.2}]]

Minimize[Jpc, k, Reals]
```

Figure B.2 : MATHEMATICA Code for Settling Time Based Cost Function

CURRICULUM VITAE

Name Surname **:** İsa Eray Akyol

Place and Date of Birth **:** Muğla, 22.05.1991

E-Mail **:** isaerayakyol@gmail.com

EDUCATION **:**

- **B.Sc.** **:** 2015, ITU, Faculty of Electrical and Elecronics Engineering, Control and Automation Engineering
- **B.Sc.** **:** 2014, ITU, Faculty of Electrical and Elecronics Engineering, Electrical Engineering

PROFESSIONAL EXPERIENCE AND REWARDS:

- R&D Engineer at Arçelik R&D Center A.¸S. since 2015

PUBLICATIONS, PRESENTATIONS AND PATENTS ON THE THESIS:

- Ümit, M.E., Baş, M.E., **Akyol,İ.E.**, Uludağ, M.Ş., Ecevit,A.B., Aslan, A.R., *"TURK- SAT 3USAT Küp Uydusu için Elektrik Güç Sistemi Tasarlanması",* Ulusal Havacılık Konferansı, Hava Harp Okulu, ˙Istanbul, Türkiye, 2012.
- Ümit, M.E., Baş, M.E., **Akyol, İ.E.**, Uludağ, M.Ş., Ecevit, A.B., Aslan ,A.R., *"Solar Emulator and Simulator Design for CUBESATS",* IAC-12-C3, 4, 9, x15321, 63rd International Astronautical Congress, Naples, Italy, 2012.
- Ümit, M.E., Baş, M.E., **Akyol. İ.E.,** Uludağ, M.Ş., Ecevit. A.B., Aslan, A.R., *"Indigenous Hardware-in-the-Loop Simulator Development for University Satellite",* IAA-B9-0510P, 9th IAA Symposium on Small Satellites for Earth Observation, Berlin, Germany, 2013.

- Aslan, R. et al, *"Development of a LEO Communication CubeSat"*, International Conference Series on Recent Advances in Space Technologies-RAST, 6th Internatioal Conference on Recent Advances in Space Technologies-RAST2013.
- Aslan. R. et al, *"QB50 Projesi kapsamında BEAGLESAT Küp Uydusunun Geliştirilmesi"*, V. Ulusal Havacılık ve Uzay Konferansı, Erciyes Üniversitesi, Kayseri ,Türkiye, 2014.
- Aslan, R. et al, *"Development and Orbit Testing of an X Ray Detector Within a 2U CubeSat",* 65th Internation Astronautical Congress, Toronto, Canada, 2014.